

Moving hotspots - Evidence from paleomagnetism and modeling

*Inaugural-Dissertation
zur Erlangung des Doktorgrades
der Fakultät für Geowissenschaften der
Ludwig-Maximilians-Universität München*

vorgelegt von
Maria Antretter

Juni 2001

1. Berichterstatter: Prof. Dr. H. C. Soffel
2. Berichterstatter: Prof. Dr. N. Petersen

Tag der mündlichen Prüfung: 25. Juli 2001

Contents

Contents	1
List of figures	4
List of tables	6
Glossary	8
Zusammenfassung	9
Summary	13
1 Introduction	17
2 The Kerguelen Plateau, a Large Igneous Province	23
2.1 LIPs and hotspots	23
2.2 Kerguelen Plateau/Broken Ridge	24
2.3 Formation of the Plateau - Geological settings	27
2.4 Summary of age variation	30
2.5 Plume - ridge interactions	31
2.6 Exploring the Kerguelen Plateau: ODP Leg 183	32
2.6.1 Background	32
2.6.2 Paleomagnetic research on Leg 183	33
3 Paleolatitudes of the Kerguelen hotspot: paleomagnetic results	35
3.1 Sampling and methods	35
3.2 The southern Kerguelen Plateau - Site 1136	37
3.3 The central Kerguelen Plateau - Site 1138	39
3.3.1 Lithostratigraphy of the basement	39
3.3.2 Rock magnetic studies	39
3.3.3 Demagnetization of the NRM	41
3.3.4 Paleosecular variation record	42
3.3.5 Paleolatitude of Site 1138	45

3.4	The northern Kerguelen Plateau - Site 1140	47
3.4.1	Lithostratigraphy	47
3.4.2	Rock magnetic studies	48
3.4.3	Demagnetization of the NRM	48
3.4.4	Paleosecular variation record	50
3.4.5	Paleolatitudes of Site 1140	51
3.5	Broken Ridge - Site 1142	53
3.6	Previous paleomagnetic investigations	53
3.7	Implications on the paleolatitudes of the Kerguelen hotspot	55
4	Paleolatitudes of the Kerguelen hotspot: True polar wander	57
4.1	True polar wander and reference frames	57
4.2	Effects of true polar wander on the Kerguelen hotspot	60
5	Paleolatitudes of the Kerguelen hotspot: hotspot motion and modeling results	63
5.1	Hotspot motion or hotspot stability?	63
5.2	Methods and theory	64
5.3	A new viscosity structure for the rising plume	67
5.4	Results for the Kerguelen hotspot motion and predictions for paleolatitudes	71
5.5	Where is the Kerguelen hotspot?	76
5.6	The influence of input-parameters on the hotspot motion results	77
5.7	Paleolatitudes of the Kerguelen hotspot: Summary	81
6	Was the Ontong Java Plateau formed by the Louisville hotspot?	84
6.1	Background	84
6.2	Modeled motion of the Louisville hotspot	85
6.3	Influence of TPW	88
7	Conclusion	91
	Bibliography	94
	Acknowledgments	102
	Appendices	103
A	Rock magnetic and paleomagnetic study on sediments from Sites 1138 and 1140	103
A.1	Methods	103
A.2	Lithologies of Sites 1138 and 1140	104
A.3	Magnetostratigraphy	108

A.3.1	Site 1138	108
A.3.2	Site 1140	110
A.4	Rock magnetism of sediments of Sites 1138 and 1140	110
A.4.1	IRM Analysis	111
A.4.2	Hysteresis Analysis	112
A.4.3	Thermomagnetic Analysis	114
B	Magnetozones in sediments, Site 1138	116

List of Figures

2.1	Global overview of LIPs	24
2.2	Bathymetry of the Kerguelen Plateau showing locations of drill holes	25
2.3	Bathymetry of Broken Ridge showing locations of drill holes	26
2.4	Plate tectonic reconstruction of the southern Indian Ocean	28
2.5	Map of the Indian Ocean showing major physiographic features	29
2.6	Summary of ODP basement drill holes on the Kerguelen Plateau	30
2.7	Concept of ridge - plume interaction	32
3.1	Thermomagnetic measurements on basalts from Site 1136	38
3.2	Lithologic units for basement of Site 1138	40
3.3	Thermomagnetic measurements on basalt from Site 1138	41
3.4	Zijderveld-diagrams for basalts from Site 1138	42
3.5	VGP scatter versus latitude for Site 1138	44
3.6	Inclination versus depth for Site 1138	46
3.7	Lithologic units for basement of Site 1140	47
3.8	Thermomagnetic measurements on basalts from Site 1140	48
3.9	Zijderveld-diagrams for basalts from Site 1140	49
3.10	VGP scatter versus latitude for Site 1140	51
3.11	Inclination versus depth for Site 1140	52
3.12	Paleomagnetically determined paleolatitudes for the Kerguelen hotspot	55
4.1	True polar wander path after <i>Besse and Courtillot</i> [1991]	58
4.2	New true polar wander paths	59
4.3	Effect of TPW on paleolatitudes of the Kerguelen hotspot	62
5.1	Proceeding for modeling of hotspot motion	65
5.2	Hotspot motion results for two different mantle-viscosity structures	67
5.3	Relationship of heat flux, dissipation number, anomalous mass flux, temperature anomaly and height above the core-mantle boundary in a plume	68
5.4	Radius of a plume as function of the height above the core-mantle boundary	71
5.5	Effect of changing viscosity in a rising plume on hotspot motion	72
5.6	Results for the motion of the Kerguelen hotspot	73

5.7	Paleolatitudes of the Kerguelen hotspot due to hotspot motion	75
5.8	Hotspot motion with different present-day positions for the Kerguelen hotspot	77
5.9	The Kerguelen hotspot motion for different anomalous mass fluxes B . . .	78
5.10	The Kerguelen hotspot motion for different initial temperature anomalies T_{in}	79
5.11	The Kerguelen hotspot motion for different pressure gradients	79
5.12	The Kerguelen hotspot motion for different initial viscosity anomalies . . .	80
5.13	Summary of paleolatitudes for the Kerguelen hotspot	82
6.1	Tectonic reconstruction for the location of the Ontong Java Plateau 120 Ma ago	85
6.2	Calculated motion for the Louisville hotspot - part 1	86
6.3	Calculated motion for the Louisville hotspot - part 2	87
6.4	Predicted paleolatitudes for the Louisville hotspot due to hotspot motion .	89
6.5	Effect of TPW on the paleolatitudes of the Louisville hotspot	90
A.1	Composite stratigraphic section for Site 1138	105
A.2	Composite stratigraphic section for Site 1140	107
A.3	Zijderveld-diagrams of sediments from Site 1138	108
A.4	Inclination data for sediments from Site 1138 and polarities.	109
A.5	Zijderveld-diagrams of sediments from Site 1140	111
A.6	IRM analysis of sediment samples of Site 1138 and 1140	112
A.7	Hysteresis curves of sediments of Sites 1138 and 1140	113
A.8	Thermomagnetic curves for sedimentes of Sites 1138 and 1140	114
B.1	Magnetozones in sediments of Site 1138	117

List of Tables

2.1	Leg 183 drilling summary	33
3.1	Paleodirectional results from the southern Kerguelen Plateau - Site 1136 . .	37
3.2	Paleodirectional results from the central Kerguelen Plateau - Site 1138 . .	43
3.3	Angular deviation and mean inclination values for Site 1138	45
3.4	Paleodirectional results from the northern Kerguelen Plateau - Site 1140 . .	50
3.5	Paleodirectional results from the Broken Ridge - Site 1142	53
3.6	Previous paleomagnetic investigations on products of the Kerguelen hotspot	54
5.1	Standard values for model parameters	68

Parts of this thesis are based on (or directly taken from) papers published or to be published in scientific journals. These papers are listed in the following:

Frey, F. A., M. F. Coffin, M. F., P. J. Wallace, D. Weis, X. Zhao, S. W. Wise, V. Wähnert, D. A. H. Teagle, P. J. Saccocia, D. N. Reusch, M. S. Pringle, K. E. Nicolaysen, C. R. Neal, R. D. Müller, C. L. Moore, J. J. Mahoney, L. Keszthelyi, H. Inokuchi, R. A. Duncan, H. Delius, J. E. Damuth, D. Damasceno, H. K. Coxall, M. K. Borre, F. Boehm, J. Barling, N. T. Arndt and M. Antretter, Origin and evolution of a submarine large igneous province: the Kerguelen Plateau and Broken Ridge, southern Indian Ocean, *Earth Planet. Sci. Lett.*, 176, 73–89, 2000.

Antretter, M., B. Steinberger, F. Heider and H. Soffel, Paleolatitudes of the Kerguelen Hotspot: new paleomagnetic results and dynamic modeling, *Earth Planet. Sci. Lett.*, submitted.

Antretter, M., H. Inokuchi and X. Zhao, Rock magnetic and paleomagnetic study on sediments from Sites 1138 and 1140, ODP Leg 183, Kerguelen Plateau *Scientific results ODP Leg 183*, submitted.

Antretter, M., F. Böhm, H. K. Coxall, H. Inokuchi, D. Lazarus, V. Liebetrau, M.-R. Petrizzio, P. G. Quilty and S. W. Wise: Integrated bio-, magneto- and Sr-isotope stratigraphy of Site 1138 (Central Kerguelen Plateau), *Scientific results ODP Leg 183*, submitted.

Glossary

The following abbreviations have been used in this thesis:

LIP	Large Igneous Province
ODP	Ocean Drilling Program
NRM	natural remanent magnetization
TRM	thermal remanent magnetization
ChRM	characteristic remanent magnetization
IRM	isothermal remanence magnetization
TPW	true polar wander
VFTB	Variable Field Translation Balance
KP	Kerguelen Plateau
SKP	southern Kerguelen Plateau
CKP	central Kerguelen Plateau
NKP	northern Kerguelen Plateau
OJP	Ontong Java Plateau

Zusammenfassung

Die Annahme, daß stationäre Hotspots unter den Lithosphärenplatten der Erde existieren, war äußerst wichtig für die Erforschung der Plattentektonik. Die Hypothese ortsfester Hotspots führt zu dem Schluß, daß Seamount Ketten geformt werden, wobei der Vulkanismus die Lithosphärenplatten durchdringt während sich diese über *Heiße Punkte* (Hotspots) von aufsteigendem Erdmantel schieben. Die Alterszunahme der Seamounts sowie deren Position kann dann verwendet werden um Plattenbewegungen in einem unabhängigen Hotspot-Referenzsystem zu rekonstruieren. Bei ortsfesten Hotspots bleibt außerdem die Richtung der charakteristischen remanenten Magnetisierung, die die Basalte beim Abkühlen erwerben, immer die gleiche. Auch wenn sich aufgrund der Plattenbewegung die Produkte eines Hotspots weit weg von seiner ursprünglichen geographischen Lage befinden, so müssen paläomagnetische Untersuchungen an den Basalten immer die Paläobreite des Hotspots ergeben. In jüngerer Zeit aber kam die Frage auf, warum sich ein Hotspot, der seinen Ursprung tief im Erdmantel hat, nicht im konvektierenden Mantel mitbewegt. In dieser Arbeit ist eine mögliche Bewegung des Kerguelen Hotspots im südlichen indischen Ozean und des Louisville Hotspots im Pazifik untersucht worden.

Der Kerguelen Hotspot ist seit ungefähr 117 Ma aktiv. Durch diesen Hotspot wurden seitdem das Kerguelen Plateau und Broken Ridge im südlichen indischen Ozean sowie das Ninetyeast Ridge gebildet, das sich als seine Hotspot Spur bis Indien nach Norden zieht. Auch die Ramajal Traps in Indien werden dem Kerguelen Hotspot zugeschrieben. Broken Ridge und das Kerguelen Plateau waren Ziel von Leg 183 im Ocean Drilling Program. Sie wurden von Dezember 1998 bis Februar 1999 von dessen Bohrschiff, der JOIDES Resolution, beprobt. Acht Bohrungen sind abgeteuft worden. In sieben der Bohrungen wurden zusätzlich zu den Basalten auch die darüberliegenden Sedimente gekernt.

In dieser Arbeit wird eine mögliche Bewegung des Kerguelen Hotspots anhand seiner Paläobreiten diskutiert. Zuerst wurden die Basalte vom Kerguelen Plateau paläomagnetisch untersucht, um die Paläobreiten des Plateaus mit der Breitenlage des Hotspots vergleichen zu können. Die Basalte von einer Bohrung im Zentralen Kerguelen Plateau (Site 1138) sowie die einer Bohrung am Nördlichen Kerguelen Plateau (Site 1140) eigneten sich zur Bestimmung ihrer Paläobreiten. Dort wurden eine ausreichende Anzahl unabhängiger Lavaflüsse durchteuft, um die Paläosäkularvariation erfolgreich herausmitteln zu können. Die charakteristische Magnetisierung sowohl des subaerisch entstandenen Sites 1138 als auch des submarinen Sites 1140 wird von Magnetit und Titanomagnetiten und -maghemiten getragen und zeigt nur eine einzige stabile Magnetisierungskomponente. Eine teilweise vorhandene, sehr schwache viskose Überprägung

konnte beim Entmagnetisieren im Labor leicht entfernt werden. Durch schrittweises Abmagnetisieren im Wechselfeld und durch schrittweises thermisches Abmagnetisieren der Proben wurde die charakteristische Inklination der Magnetisierung sehr genau bestimmt. Aus den mittleren Inklinationen eines Sites ergaben sich eine Paläobreite von $\lambda = 43.6^\circ\text{S}$ (max.: 47.8°S ; min.: 37.9°S) für Site 1138 am Zentralen Kerguelen Plateau sowie eine Paläobreite $\lambda = 35.8^\circ\text{S}$ (max: 43.0°S ; min.: 28.9°S) für Site 1140 am Nördlichen Kerguelen Plateau. In Site 1136 am Südlichen Kerguelen Plateau wurden nur 2 Lavaflüsse durchteuft, und die Paläosäkularvariation konnte dadurch nicht ausreichend herausgemittelt werden. Aus seismischen Vorerkundungen des Gebietes ergab sich, daß Site 1142 am Broken Ridge nach seiner Entstehung tektonisch gekippt worden ist, und die Inklination der Magnetisierung konnte daher nicht zur Paläobreitenbestimmung verwendet werden. Verglichen mit der Breitenlage des Kerguelen Hotspots bei 49°S liegen die Paläobreiten vom Zentralen und Nördlichen Kerguelen Plateau weiter nördlich. Dieses Ergebnis stimmt mit früheren paläomagnetischen Arbeiten vom Südlichen Kerguelen Plateau und vom Ninetyeast Ridge überein. Auch dort ergaben sich Paläobreiten, die auf eine Entstehung nördlich der heutigen Hotspotlage deuten. Diese Differenz weist auf eine Südwärtsdrift des Hotspots seit der Kreidezeit relativ zur Rotationsachse der Erde hin. Die Bewegung kann prinzipiell durch die Verschiebung des gesamten Erdmantels relativ zur Spinachse (True Polar Wander) oder durch eine Bewegung des Hotspots im Erdmantel erklärt werden.

Als nächstes wurde daher die Möglichkeit untersucht, daß True Polar Wander für die Differenz zwischen paläomagnetischen Daten und Breitenlage des Hotspots verantwortlich ist. Drei unabhängig voneinander bestimmte True Polar Wander Kurven, die eine Bewegung des gesamten Erdmantels (mit den Hotspots) gegen die Rotationsachse (bzw. magnetische Achse) der Erde aufzeichnen, wurden dafür verwendet. Alle drei Kurven weisen darauf hin, daß zur Zeit der Entstehung des Zentralen und Südlichen Kerguelen Plateaus der Erdmantel so verschoben war, daß die paläomagnetischen Untersuchungen südlichere Paläobreiten ergeben müssten - also im Gegensatz zu den wirklichen Ergebnissen. Der känozoische Teil der drei experimentell bestimmten True Polar Wander Kurven stimmen innerhalb ihrer Fehler ungefähr mit einer numerisch berechneten Kurve überein, welche Änderungen der Trägheitsmomente der Erde berücksichtigt. Daraus folgt, daß der Unterschied zwischen den paläomagnetischen Daten und der Lage des Hotspots unter Berücksichtigung von True Polar Wander nicht erklärt werden kann, sondern sogar noch vergrößert wird. Daher wurde als nächstes die Möglichkeit von Hotspotbewegung untersucht.

Zur Bestimmung der Hotspotdrift sind geodynamische Modellrechnungen durchgeführt worden. Dabei nimmt man an, daß ein von der Kern-Mantel Grenze aufsteigender

Mantelplume im konvektierenden Mantel mitgezogen wird, was sich an der Erdoberfläche als Verschiebung des Hotspots auswirkt. Dafür wurden seismische Tomographie-Modelle in Dichtemodelle für den Erdmantel konvertiert. Daraus wiederum wurde ein Geschwindigkeitsfeld, das aufgrund der ausgleichenden Massenbewegungen zwischen den Dichteheterogenitäten entsteht, für den konvektierenden Mantel berechnet. Ein aufsteigender Mantelplume wird dann in diesem Geschwindigkeitsfeld abdriften. Sieben verschiedene tomographische Modelle wurden zur Berechnung von Geschwindigkeitsfeldern verwendet. Alle sieben Modelle ergeben eine Südwärtsbewegung des Kerguelen Hotspot seit seinem ersten Auftreten vor ungefähr 117 Ma. Die Bewegung hat für die verschiedenen Modelle die ähnliche Richtung und liegt zwischen 5 und 10 Grad.

Das Programm zur Modellierung der Hotspotbewegung nahm bisher eine konstante Viskosität im aufsteigendem Plume an. Realistischer ist die Annahme eines tiefenabhängigen Plumeradius, basierend auf Abschätzungen von Temperatur- und daher Viskositätsänderungen innerhalb des Plumes. Dies wurde als Subroutine in das Programm integriert. Der Plumeradius wirkt sich auf das Aufsteigen des Plumes aus. Ein Plume mit größerem Radius steigt schneller durch den Mantel, und wird daher eine stärkere Tendenz zu geradelinigem Auftrieb haben. Ein Plume mit kleinem Radius steigt dagegen langsamer auf und wird stärker vom Geschwindigkeitsfeld des Mantels beeinflusst. Unter Berücksichtigung der Viskositätsänderungen in den aufsteigenden Plumes sind die Hotspotbewegungen neu berechnet worden. Diese neuen Ergebnisse und eine Gegenüberstellung der resultierenden Hotspotbewegungen bei veränderten Eingabeparametern zeigen, daß die Berechnungen von den einzelnen Parametern relativ unabhängig ist. Nach wie vor weisen die Modellierungen auf eine Südwärtsbewegung zwischen 5 und 10 Grad hin, nur der Verlauf der Hotspotspur verändert sich leicht.

Die Südwärtsbewegung von 5 bis 10 Grad, die in den Modellierungen für den Kerguelen Hotspot gefunden wurde, kann die Differenz zwischen den paläomagnetischen Paläobreiten und der heutigen Hotspotlage erklären. Sogar die Kombination mit True Polar Wander, welche diese Differenz sogar noch vergrößert, ist bei einer Hotspotbewegung dieser Größenordnung erlaubt. Die Übereinstimmung der paläomagnetischen Ergebnisse (zumindest innerhalb ihrer Fehlergrenzen) mit den Modellierungen ist ein deutlicher Hinweis auf die Gültigkeit der Modellrechnungen, und läßt den Schluß zu, daß sich der Kerguelen Hotspot seit seinem ersten Auftreten vor 117 Ma tatsächlich um einige Grad südwärts bewegt hat.

Eine Magnetostratigraphie, die aus den Sedimenten der Bohrlokationen von ODP Leg 183 angefertigt wurde, hat einen Beitrag zur möglichst exakten Altersdatierung der Basalte geliefert. Paläomagnetische Untersuchungen an den Sedimenten von Leg

183 haben zur Erstellung einer kombinierten Bio/Magnetostratigraphie beigetragen. Die Stratigraphie hilft, das Minimalalter der darunterliegenden Basalte zu bestimmen. Anhand der gefundenen Reversals in der Magnetisierung und der Korrelation mit den paläontologischen Ergebnissen wurden für die tiefstliegenden Sedimente von Site 1136 (Südliches Kerguelen Plateau) ein Alter in der frühen Kreide, von Site 1138 (Zentrales Kerguelen Plateau) ein Alter der späten Kreide gefunden. Die ältesten Sedimente von Site 1140 (Nördliches Kerguelen Plateau) haben wir dem frühen Oligozän zugeordnet. Diese Ergebnisse sind nun auch durch genaue $^{40}\text{Ar}/^{39}\text{Ar}$ -Altersdatierungen der Basalte bestätigt worden, welche für Site 1138 ein Alter von 100 Ma und für Site 1140 von 35 Ma ergaben.

Das Ontong Java Plateau, eine große Eruptivprovinz im westlichen Pazifik, ist wahrscheinlich ebenfalls von einem aufsteigendem Mantelplume in der Anfangsphase eines Hotspots geformt worden. Nach einer neuen Plattenrekonstruktion ist das Plateau jedoch nördlich von der heutigen Lage des Louisville Hotspots gebildet worden, welchem das Plateau bisher zugeschrieben wurde. In dieser Arbeit wird gezeigt, daß eine Bildung des Plateaus durch den Louisville Hotspot möglich wäre, wenn man annimmt, daß dieser sich in einem konvektierenden Erdmantel bewegt. Mit Hilfe der Methoden, die bereits für den Kerguelen Hotspot angewandt wurden, ist die Bewegung des Louisville Hotspots für die letzten 120 Millionen Jahre modelliert worden. Die Modellrechnungen zeigen, daß sich der Hotspot seit seinem ersten Auftreten vor ungefähr 120 Ma wahrscheinlich um mehrere Grad nach Süden verschoben hat. Jedoch gibt es erhebliche Unterschiede zwischen den Modellergebnissen, die aus den unterschiedlichen Dichtemodellen des Mantels resultieren. Da der Louisville Hotspot für die Bildung des Plateaus jetzt zu weit südlich liegt, könnte er unter Berücksichtigung einer Südwärtsbewegung vor 120 Ma passend positioniert gewesen sein. Am Beispiel der Bewegung des Louisville Hotspots wird gezeigt, daß die Drift von Hotspots Auswirkungen auf Plattentektonik und tektonische Rekonstruktionen haben kann und berücksichtigt werden sollte.

Summary

The assumption that stationary hotspots underlie the Earth's lithospheric plates has been most important in the development of the theory of plate tectonics. According to the fixed hotspot hypothesis seamount trails are formed by volcanism penetrating the lithospheric plates whilst moving over "hotspots" of upwelling mantle. In turn, the azimuths and age progressions of seamount trails can be used to quantify plate motions with respect to an independent reference frame of hotspots in the mantle. Also, assuming fixed hotspots, the direction of characteristic remanent magnetization in the basalts acquired during cooling should always be the same. Even if due to plate motion the products of the hotspot are located far away from the position of the hotspot itself, paleomagnetic studies on the basalts must always provide the position of the hotspot itself. Recently the question arose, why a hotspot with its origin deep in the mantle would not get advected in the convecting mantle of the Earth. - In this thesis a possible motion of the Kerguelen hotspot in the southern Indian Ocean and of the Louisville hotspot in the Pacific has been studied.

The Kerguelen hotspot is active since approximately 117 Ma. Since then it formed the Kerguelen Plateau and the Broken Ridge in the southern Indian Ocean as well as the Ninetyeast Ridge, which is the hotspot track going north up to India, and the Ramajal Traps in India. Drilling into basement rocks of Broken Ridge and the Kerguelen Plateau was aim of the Ocean Drilling Program, Leg 183, from December 1998 to February 1999. Eight sites have been drilled. In seven of the sites also the sediments have been recovered.

In this thesis, a possible motion of the Kerguelen hotspot has been studied by determining its paleolatitudes. First, basalts from the Kerguelen Plateau have been studied paleomagnetically to compare the paleolatitudes with the latitude of the hotspot itself. Basement from a drillsite on the central Kerguelen Plateau (Site 1138) and of a site on the northern Kerguelen Plateau (Site 1140) were suitable for a determination of paleolatitudes. A sufficient number of independent lavafloes has been penetrated and sampled there to properly average out paleosecular variation, an important requirement for determining paleolatitudes. The characteristic magnetization from the subaerial Site 1138 with AA- and Pahoehoe lava and of the submarine Site 1140 with its pillow basalts is carried by magnetite and titanomagnetites and -maghemites and consists of a single remanence component with sometimes a small viscous overprint, that could easily be removed during demagnetization. Stepwise demagnetization in an alternating field and stepwise heating of the specimens provided the inclination value of the characteristic magnetization very precisely with small error. Conversion of the mean-site inclination into the paleolatitude of a site provided a latitude of $\lambda = 43.6^\circ\text{S}$ (max.: 47.8°S ; min.: 37.9°S) for Site 1138 on the central Kerguelen Plateau and a latitude of $\lambda = 35.8^\circ\text{S}$ (max.: 43.0°S ; min.: 28.9°S) for Site 1140 on the northern Kerguelen Plateau. In Site 1136

on the southern Kerguelen Plateau only two lava flows have been sampled. Therefore paleosecular variation could not be averaged out properly. Site 1142 on the Broken Ridge has been tilted and deformed tectonically after its formation, as was found from seismic explorations prior to drilling, and the inclination of the magnetization could therefore not be used for a determination of paleolatitudes. Compared to the latitude of the Kerguelen hotspot at 49°S, the paleolatitudes of the central and northern Kerguelen Plateau are further north. This result agrees with previous paleomagnetic studies on the southern Kerguelen Plateau and the Ninetyeast Ridge, where paleolatitudes have been found that indicate also a formation north of the present-day hotspot position. This difference indicates a southward movement of the hotspot since the Cretaceous relative to the spin axis of the Earth. The motion can be explained with a rotation of the whole mantle of the Earth relative to the spin axis (true polar wander) or with a motion of the hotspot within the Earth's mantle.

Therefore, the possibility was studied whether true polar wander can be responsible for the difference between the paleomagnetic data and the present-day latitude of the hotspot. Three independently obtained true polar wander paths have been used, that describe the motion of the whole mantle (with the hotspots) relative to the rotation or dipole axis. All three curves point to a shift of the mantle at the time when the central and southern Kerguelen Plateau formed in such a way that higher southern paleolatitudes should be observed. This prediction is just the opposite to what was found in the paleomagnetic studies. The Cenozoic parts of the three experimentally obtained true polar wander paths roughly agree within their uncertainties with a numerically calculated path that accounts for changes of moments of inertia of the mantle. This means that the difference between paleomagnetic data and the present-day position of the hotspot can not be explained by true polar wander. The next starting point to explain the discrepancy is hotspot motion.

For the determination of hotspot drift, geodynamic modeling has been carried out. Assuming that a mantle plume rising from the core-mantle boundary is advected in a convecting mantle, a hotspot could move relative to the surface of the Earth. Seismic tomography models were converted into density models of the Earth's mantle. Then a velocity field derived from the mass motion due to the density heterogeneities is calculated. The rising mantle plume is then inserted into the model and becomes advected in the velocity field. Seven different tomographic models have been used to obtain velocity fields. All seven models result in a southward motion for the Kerguelen hotspot since its first appearance approximately 117 Ma ago. The motion is in a similar direction for the different models, and its magnitude varies from 5 to over 10 degrees.

So far, the program to model the hotspot drift assumed a constant viscosity within the rising plume. More realistic is the assumption of a depth-dependent plume radius, based on estimates of temperature- and hence viscosity variations within the plume. This has been integrated as a subroutine into the program. The plume radius affects the buoyancy of the plume. A plume with larger radius rises faster through the mantle, and will hence have a stronger tendency to straighten up. In contrast, a plume with smaller radius rises slowly and will be influenced more strongly by the velocity field of the mantle. Allowing for the variation of viscosity within the plume, the hotspot motion was calculated again. A comparison of the resulting hotspot motion for various input parameters showed that the result is rather independent of the parameters. The calculations also yield a southward motion of 5 to 10 degrees, only the shape of the hotspot path is somewhat changed.

This southward motion of the Kerguelen hotspot by 5 to 10 degrees can explain the difference between the paleomagnetic data and the present-day position of the hotspot. Even combined with true polar wander it fits the paleomagnetic results, although true polar wander, taken by itself, even increases the difference that has to be explained. The consistency of paleomagnetic results with the model calculations allows the conclusion that the Kerguelen hotspot indeed moved southward by some degrees since its first occurrence 117 Ma ago.

A magnetostratigraphy has been made using the sediments of ODP Leg 183. It yielded a contribution to the age dating of the basalts prior to $^{40}\text{Ar}/^{39}\text{Ar}$ dating. Paleomagnetic studies on the sediments contributed to a combined Bio/Magnetostratigraphy. The stratigraphy helps to determine the minimal age of the underlying basalts. Using the reversals found in the magnetization and a correlation with the paleontological data, the lowermost sediments of Site 1136 (southern Kerguelen Plateau) are dated to have an age in the Early Cretaceous, Site 1138 (central Kerguelen Plateau) in the Late Cretaceous, and Site 1140 (northern Kerguelen Plateau) in the Oligocene. These results are meanwhile confirmed by precise $^{40}\text{Ar}/^{39}\text{Ar}$ age dating of the basement yielding an age of 100 Ma for Site 1138 and of 35 Ma for Site 1140.

The Ontong Java Plateau, a Large Igneous Province in the western Pacific, was thought to be formed by the rising mantle plume of the Louisville hotspot approximately 120 Ma ago. However, according to a recent plate reconstruction, the plateau has been formed well to the north of the location of this hotspot. In this thesis it could be shown that the formation of the Ontong Java Plateau by the Louisville hotspot is possible if hotspot motion in the convecting mantle is allowed. For this purpose, the motion of the Louisville hotspot for the last 120 Ma years has been modeled, using the same method as already

applied for the Kerguelen hotspot. The calculations indicate, that the Louisville hotspot has probably shifted by some degrees to the south since its first occurrence approximately 120 Ma ago. There is a considerable variation between different model results, though. The Louisville hotspot is now located too far south to be responsible for the formation of the Plateau. However, it could have been in the right place at the time of the formation 120 Ma ago if hotspot motion is considered. This is an example that the drift of hotspots can affect plate tectonics and tectonic reconstructions and that it should be considered.

Chapter 1

Introduction

Yves Joseph de Kerguelen-Trémarac discovered La France Australe (today's Kerguelen chain in the Indian Ocean just north of Antarctica) in 1772, and in the same year claimed this "southern motherland" for France. Upon returning home, his eloquent rhapsodizing to the reigning French monarch about Kerguelen's superb agricultural and mineral potential resulted in the king dispatching three ships and 700 men to colonize Kerguelen in 1773. However, once there, 699 pairs of eyes couldn't lie. They saw only the tiny volcanic islands but no massive continent as Kerguelen had claimed. Indeed, they had no way of knowing then that the volcanic islands they saw were the tips of a small continent (the Kerguelen Plateau) which lay submerged about two kilometers below the ocean surface. Upon Kerguelen's second homecoming to France, he was court-martialed, sentenced to 20 years in prison, and dismissed from the Navy for exaggerating his findings.

In contrast, James Cook dubbed Kerguelen the "Isles of Desolation" after landing there in 1776. This may have been closer to the mark, for geologically, the Kerguelen Plateau is a massive, enigmatic, mafic, and heavily-structured large igneous province (LIP). From Coffin [1998].

Large Igneous Provinces and hotspots Large igneous provinces are a significant type of planetary volcanism found on Earth, the moon, Venus, and Mars. They represent large volumes of magma emplaced over relatively short time periods, such as expected from decompression of upwelling, relatively hot or wet mantle [Coffin and Eldholm, 1994]. This process explains hotspot magmatism at the Earth's surface and is conceptually described by various plume head and tail models applicable to the Earth's sublithospheric mantle [e.g. Richards *et al.*, 1989]. In such models, the plume head leads to oceanic plateaus and continental flood basalts, and the tail leads to volcanic chains known as hotspot tracks. These volcanic islands chains show a progressive increase in age in the direction of plate motion and seem to be tracks originating from localized hotspots

fixed in the mantle. The most famous among the hotspot tracks is the Hawai'ian - Emperor Seamount chain in the Pacific Ocean. In the Indian Ocean, the largest of these volcanic features is the Ninetyeast Ridge, the hotspot chain that has been formed by the Kerguelen hotspot, as well as the Kerguelen Plateau - Broken Ridge, which is the associated Large Igneous Province (chapter 2).

"Fixed hotspots gone with the wind" *Wilson* [1965] was the first to recognize that certain chains of volcanic islands such as Hawai'i show a progressive increase in age in the direction of plate motion and seem to be tracks originating from localized hotspots in the mantle beneath the plate. *Morgan* [1971] recognized that the various hotspot tracks on the Pacific plate can be explained by assuming that the hotspots are fixed relative to one another. He introduced the concept of deeply anchored mantle plumes. Hotspots are commonly seen as fixed points to which absolute plate motion can be referred and are used as a reference frame for plate reconstructions.

However, a direct test of moving hotspots has been made by *Molnar and Stock* [1987]. They show results of a detailed comparison between the tracks of Hawai'i and hotspots in other oceans with their predicted tracks, calculated using the fixity assumption and relative plate motions. They found systematic displacements between Hawai'i and the other hotspots (Iceland and Tristan de Cunha in the Atlantic; Reunion, St Paul's and Kerguelen in the Indian Ocean). The results indicate a southward drift of the Hawai'ian hotspot, consistent with paleomagnetic results of *Sager and Bleil* [1987] and *Tarduno and Cottrell* [1997]. These paleomagnetic studies gave paleolatitudes from the Pacific generally and the Hawai'ian seamounts specifically, that are too far north for the present-day position of the hotspot and hence indicate a southward motion.

Aim of this thesis is to answer the question about fixity or motion of the Kerguelen hotspot in the southern Indian Ocean and the Louisville hotspot in the Pacific: new paleomagnetically obtained paleolatitudes for the Kerguelen hotspot will be compared to its present-day latitude (chapter 3). The effect of true polar wander on the paleolatitudes will be discussed (chapter 4 and chapter 6) and the drift of the hotspots in the convecting mantle will be modeled (chapter 5 and chapter 6).

Sampling the Kerguelen Plateau - Broken Ridge: ODP Leg 183 Despite the huge size of some oceanic plateaus and their potential role in contributing to our understanding of Cretaceous mantle circulation and environmental change, they are among the least understood features in the ocean basins. The Kerguelen Plateau and Broken Ridge, an oceanic plateau that has been separated from Kerguelen Plateau in the

Early Tertiary and is now located 1600 km north of the Kerguelen Plateau, were formed by the mantle plume of the Kerguelen hotspot. The igneous crust of the Kerguelen Plateau and Broken Ridge have been sampled by dredging and drilling. In particular, Leg 183 (December 98 to February 99) of the Ocean Drilling Program focused on the development of this Large Igneous Province in time and space by drilling and coring five holes into igneous crust of the Kerguelen Plateau and two into Broken Ridge (chapter 2). The Ocean Drilling Program (ODP) is an international partnership of scientists and research institutions organized to explore the evolution and structure of the Earth. The *JOIDES Resolution* is the drill and research vessel of ODP, equipped with shipboard laboratories that include a fully equipped paleomagnetic laboratory. During Leg 183 the *JOIDES Resolution* was on her way from Freemantle (Australia) to the southern Indian Ocean and back to Freemantle with the aim of drilling into the basement of the Kerguelen Plateau. Six sites consisting of one hole each have been drilled on the Kerguelen Plateau (Sites 1135 - 1140) and two on Broken Ridge (Sites 1141 and 1142). The total penetration (including the overlying sedimentary section and the basement) ranges from 142 m in Site 1142 to 843 m in Site 1138.

Paleomagnetic studies on rock material from the Kerguelen Plateau All cores recovered on ODP cruises get split into two halves: an archive and a working half. Paleomagnetic measurements have been conducted during Leg 183 on the archive halfcores in the shipboard laboratory as well as on discrete samples taken from the working halves upon return to Munich. Two paleomagnetists joined the scientific party of Leg 183 (Hiroo Inokuchi, Kobe University and Maria Antretter, LMU München) and have been responsible for shipboard as well as for onshore paleomagnetic studies. The eight drilled sites have been divided into even and odd numbered sites for onshore studies. In this work the results of the even numbered sites will be presented.

In three of the sites studied, sediments as well as basement rocks have been cored. From the last site that has been drilled during Leg 183, Site 1142 on the Broken Ridge, sediments have been washed out and only basement has been recovered. According to the lithologic division into sediments and basement, the paleomagnetic work on the samples can be separated into two main subjects:

(1) Studies of the sedimentary sections (Appendix A): Demagnetization of the archive halves and of discrete samples provide a determination of the inclination of the characteristic remanence. Because of the relatively high southerly latitude of the investigated sites, the inclinations provide a clear information about magnetic polarities. The magnetic polarities, combined with biostratigraphic data, result in a bio-magnetostratigraphy, which is used for age estimations of the different lithological units. It was also used to get a minimal age of the underlying basement before the onshore $^{40}\text{Ar}/^{39}\text{Ar}$ age dating. Correlation

of age-dated stratigraphy with drilling depth provides information about sedimentation rates.

(2) Studies of the basement sections (chapter 3): Major aim is the determination of the paleolatitudes for different parts of the Kerguelen plateau. Thermal and alternating field demagnetization of discrete basalt samples provide inclinations of the characteristic remanent magnetization, which can then be converted into paleolatitudes. An assumption in paleomagnetic studies is the axial geocentric dipole hypothesis. Only if this hypothesis holds, determination of paleolatitudes is possible. However, the axial geocentric dipole takes no account of secular variation, although its effect must be averaged out before paleomagnetic measurements are said to conform with the model. One of the major risks when determining paleolatitudes, especially when dealing with older rocks, is that only part of the secular variation record will be retrieved. This will cause an artificial underestimation of the secular variation. It is, therefore, very important to sample a sufficient number of time-independent lava units. Tectonic tilting of the basement units would bias the inclination registered in the basalts and must be excluded when determining paleolatitudes. Seismic investigations of the areas that include the drilled sites have been conducted prior to Leg 183. They provide information about tilting and deformation of the seafloor and, hence, about reliability of the inclination data obtained from the basement.

Test for hotspot motion from paleolatitudes It was commonly thought that the Kerguelen hotspot and all the other hotspots on the Earth were stationary. They have therefore been used as a reference frame for plate tectonic reconstructions. However, several recent studies put this hypothesis under question. There are different ways to control the fixity of hotspots. One of them is to determine the paleolatitudes of the basalts produced by the hotspot. If the hotspot does not move relative to the dipole axis of the geomagnetic field, then the paleolatitudes of all basalts in every time range must be identical with the latitude of the hotspot itself. If the paleolatitudes differ from the hotspot's latitude, then the hotspot must have moved after producing the sampled basalts.

There have been several previous paleomagnetic studies on products of the Kerguelen hotspot [*Klootwijk*, 1971; *Klootwijk et al.*, 1991; *Inokuchi and Heider*, 1992; *Henry and Plessard*, 1997]. They provide paleolatitudes for the Kerguelen Island, the southern Kerguelen Plateau and the Ninetyeast Ridge (the seamount chain produced by the Kerguelen hotspot during the fast northward drift of the Indian plate). Together with the paleolatitudes obtained from ODP Leg 183 they can be used to test the question about hotspot motion: if the paleolatitudes correspond to the present-day position of the hotspot, no hotspot motion seems to have occurred since its formation. If they differ,

hotspot motion might have occurred.

Besides hotspot motion, also "true polar wander" can cause changes in hotspot paleolatitudes:

True polar wander True polar wander is generally understood as the drift of the rotation pole of the Earth relative to the Earth's mantle (or some reference frame fixed in the Earth). True polar wander changes the position of the Earth's mantle (with the hotspots) relative to the rotation axis (which is an averaged dipole axis, according to the axial geocentric dipole hypothesis). In this way, true polar wander is able to affect the paleolatitudes of hotspots. Several attempts have been made to determine the amount of true polar wander with time and true polar wander curves have been generated. Three recent determinations of true polar wander by *Besse and Courtillot* [1991], *Besse* [2000] and *Prévoit et al.* [2000] have been used in this thesis to determine the influence on the paleolatitudes of the Kerguelen hotspot (chapter 4) and of the Louisville hotspot (chapter 6).

Modeling of hotspot motion Mantle plumes are upwelling structures of relatively hot or wet mantle that originate probably at the core-mantle boundary and rise through the mantle to the Earth's surface forming large igneous provinces and hotspot chains. Mantle plumes have been thought to be fixed in the mantle and have been used as a reference frame for plate motions.

On the contrary, mantle flow calculations based on velocity models derived from seismic tomography imply that much of the return convective flow that balances plate motion occurs in the lower mantle of the Earth [*Hager and O'Connell*, 1979, 1981]. This lower mantle can therefore not be the immobile basic layer through which fixed plumes rise. *Steinberger and O'Connell* [1998] calculated a global mantle-circulation model for the past, using buoyancy forces inferred from tomographic anomalies and taking the present and past plate motions as boundary conditions. Then, they inserted plume conduits and calculated how these conduits are advected by the mantle when rising from the core-mantle boundary up to the Earth's surface. In this thesis, their concept will be extended and applied to calculate the motion of the Kerguelen hotspot (chapter 5) and the Louisville hotspot (chapter 6).

In this simplified model, the rising mantle conduit of the hotspots is horizontally advected in large-scale mantle flow and the conduit elements rise buoyantly through the surrounding viscous mantle. The method of *Hager and O'Connell* [1979, 1981] is used to calculate the large-scale mantle flow field in a spherical shell. Several tomographic models have been used to compute mantle flow fields, and the advection of the rising Kerguelen plume has been calculated for each of these flow fields.

A comparison of paleolatitudes for the Kerguelen hotspot summarizes the paleomagnetic results, the effect of true polar wander, the effect of hotspot motion and the combination of true polar wander and hotspot motion.

The Ontong Java Plateau - the Louisville hotspot The Ontong Java Plateau is a Cretaceous large igneous province in the western Pacific (chapter 6). It is the largest of the igneous provinces and was thought to be formed by the rising plume head in the initial stage of the Louisville hotspot. However, a recent plate reconstruction [Neal *et al.*, 1997] suggests that the plateau was formed well to the north of this hotspot's current location. Therefore, recently, it was doubted, if the Ontong Java Plateau has in fact been formed by the Louisville hotspot. According to the plate reconstruction, the center of the Ontong Java Plateau at approximately 125 Ma was at approximately 42°S, 159°W and therefore 9° north of the Louisville hotspot. No hotspot is known to exist today in the vicinity of the location of the plateau in the 125 Ma reconstruction at about 42°S.

The effect of hotspot motion could explain the discrepancy between the plate reconstruction's paleolatitude and the Louisville hotspot's latitude. For example, a southward motion of the Louisville hotspot of approximately 10° since 120 Ma ago would allow the formation of the Plateau by the Louisville hotspot. In this thesis, the motion of the Louisville hotspot has been modeled to find out whether it could explain the discrepancy between plate reconstruction and hotspot position.

Chapter 2

The Kerguelen Plateau, a Large Igneous Province

Drilling into basement rocks of the Kerguelen Plateau, a Large Igneous Province in the southern Indian Ocean, and understanding its formation and development was the aim of Leg 183 (December 1998 to February 1999) of the Ocean Drilling Program. This chapter gives a short introduction into the development and significance of Large Igneous Provinces in general and specifically to the formation of the Kerguelen Plateau. It also summarizes some results of previous drilling on the Plateau (Leg 119 and 120) and presents main aspects of Leg 183.

2.1 LIPs and hotspots

Large igneous provinces (LIPs) are a significant type of planetary volcanism found on the Earth, the Moon, Venus, and Mars [*Coffin and Eldholm, 1994*]. Figure 2.1 summarizes the locations of LIPs on Earth, showing continental as well as oceanic flood basalts. LIPs represent large volumes of magma emplaced over relatively short time periods, such as expected from decompression melting of upwelling, relatively hot or wet mantle. This process explains hotspot magmatism at the Earth's surface and is conceptually described by various plume-head and -tail models applicable to the Earth's sublithospheric mantle. In such models, the plume head is responsible for oceanic plateaus and continental flood basalts, whereas the tail leads to volcanic chains known as hotspot tracks. The most famous hotspot track is probably the Hawai'i-Emperor seamount chain, produced by the Hawai'ian hotspot. This type of volcanism differs in style, location and geochemical characteristics from volcanism at divergent plate boundaries (mid-ocean ridge spreading centers) and convergent plate boundaries (arc volcanoes associated with plate subduction). Many LIPs formed during Cretaceous time. The two most voluminous LIPs are Cretaceous oceanic plateaus, Ontong Java in the Pacific Ocean and Kerguelen Plateau/Broken

Ridge in the southern Indian Ocean (Figure 2.1).

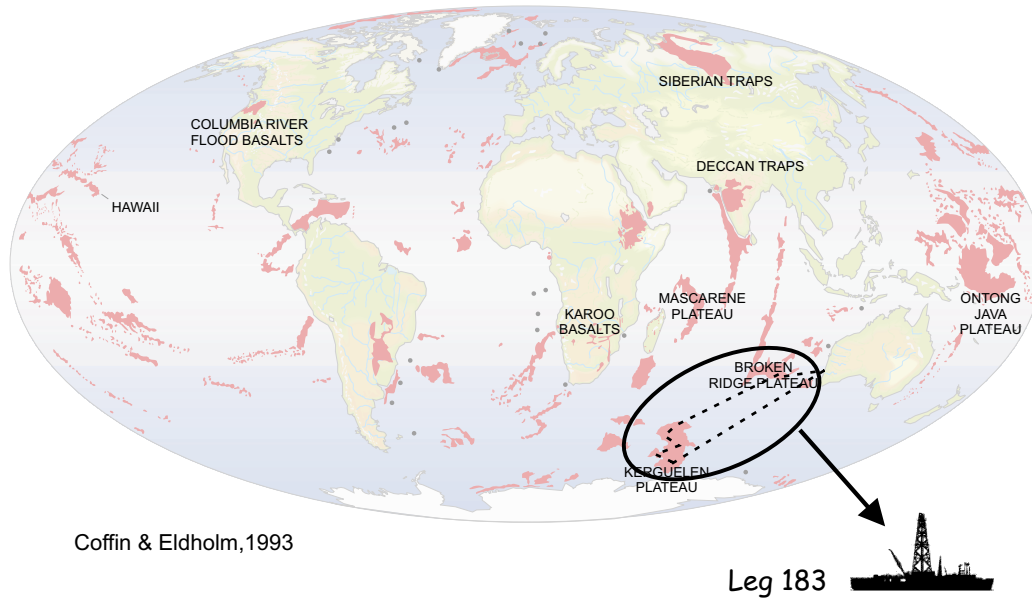


Figure 2.1: Global LIPs, including continental flood basalts and associated intrusive provinces, oceanic plateaus, submarine ridges, ocean basin flood basalts, and seamount groups [Coffin and Eldholm, 1993]. The two most voluminous LIPs are Cretaceous oceanic plateaus, Ontong Java in the Pacific Ocean and Kerguelen Plateau/Broken Ridge in the southern Indian Ocean. ODP Leg 183 (December-February 1998/99) drilled seven basement sites into the Kerguelen/Broken-Ridge Plateau complex.

They cover vast areas ($\sim 2 \cdot 10^6$ km²), stand 2 to 4 km above the surrounding ocean floor and have thick mafic crusts of 20 to 40 km compared to the typical oceanic crustal thickness of 7 km [Larson, 1991; Coffin and Eldholm, 1994]. This intense igneous activity, perhaps reflecting a more vigorous mode of whole mantle convection than the present [Stein and Hofmann, 1994], temporarily increased the flux of material and energy from the mantle to the crust, hydrosphere, biosphere and atmosphere. Possible consequences are global environmental changes involving climate, sea level, oceanic anoxia, seawater composition and biological extinctions.

2.2 Kerguelen Plateau/Broken Ridge: Background

The Kerguelen Plateau is a broad (200 to 600 km wide) bathymetric high in the southern Indian Ocean (Figure 2.1), extending for ~ 2300 km between 46°S and 64°S (Figure 2.2). It is divided into distinct domains: the southern (SKP), central (CKP), and northern Kerguelen Plateau (NKP) and the Elan Bank (Figure 2.2). Multichannel seismic reflection data show numerous dipping intra-basement reflections interpreted as subaerial flood basalts that form the uppermost igneous crust of the Kerguelen Plateau [Coffin et al., 1990; Schaming and Rotstein, 1990]. The entire

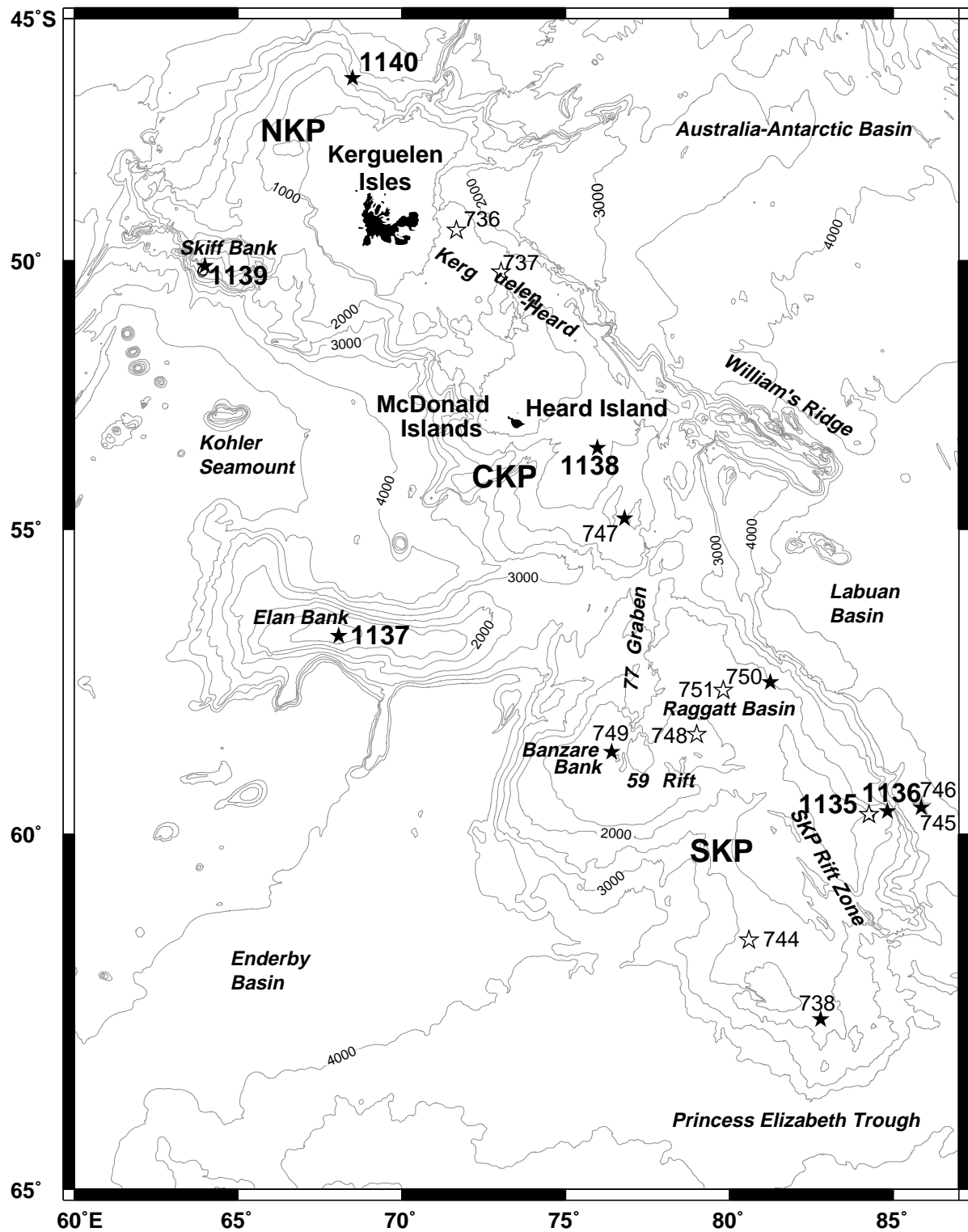


Figure 2.2: Bathymetry of the Kerguelen Plateau. Leg 119, 120 and 183 drill sites that recovered igneous basement are indicated by filled stars. Sites that bottomed in sediment are shown as open stars. Contour interval = 500 m. Paleomagnetic studies on even numbered Sites of Leg 183 (1136, 1138 and 1140) are presented in this thesis.

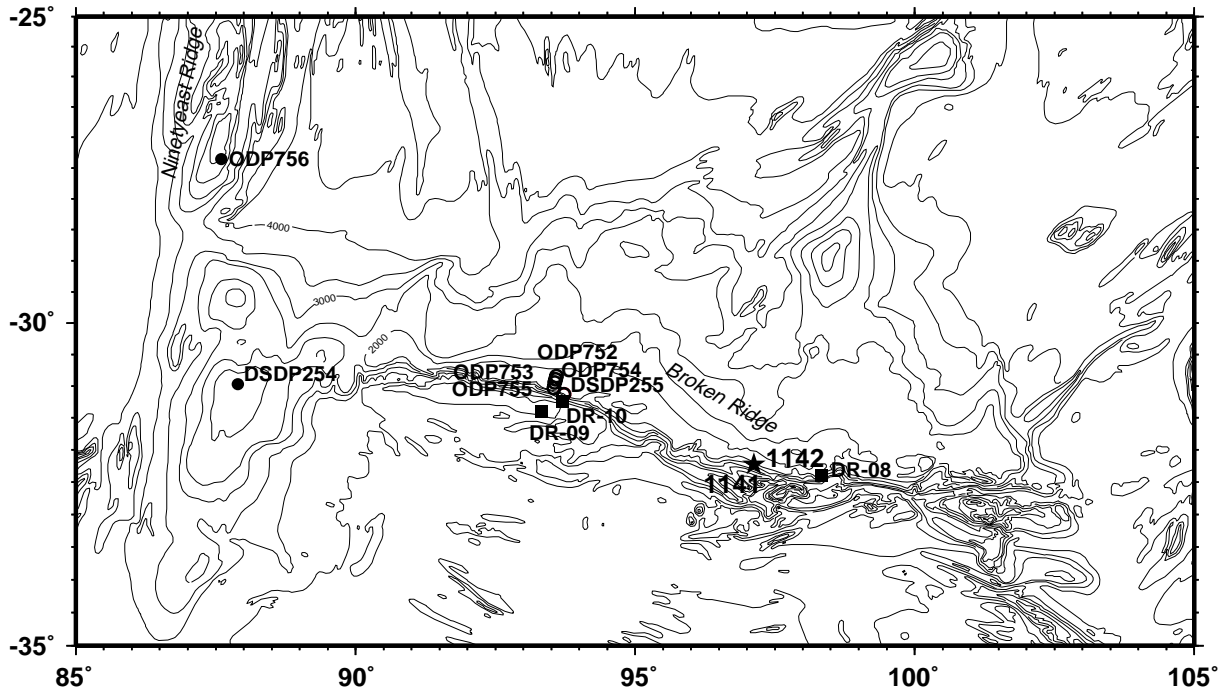


Figure 2.3: Bathymetry of Broken Ridge. Previous DSDP and ODP drill sites that recovered igneous basement are indicated by solid circles. Sites that bottomed in sediment are shown as open circles. Dredge locations that recovered igneous basement are indicated by solid squares. Leg 183 Sites 1141 and 1142 are indicated by a star. Paleomagnetic studies on Site 1142 of Leg 183 are presented in this thesis.

igneous crust of the Plateau is 19 to 22 km thick [Coffin *et al.*, 1986; Rotstein *et al.*, 1992].

The southern Kerguelen Plateau lies at water depths of 1.5 to 2 km. The central Kerguelen Plateau with water depths similar to the southern Kerguelen Plateau includes the volcanically active Heard and McDonald Islands. The central Kerguelen Plateau and Broken Ridge formed as a single entity; subsequently, at ~ 40 Ma Broken Ridge and the central Kerguelen Plateau began to separate along the nascent Southeast Indian Ridge [Mutter and Cande, 1983]. Broken Ridge, now ~ 1800 km north of the Kerguelen Plateau, is a narrow and elongated oceanic plateau (100-200 km by ~ 1000 km at ~ 2 km water depth) that trends west-northwest (Figure 2.3). It is markedly asymmetric in cross section, dipping gently ($< 2^\circ$) toward the north but with a steeply dipping ($> 10^\circ$) southern flank. This southern flank was uplifted, perhaps by more than 2000 m, during the Early Tertiary separation from the Kerguelen Plateau [Weissel and Karner, 1989]. Elan Bank, a structure unit extending westward from the boundary between the central Kerguelen Plateau and southern Kerguelen Plateau (Figure 2.2), has water depths from < 1000 to 2000 m. The northern Kerguelen Plateau, dominantly at water depths < 1 km, includes the still volcanically active Kerguelen Archipelago.

2.3 Formation of the Plateau - Geological settings

The Cretaceous Kerguelen Plateau/Broken Ridge LIP is interpreted to represent voluminous volcanism associated with the arrival of the Kerguelen plume head below young Indian Ocean lithosphere. A schematic plate tectonic reconstruction of the southern Indian Ocean for the last 120 Ma is shown in Figure 2.4 [Duncan and Storey, 1992; Weis et al., 1992; Morgan, 1981; Royer and Rollet, 1997; Müller et al., 1993] and can be summarized as follows:

Sea-floor spreading initiates at ~ 133 Ma between Western Australia and Greater India [Markl, 1978]; a minimum estimate for the initiation of sea-floor spreading between Australia and Antarctica is slightly later at ~ 125 Ma [Stagg and Willcox, 1992]. Between 130.9 and 118.7 Ma, Antarctica migrates to the SE relative to the Kerguelen hotspot. The first massive pulse of Kerguelen magmatism creates the southern Kerguelen Plateau (SKP) at ~ 110 Ma and possibly Elan Bank (EB), as Indian Ocean lithosphere migrates SE relative to the Kerguelen hotspot.

India continues its northward drift relative to Antarctica, and the Kerguelen hotspot is predicted to have remained close to the NE edge of the central Plateau (CKP) and Broken Ridge (BR), which form at ~ 100 to 85 Ma. Rapid northward movement of the Indian plate over the plume stem formed a 5000 km long, ~ 82 to 38 Ma, hotspot track, the Ninetyeast Ridge.

At ~ 40 Ma, seafloor spreading stopped between India and Australia and resumed as the newly formed Southeast Indian Ridge (SEIR), that intersected the plume's position. With the formation of the SEIR, the plate boundaries are at their present-day configuration. As the SEIR migrated northeast relative to the plume, hotspot magmatism became confined to the Antarctic plate. At ~ 40 Ma, sea-floor spreading commences between the central Kerguelen Plateau and Broken Ridge. The hotspot generates the northern Kerguelen Plateau (NKP), and since 40 Ma, as Broken Ridge and the Kerguelen Plateau continue to separate, produces the Kerguelen Archipelago (Figure 2.4).

This plate reconstruction model has been confirmed by previous drilling and age-dating of both basement basalt and overlying sediments (see section 2.4). Igneous basement of the Ninetyeast Ridge established a systematic south to north progression of ages from ~ 82 to 38 Ma along this hotspot track. The clear association with this long linear volcanic ridge is a unique aspect of the Kerguelen Plateau. In addition, the Kerguelen Archipelago and Heard Island have a volcanic record from ~ 38 Ma to the present. Thus, a ~ 115 Ma record of volcanism is attributed to the Kerguelen plume. An overview of the present-day features in the Indian Ocean, showing the products of the Kerguelen plume and the sites drilled prior to ODP Leg 183, is given in Figure 2.5.

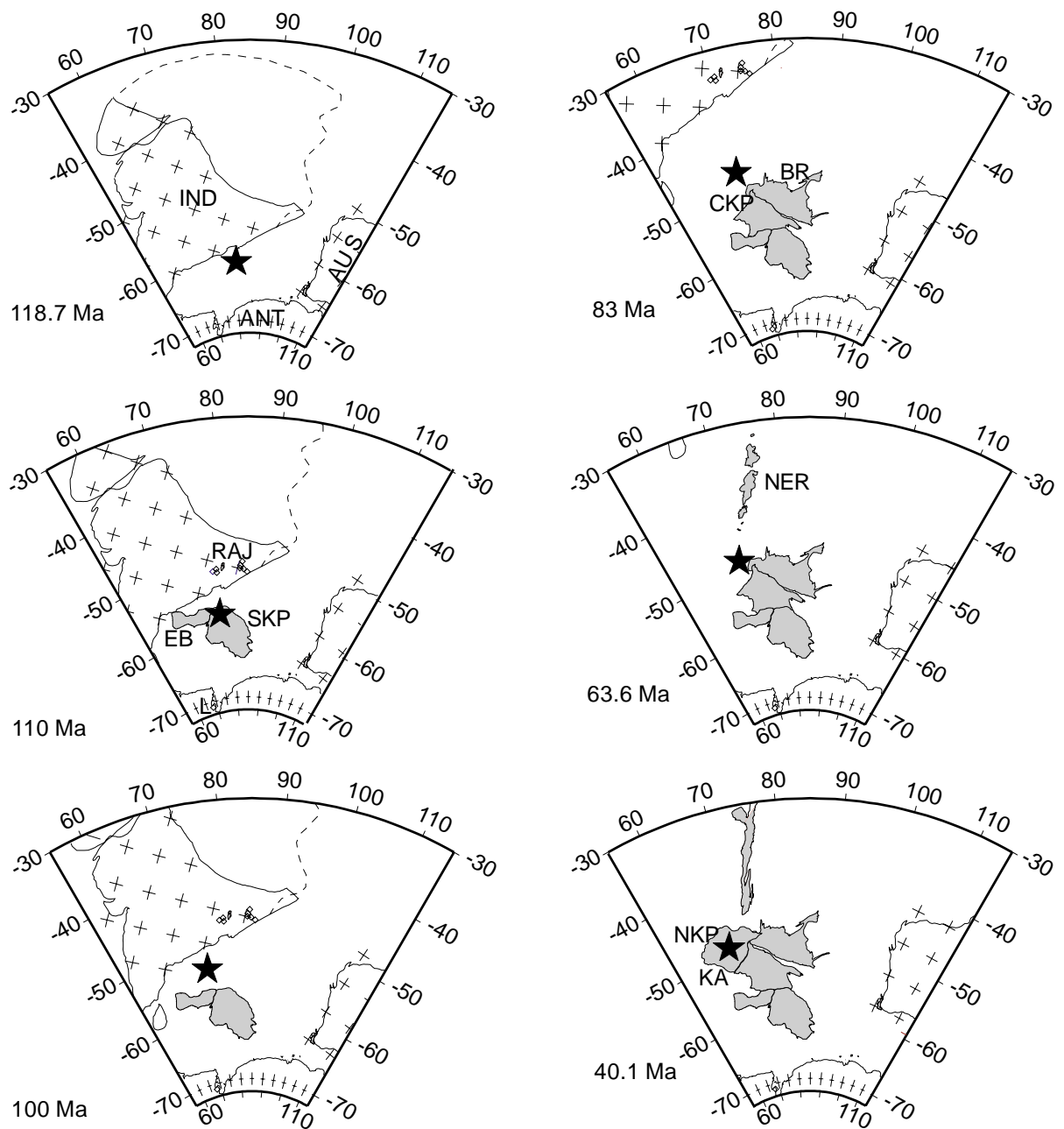


Figure 2.4: Schematic plate reconstruction of the southern Indian Ocean region and the formation of the Kerguelen Plateau [Royer and Rollet, 1997; Müller *et al.*, 1993]. Antarctica is fixed, the position of the Kerguelen hotspot is indicated by black stars. The hotspot is assumed to be fixed relative to other hotspots (not to Antarctica and this is why it apparently moves in this figure where Antarctica is kept fixed). Volcanic rock associated with the Kerguelen hotspot is indicated in grey. Dashed line indicates a possible northern boundary for Greater India now subducted. IND: India; ANT: Antarctica; AUS: Australia; RAJ: Rajmahal traps; SKP: southern Kerguelen Plateau; EB: Elan Bank; BR: Broken Ridge; CKP: central Kerguelen Plateau; NER: Ninetyeast Ridge; NKP: northern Kerguelen Plateau; KA: Kerguelen Archipelago.

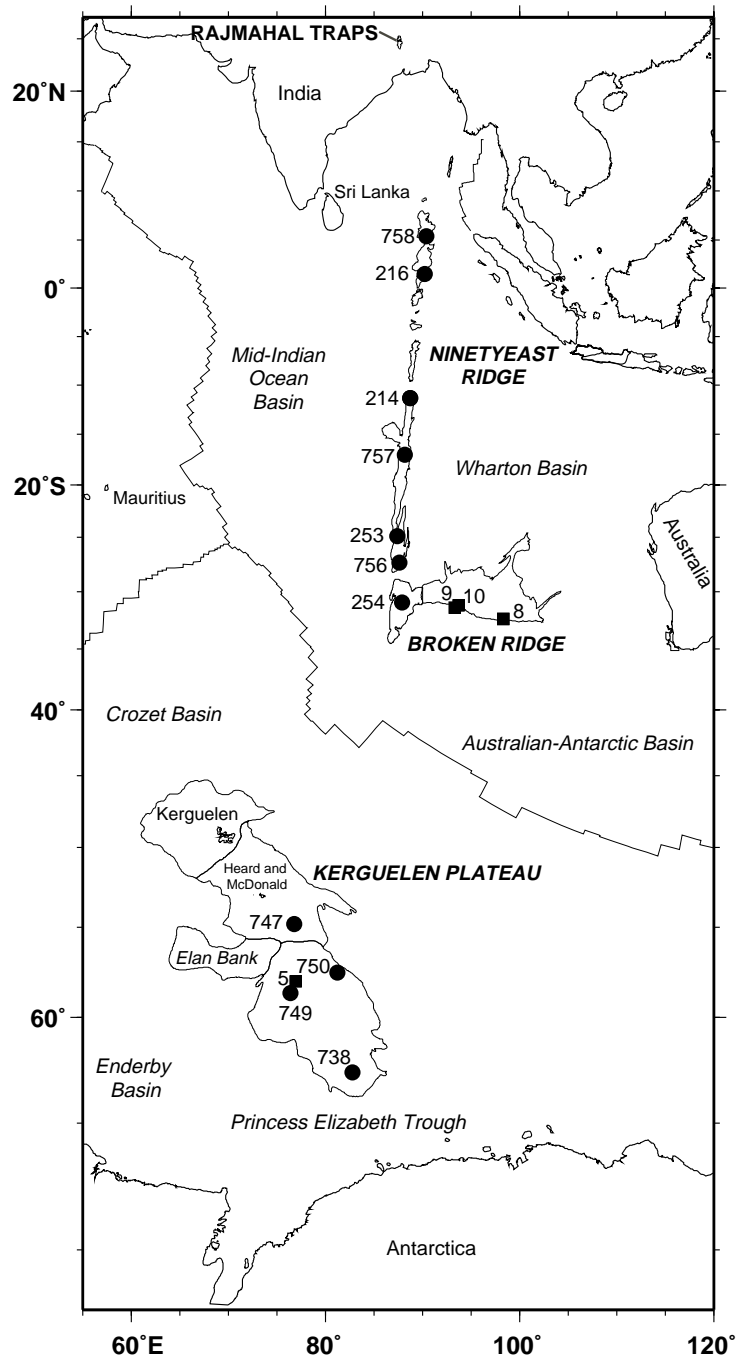


Figure 2.5: Map of the Indian Ocean showing major physiographic features and pre-Leg 183 sites where igneous basement was recovered from the Ninetyeast Ridge, Broken Ridge, and Kerguelen Plateau by DSDP and ODP drilling (circles) and dredging (squares). The Rajmahal Traps are continental volcanics that have been postulated to be related to the Kerguelen plume.

2.4 Summary of age variation

A summary of previous age dating of the basalts is given and the bio- magnetostratigraphic age constraints for the Leg 183 basalts using the sediments are summarized in this section. Previous dating of basalts recovered at four spatially diverse locations on the southern Kerguelen Plateau (ODP Sites 738, 749 and 750, Figure 2.2) has shown that the uppermost igneous crust formed over a relatively short time interval at ~ 110 Ma (*Leclaire et al.* [1987], *Storey et al.* [1977], *Pringle et al.* [1994] and Figure 2.6). Middle Albian (~ 104.5 to 106.5 Ma) shallow-water sands and clays overlying basaltic flows recovered from Site 1136 (Figure 2.6) also support a ~ 110 Ma age for the SKP.

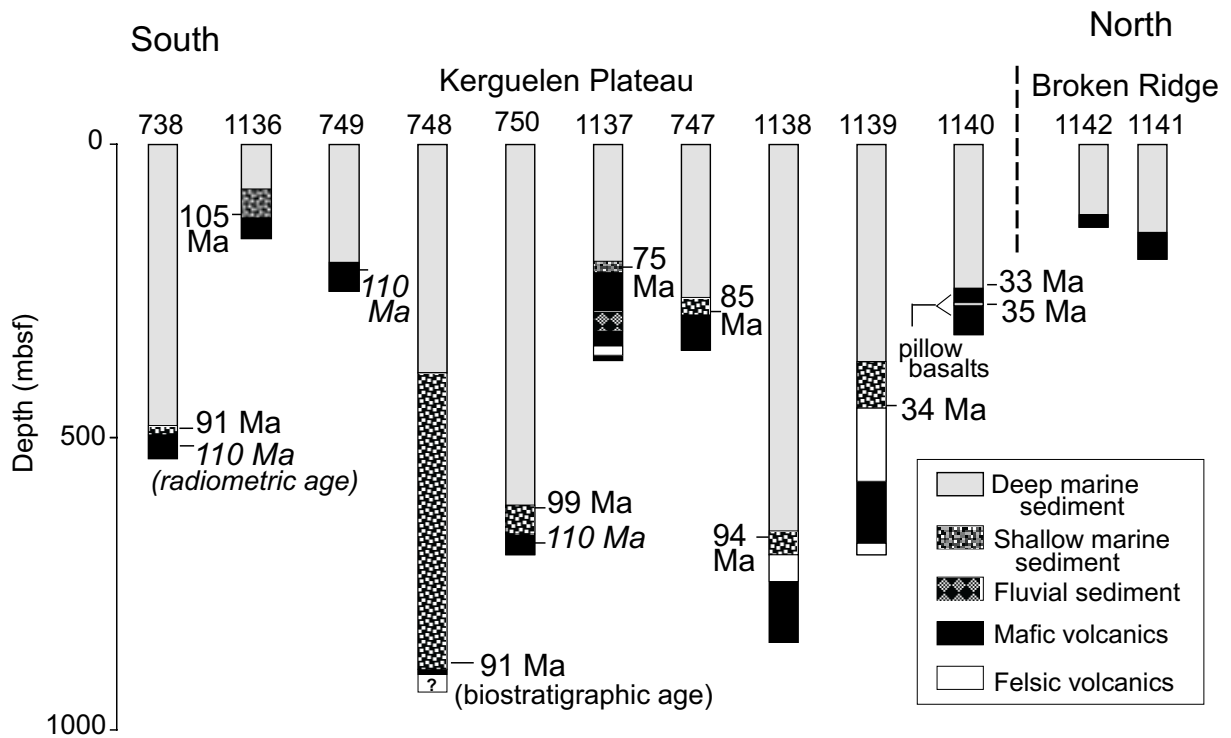


Figure 2.6: Summary of ODP drill holes on the Kerguelen Plateau that recovered volcanic rocks. Data are shown for Leg 119 (Site 738), Leg 120 (Sites 747, 748, 749, and 750) and Leg 183 (Sites 1136, 1137, 1138, 1139, 1140, 1141, and 1142). Multichannel seismic reflection profiles indicate that the volcanic rocks at all sites except Site 748 were recovered from the uppermost basement of the plateau, which lies beneath younger sedimentary cover. Basalt at Site 748 was recovered ~ 200 m above the seismically defined basement and overlies a poorly recovered zone that contains smectitic clay and highly altered basalt. Radiometric ages for basalts are shown in italics. Biostratigraphic ages of sediments overlying basement are also indicated.

In contrast, basement basalts from Site 747 on the central Kerguelen Plateau may be much younger, ~ 85 Ma [*Storey et al.*, 1977]. This age is similar to the 83-88 Ma age for lavas from Broken Ridge dredge sites 8 and 10, which were close to Site 747 prior to separation between Broken Ridge and the central Kerguelen Plateau. Also, piston coring of sediments on the northeast flank of the central Kerguelen Plateau between the

Kerguelen Archipelago and Heard Island recovered cherts and calcareous oozes of probable Santonian age (83.5-85.5 Ma) [Fröhlich and Wicquart, 1989]. Site 1138 basalts from the central Kerguelen Plateau are overlain by Cenomanian-Turonian (~ 94 Ma) sandstone. The first recovery of igneous basement from Elan Bank was at Site 1137; basement is overlain by late Campanian (~ 75 Ma) packstone (Figure 2.6). Igneous basement is likely to be somewhat older, as the packstone is at the top of a basal sedimentary sequence that thickens markedly to the east of Site 1137. These sparse data show that most of the Kerguelen Plateau and Broken Ridge formed in Cretaceous time, but the SKP is distinctly older than the central Kerguelen Plateau and Broken Ridge. In contrast, Cenozoic magmatism (~ 40 Ma to present) has formed the northern Kerguelen Plateau and Kerguelen Archipelago, as well as numerous volcanic edifices on the Cretaceous central Kerguelen Plateau: Heard and McDonald Islands, and the bathymetric/gravity highs between the Kerguelen Archipelago and Heard Island [Nicolaysen *et al.*, 2000]. The first recovery of submarine igneous basement from the northern Kerguelen Plateau was at Site 1139 on Skiff Bank and Site 1140 on the northernmost Kerguelen Plateau (Figure 2.2). On Skiff Bank, chalk at the base of the pelagic sedimentary section is earliest Oligocene (32.8-34.3 Ma) in age (Figure 2.6). This minimum age is consistent with the oldest rocks (~ 38 Ma) from the Kerguelen Archipelago [Giret and Lameyre, 1983]. At Site 1140 pelagic sediment of late Eocene age (~ 35 Ma) is intercalated with basalt flows (Figure 2.6).

2.5 Plume - ridge interactions

Mantle plumes and upwelling beneath ridges represent the two dominant modes of material transport between the Earth's deep interior and the surface of the Earth. They contribute independently to the crustal accretion process. However, it is becoming increasingly clear that the two modes interact and that even the dispersion of plumes might be modulated by mid-ocean ridges.

The simplest mode of interaction is when the plume is centered on the ridge. Of these so called "on-axis" plumes, Iceland on the spreading Reykjanes Ridge is the best known example.

The Kerguelen plume is an example for the so called "off-axis" plumes; it is not centered on the Southeast Indian Ridge (SEIR) but located rather distant from it. Morgan [1978] suggested that in the case of an off-axis plume a pipeline-like flow from the plume to the ridge axis on the base of the rigid lithosphere may develop. In the numerical model of Yale and Phipps Morgan [1998], the Kerguelen hotspot, now located beneath the stationary Antarctic Plate, must supply asthenosphere to the ridge to accommodate the large shear and pressure fluxes generated by the (in contrast to the Antarctic Plate) rapidly moving Indian Plate. Their model also suggests a pipeline-like flow from the plume to the ridge.

At ~ 40 Ma the newly formed SEIR intersected the position of the Kerguelen plume,

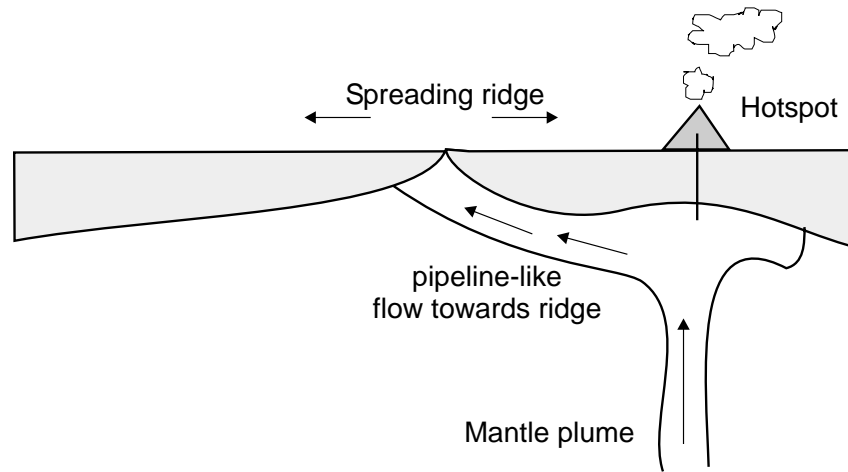


Figure 2.7: This cartoon illustrates the conceptual model for the interaction of off-axis (but near-ridge) plumes with spreading ridges. The plume rises and then a pipeline-like flow from the off-axis plume toward the ridge axis at the base of the rigid lithosphere develops. This could be the case for the Kerguelen plume after formation of the Southeast Indian Ridge approximately 40 Ma ago and may have influenced the formation of the younger hotspot products (the northern Kerguelen Plateau including the Kerguelen Archipelago). After *Morgan* [1978].

followed by the northeastward migration of the ridge relative to the plume. The northern Kerguelen Plateau was formed at that time. Therefore, the volcanic events that formed the northern Kerguelen Plateau and the Kerguelen Island may have been affected by plume-ridge interactions.

2.6 Exploring the Kerguelen Plateau: ODP Leg 183

The *Ocean Drilling Program* (ODP) is an international partnership of scientists and research institutions organized to explore the evolution and structure of the Earth. The *JOIDES Resolution* is the drill and research vessel of ODP, equipped with shipboard laboratories. During Leg 183 (December 98 to February 99) her aim was drilling basement of the Kerguelen Plateau.

2.6.1 Background

Despite the huge size of some oceanic plateaus and their potential role in contributing to our understanding of Cretaceous mantle circulation and environmental change, they are among the least understood features in the ocean basins. The igneous crust of the Kerguelen Plateau and Broken Ridge has been sampled by dredging and drilling; in particular, Leg 183 focused on the development of this LIP in time and space by drilling and coring five holes into igneous crust of the Kerguelen Plateau and two into Broken Ridge (Figure 2.2 and 2.3). A drilling summary of Leg 183 sites is given in Table 2.1.

During Leg 183, basement was reached on 7 Sites (1136-1142), while on Site 1135 only sediments have been recovered.

Site/ Location	Water depth (m)	Sediment penetration (m)	Sediment recovery (m)	Basement penetration (m)	Basement recovery (m)	Total penetration (m)
1135 SKP	1566.6	526.0	208.7	0	0	526.0
1136 SKP	1930.6	128.1	54.2	33.3	18.4	161.4
1137 EB	1004.5	219.5	113.9	151.7	105.5	371.2
1138 CKP	1141.4	698.2	343.0	144.5	69.0	842.7
1139 SB	1415.3	461.7	269.6	232.5	87.3	694.2
1140 NKP	2394.1	234.0	95.8	87.9	49.1	321.9
1141 BR	1196.9	113.5	57.7	72.1	39.1	185.6
1142 BR	1200.8	91.0	No Coring	50.9	17.3	141.9

Table 2.1: Leg 183 drilling summary. Samples from the sites printed in bold face (even numbered sites) have been used for the paleo- and rock magnetic studies presented here.

Site 1135 and 1136 are located on the southern Kerguelen Plateau, Site 1137 on the Elan Bank, Site 1138 on the central Kerguelen Plateau, Site 1139 on Skiff Bank, Site 1140 on the northern Kerguelen Plateau, close to the Kerguelen Archipelago, and Site 1141 and 1142 on Broken Ridge.

Shipboard studies indicate that much of the southern and central Kerguelen Plateau formed subaerial landmasses whose surfaces range in age from ~ 110 Ma in the south to ~ 85 Ma in the central part of the plateau. In contrast, the uppermost lavas of the northern Kerguelen Plateau are Cenozoic. At three Leg 183 drillsites, plateau construction ended with explosive eruption of highly evolved felsic magmas that may have had significant environmental consequences.

2.6.2 Paleomagnetic research on Leg 183

Paleomagnetic research on samples of Leg 183 focussed on two main subjects. Although Leg 183 was a so called "hard-rock" Leg, i.e. with the aim of drilling and studying basement rocks of the Plateau, the overlying sediments have been cored, too, at 7 of 8 sites. Their characteristic remanent magnetization has been used to determine a magnetostratigraphy, which in combination with biostratigraphic data, provide an age-estimation of the underlying basement. Moreover, the bio-magnetostratigraphy has been used to date the ages of individual lithologic units and to determine sedimentation rates on the Kerguelen Plateau. Rock magnetic and paleomagnetic studies on sediments of the Kerguelen Plateau are presented in Appendix A of this thesis, and magnetozones found in sediments of Site 1138 in Appendix B.

Main part of the paleomagnetic research, however, was the determination of the characteristic remanent magnetization of the basalts. It has been used to obtain paleolatitudes of the Kerguelen Plateau. These paleolatitudes help to test the question if the Kerguelen hotspot has been moving or is fixed (see chapter 3).

Two paleomagnetists joined the scientific party of Leg 183 (Hiroo Inokuchi, Kobe University and Maria Antretter, LMU München). During Leg 183, it was decided to divide the sample material in even and odd numbered sites for onshore studies. For the work presented here, shipboard measurements and samples of the even numbered sites (Site 1136 on the southern Kerguelen Plateau, Site 1138 on the central Kerguelen Plateau, Site 1140 on the northern Kerguelen Plateau and Site 1142 on the Broken Ridge) have been used.

Discrete samples used in this work are identified according to Ocean Drilling Program conventions. A site can exist of several holes (hole A, B, etc.), however, during Leg 183 only one hole per site was drilled (only holes A). Drilling a hole proceeds with 9 m long cores, which are subdivided into 1.5 m long sections. Several drilling methods are possible; however, during Leg 183 only the rotary core barrel (identified with "R") has been used. A typical sample identification could for example be:

Sample 183-1138A-80R-2,114 cm, which means: Leg 183, Site 1138, Hole A, Core 80 drilled with a rotary core barrel R, Section 2 in this core, at 114 cm in this section.

Chapter 3

Paleolatitudes of the Kerguelen hotspot: paleomagnetic results

Are hotspots stationary or do they move in a convecting mantle? And if they move, is the magnitude of the motion big enough to be recorded with paleomagnetic methods?

If a hotspot is stationary relative to the pole, the paleolatitudes of the products of the hotspot should always be identical with the latitude of the present-day position of the hotspot itself. This means for the Kerguelen hotspot that paleomagnetic investigations on its products (the southern, central and northern Kerguelen Plateau, the Ninetyeast Ridge as well as the Broken Ridge) should provide a paleolatitude of 49°S, which is the assumed present-day latitude of the Kerguelen hotspot. The position at 49°S underneath Kerguelen Island is the preferred present-day position for the hotspot, however, it could possibly be further south underneath Heard Island or inbetween Kerguelen and Heard Island. The position of the hotspot below Kerguelen Island gives the best and most reliable fit with the data, as discussed in chapter 5 section 5.8.

In this chapter the basalts from the Kerguelen Plateau that have been drilled during Leg 183 of the Ocean Drilling Program (December 98 to February 99) are used to determine paleolatitudes of the plateau. Previous paleomagnetic studies on Kerguelen basalts are summarized and compared to the new results. The paleolatitudes are used to test the question about fixity or motion for the Kerguelen hotspot.

3.1 Sampling and methods

During ODP Leg 183, eight Sites (1135 to 1142) have been drilled into the Kerguelen Plateau and Broken Ridge and on Sites 1136 to 1142 basement rock has been cored. Two paleomagnetists (Hiroo Inokuchi, Kobe University, and Maria Antretter) joined the scientific party of Leg 183 and took care of shipboard paleomagnetic measurements as well as of subsequent onshore paleomagnetic research. Sample material from the eight drillsites

have been shared; the division was made into odd and even numbered sites for onshore studies. Results from measurements on basement rocks from the even numbered sites are presented here (1136 on the southern Kerguelen Plateau, 1138 on the central Kerguelen Plateau, 1140 on the northern Kerguelen Plateau and 1142 on the Broken Ridge).

All cores during Leg 183 have been rotary drilled, and therefore no azimuthally oriented material has been recovered. During shipboard procedure, the cores are split into an archive and a working half. Shipboard routine measurements consist in stepwise AF demagnetization of the archive half cores up to 80 mT using a 2-G Enterprises pass-through cryogenic magnetometer in 1 cm intervals for igneous rocks when continuous pieces longer than 15 cm were available. These data have been analyzed during Leg 183, and based on these results core intervals of stable remanence have been chosen for discrete sampling. These intervals generally correspond to the massive and less altered parts of the flows.

For shorebased paleomagnetic studies, cylindrical inch-cores (12 cm³) were drilled from long basalt pieces of the working halves using a water-cooled nonmagnetic drill bit attached to a standard drill press. The inch-cores are oriented with an arrow pointing in the uphole direction. Where sufficient material was recovered, at least 7 inch-cores have been taken in each basement unit.

25 inch-cores have been taken from basement of Site 1136, 151 inch-cores from Site 1138, 86 from Site 1140 and 20 inch-cores from Site 1142. All samples have been analyzed in the Paleomagnetic Laboratory at the University of Munich, Germany. Overlying sediments have not been used for paleolatitude analysis because of high disturbances in the rotary drilled sediment cores. Most of the samples were subjected to detailed thermal demagnetization. Some samples were also demagnetized using stepwise alternating field treatment in increments of 3 to 20 mT. Thermal and AF demagnetization were equally effective for determining the characteristic remanent magnetization (ChRM). Measurement and stepwise demagnetization of the NRM were performed in the magnetically shielded room at the paleomagnetic laboratory of the University of Munich in Niederlippach. Because of high NRM intensities, all remanence measurements were carried out using a Molspin spinner magnetometer. The low-field magnetic susceptibility was measured at room temperature for every sample and after each thermal demagnetization step using a KLY-2 kappa bridge.

At least one sample from every flow was used for a set of rock magnetic measurements. IRM-acquisition, backfield curves, hysteresis loops at room temperature and thermomagnetic curves ($B_{max} = 400$ mT, $T_{max} = 600^{\circ}\text{C}$) for each of these samples were measured with a Variable Field Translation Balance (VFTB).

3.2 The southern Kerguelen Plateau - Site 1136

In Site 1136 on the southern Kerguelen Plateau, from 128.1 to 161.4 mbsf (meters below sea floor), three normally magnetized basalt flows with 55% recovery have been cored. From the uppermost ~10-m-thick flow, 6.2 m have been recovered. This flow probably formed as an inflated pahoehoe flow. Basalt from the central flow (13.3 m recovered from a ~20-m-thick flow) also indicate an inflated, large-volume pahoehoe flow. Only 53 cm of a vesicular basaltic breccia that forms the rubbly flow top of the lower flow have been recovered. The inference that the flows are inflated pahoehoe and the absence of features indicating submarine volcanism (e.g., pillows and quenched glassy margins) suggest sub-aerial eruption. 7 inch-cores from Unit 1 and 8 inch-cores from Unit 2 have been taken from the massive, relatively unaltered interiors of the flows for the paleomagnetic studies. Thermal and alternating field results are consistent and equally effective in determining the ChRM. All of the samples show a stable component, that allowed calculation of a characteristic direction with principal component analysis. Table 3.1 lists the mean inclination values and precision parameters for the two sampled lava flows, that have been determined after *McFadden and Reid* [1982].

Unit number	N/n	Inc [°]	k	α_{95} [°]
1	7/7	-73.6	1078	2.0
2	8/8	-67.3	594	2.4

Table 3.1: Paleodirectional results from the southern Kerguelen Plateau. For every sampled lava flow the mean inclination as well as the precision parameter k and the α_{95} are shown. Also given is the number of samples treated (N) versus the number of samples used (n) for calculating the mean direction.

An important assumption for a proper determination of paleolatitudes is the averaging out of the paleosecular variation within the sampled lithologic sequence. A first requirement is that several time independent lava flows or basement units have been drilled and sampled. In Site 1136, only 3 lava flows were recovered, and only two of them could be sampled for paleomagnetic studies. Obviously the paleosecular variation can not be averaged out based on two lava flows. Hence, the determination of the paleolatitude for the southern Kerguelen Plateau at the time of its formation 120 Ma ago is not possible based solely on paleomagnetic data of Site 1136.

Analysis of backfield- and hysteresis measurements according to *Day et al.* [1977] indicate a grain size distribution characterized by pseudo-single domain particles. Strong field thermomagnetic $M_s(T)$ curves are shown in Figure 3.1A for a sample of Unit 1 and Figure 3.1B for a sample of Unit 2. Both curves are reversible with unblocking temperatures at 550 - 580°C and indicate magnetite or low Ti-magnetite as magnetic carriers. Based on the reversibility of the $M_s(T)$ curves, few paleointensity experiments

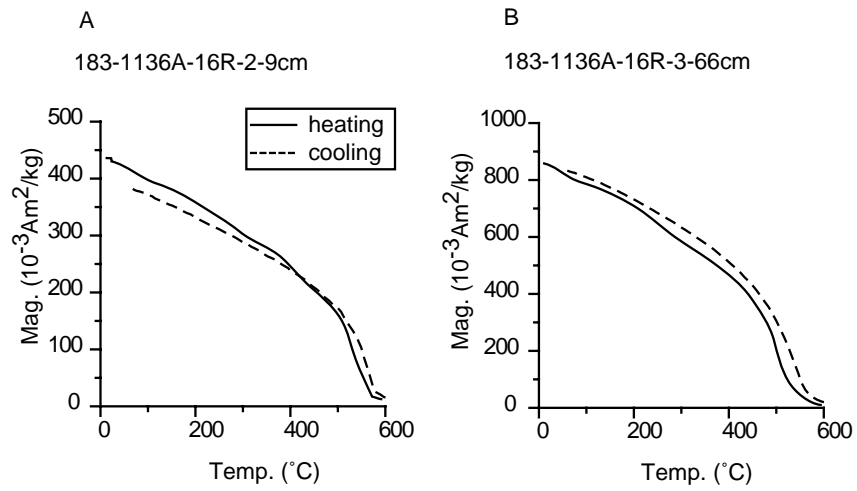


Figure 3.1: Thermomagnetic measurements on basalts from Site 1136

have been conducted on bulk samples of Site 1136, using the Thellier-Thellier method [Thellier and Thellier, 1944]. However, measurements did not give useful results, and an interpretation of the data was not possible.

3.3 The central Kerguelen Plateau - Site 1138

A lava flow sequence of the central Kerguelen Plateau was recovered in Site 1138. Several samples of the different flows were taken and were subjected to various paleo- and rock magnetic experiments in order to investigate the directional behavior of these cretaceous rocks from the Kerguelen hotspot.

3.3.1 Lithostratigraphy of the basement

In Site 1138 on the central Kerguelen Plateau (Hole 1138A: 53°40'S, 75°35'E), 144.5 m of massive lava flows were penetrated and 69.0 m of cores were recovered. The basalt sequence can be separated into 22 lithologic units (Figure 3.2).

Basement Unit 1 includes rounded cobbles of flow-banded, aphyric to sanidine-phyric dacite. Unit 2 is a complex succession of volcanoclastic rocks overlying basalt lava flows (Units 3 through 22). Basement Units 3 - 22 are ~5-m-thick subaerial basaltic lava flows that range from inflated pahoehoe to classic aa. Several boundaries are oxidized, suggesting subaerial weathering between eruptions. The massive parts of flow Units 3 - 22 are slightly to locally highly altered. Sample material for paleomagnetic measurements have been taken from the less altered parts.

Several observations indicate that the flows are near vent flows: (1) aa and slab pahoehoe flows rarely travel more than a few tens of kilometers from vents, (2) abundant small vesicles indicate that the lavas did not flow far enough for vesicles, which formed at vents, to coalesce, and (3) clasts in some of the welded basal breccias appear to be spatter, which only forms close to vents [Coffin *et al.*, 2000].

3.3.2 Rock magnetic studies

Plotting the parameters of the hysteresis and backfield measurements in a *Day et al.* [1977] plot results in a clustering of the samples within the pseudo single domain (PSD) grain size range. Thermomagnetic ($M_S T$) curves revealed three different types of blocking temperature distributions (Figure 3.3). The uppermost units (Units 2-14) are characterized by a single Curie temperature between 500 and 570°C (Figure 3.3A), indicating magnetite or low Ti-magnetite as the only magnetic carrier. These samples show reversible thermomagnetic curves. Intermediate Curie temperatures (200 - 300°C) were detected in samples from unit 19 and 22. Magnetization is probably carried by Ti-magnetite. Two Curie temperatures (200 - 300°C and 400 - 500°C) were found in samples from Unit 16, 17, 20 and 21, indicating the presence of low and high Ti-magnetite.

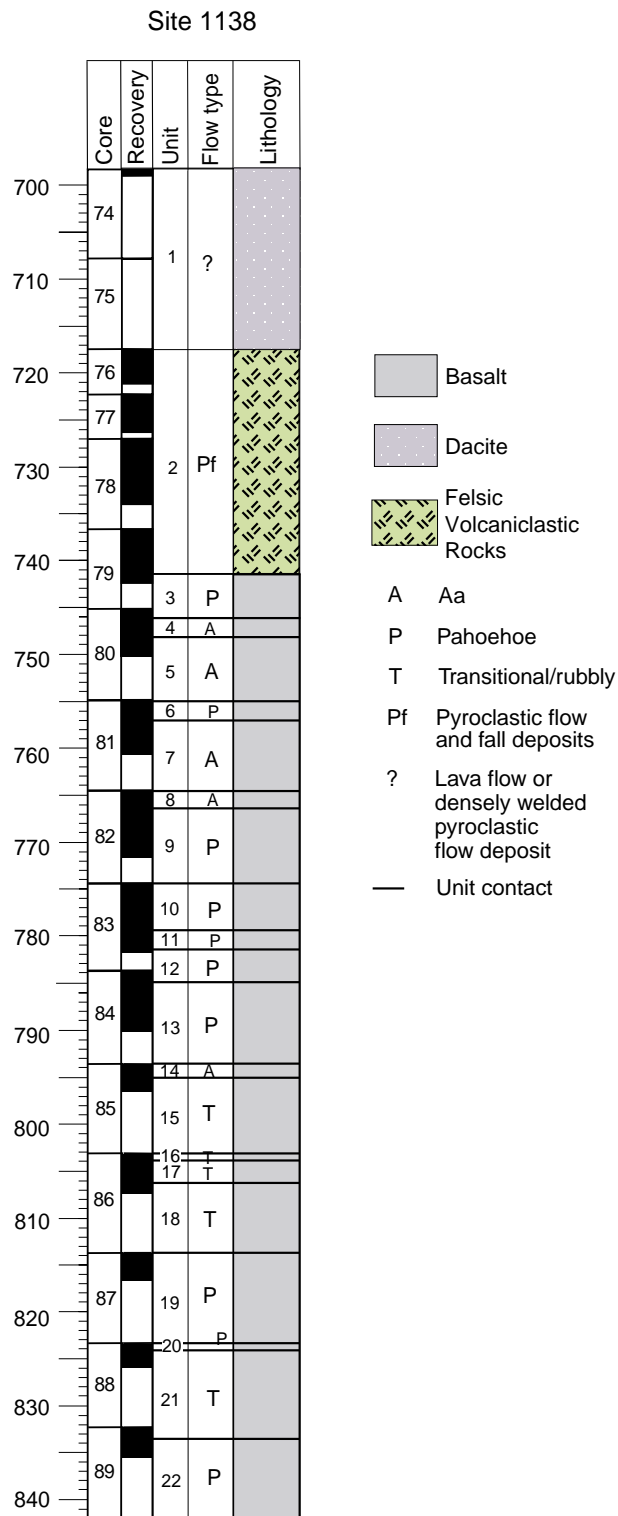


Figure 3.2: Lithology of basement of Site 1138. Core numbers are shown versus depth. Black zones in the recovery column indicate recovery, white zone indicate no recovery.

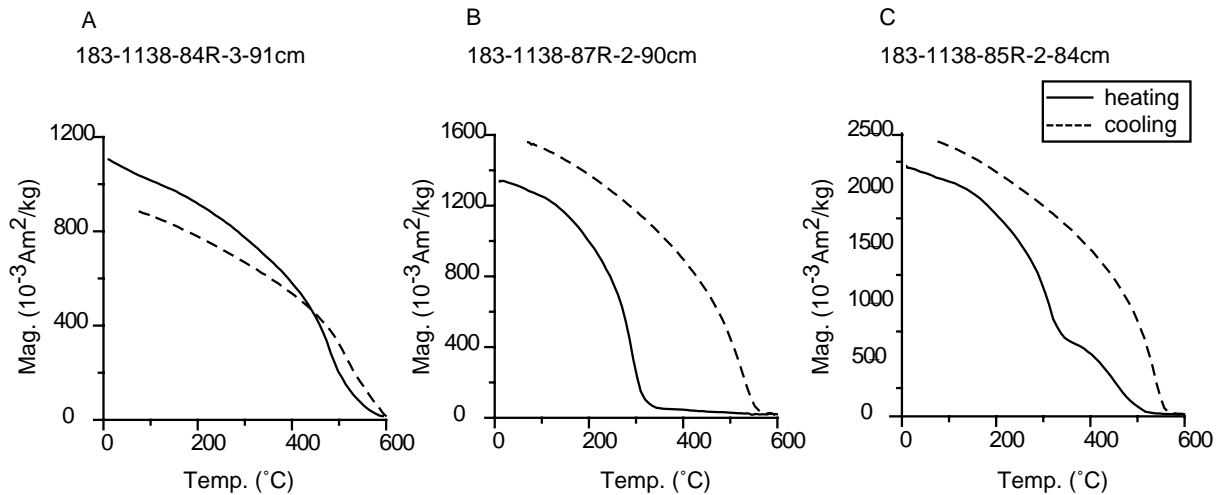


Figure 3.3: Thermomagnetic curves from basalt samples from Site 1138. A: Most of the sampled lava flows are characterized by Curie-temperatures between 500 and 570°C. B: Intermediate Curie temperatures (200 - 300°C) were found in samples from unit 19 and 22. C: Unit 16, 17, 20 and 21 are characterized by two phases with Curie-temperatures from 200 - 300°C and 400 - 500°C.

3.3.3 Demagnetization of the NRM

151 inch-cores have been taken from basement Units 2 - 22 of Site 1138. Thermal and alternating field results are consistent and equally effective in determining the ChRM. Typical demagnetization diagrams are shown in Figure 3.4.

During both demagnetization techniques, most of the samples show a stable component, indicated by straight tracks in the orthogonal projection pointing toward the origin in the higher temperature and alternating field range. Some samples had a viscous overprint, but these could easily be removed at demagnetization steps up to 200°C and 30 mT. The univectorial behavior during demagnetization allowed calculation of a characteristic direction with principal component analysis. In Table 3.2 the mean inclinations for the flows are listed. Mean inclinations for the flows as well as mean site inclination have been calculated after *McFadden and Reid* [1982].

All the ChRM's of samples of Site 1138 have negative inclination. Assuming a southern hemisphere origin, the negative inclinations denote normal polarity. Not enough oriented material was recovered in lithologic Units 1, 15 and 18 to obtain reliable paleomagnetic directions. A few samples with unstable directions were excluded from the directional analysis. Overall the within-flow scatter is small. The α_{95} values are $<5^\circ$ in most flow units, except of units 8, 16, 17 and 19 - 22. In the remaining, except of Unit 16, the α_{95} values are $<10^\circ$, associated with k values above 80, which underlines the high quality of the directional data (Table 3.2).

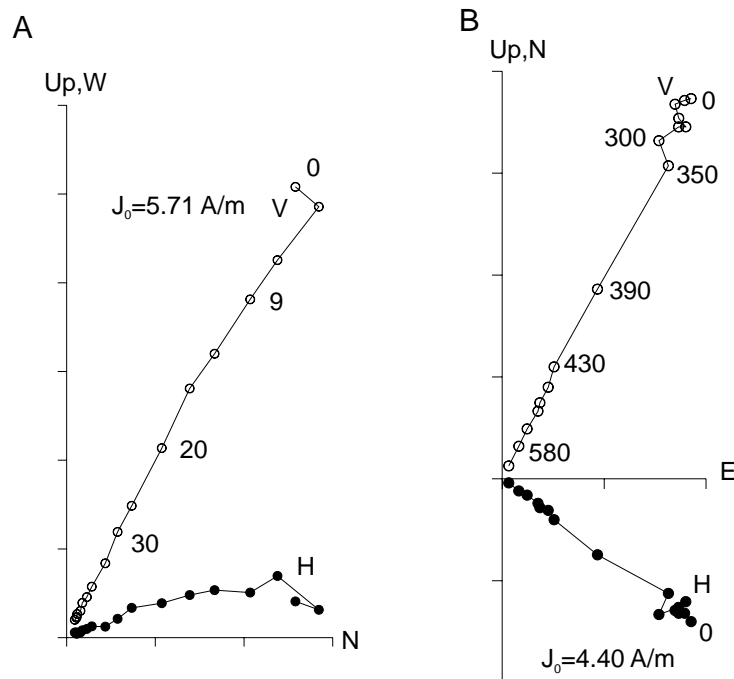


Figure 3.4: A.,B.: Characteristic behavior of samples of Site 1138 during alternating field and thermal demagnetization, respectively. The orthogonal vector diagrams [Zijderveld, 1967] show nearly univectorial decay to the origin after the removal of a small viscous overprint. Temperature steps and field steps are 50-25°C and 2-5 mT, respectively. Sample identifications following conventions of the Ocean Drilling Program are as follows: A.: 183-1138A-80R-2,114-116cm; B.: 183-1138A-80R-3,40-42cm. V: vertical component; H: horizontal component; J_0 : starting magnetization.

3.3.4 Paleosecular variation record

An assumption in paleomagnetic studies is the axial geocentric dipole hypothesis. This hypothesis must hold for the determination of paleolatitudes. However, the axial geocentric dipole takes no account of secular variation, although its effect must be averaged out before paleomagnetic measurements are said to conform with the model. Hence, before converting mean inclinations of a site to paleolatitudes, it must be controlled if paleosecular variation is properly averaged out.

One of the major risks of analysis of paleosecular variation, especially when dealing with older rocks, is that only part of the secular variation record will be retrieved, which will cause an artificial underestimation of the secular variation. It is, therefore, very important to sample a sufficient number of lava units. It is also important that the sampled lava flows are not correlated but of independent origin and that the sampled sequence through the flows cover a time span of some thousands of years. On Site 1138, 22 basement units have been sampled. This relatively large number of sampled units indicates a covered time span which is long enough for averaging out the secular variation. According to Lipman [1995], who estimated the growth-rate of shield volcanos to 4 mm/year, the penetrated 180 m of basalt in Site 1138 correspond to approximately 45 000 years.

Unit number	N/n	Inc [°]	k	α_{95} [°]
1	0/0	–	–	–
2	7/7	-65.0	691	2.4
3	9/9	-62.3	392	2.7
4	6/6	-61.5	654	2.9
5	9/8	-60.2	937	1.9
6	7/7	-54.6	682	2.5
7	9/8	-53.2	664	2.2
8	6/6	-62.6	144	6.2
9	12/10	-68.3	306	2.8
10	10/10	-73.0	371	2.5
11	6/6	-73.5	2344	1.5
12	7/7	-71.9	671	2.5
13	16/16	-68.3	141	3.0
14	11/10	-64.0	154	3.9
15	0/0	–	–	–
16	3/3	-60.3	82	22.7
17	5/5	-52.5	130	7.8
18	1/0	–	–	–
19	6/6	-56.0	187	5.4
20	7/7	-51.4	92	6.7
21	7/7	-55.1	80	7.2
22	7/6	-53.8	171	5.7
mean	151/244	-62.3	63	4.2

Table 3.2: Paleodirectional results from the central Kerguelen Plateau. For every sampled lava flow the mean inclination as well as the precision parameter k and the α_{95} are shown. Also given is the number of samples treated (N) versus the number of samples used (n) for calculating the mean direction.

However, this estimation might not be appropriate to the formation of a Large Igneous Province like the central Kerguelen Plateau.

In order to quantify the amount of paleosecular variation recorded in the lava sequence of Site 1138, the angular dispersion of the data has to be determined. Cores from Site 1138 have been rotary drilled, and therefore an azimuthal orientation was not possible. As only inclination is available, it is necessary to consider its statistical distribution so that estimates of the mean inclination and its confidence interval can be made. The statistical distribution of the inclination data is considered by *McFadden and Reid* [1982] and it provides estimations of mean inclination and dispersion for every flow unit (Table 3.2). The same statistics provide the mean total site dispersion S_T . The dispersion S_T of the directions has to be transformed into pole-space after calculations of *McElhinny and Merrill* [1975]. S_T has to be corrected with the within-site-scatter S_W after *McElhinny and Merrill* [1975]. The resulting between-site scatter S_B was calculated with lower and

upper 95% confidence limits after *Cox* [1969] ($S_B = 14.14$; max = 18.10; min = 11.61).

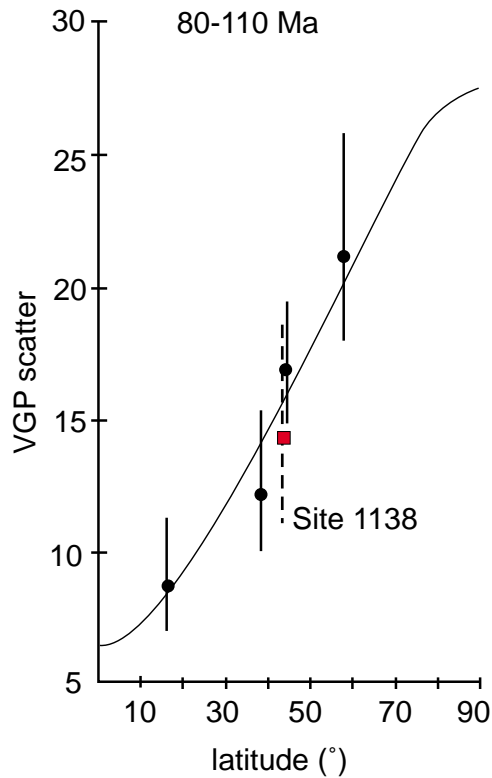


Figure 3.5: The dispersion of the mean direction of Site 1138 (square and dashed line) corresponds with the dispersion of data of similar latitude and age, taken from a global databank and calculated by *McFadden et al.* [1991] (dots and solid lines). This indicates a complete averaging out of paleosecular variation, which is an important condition for a proper determination of paleolatitudes.

One way to control the quality of the paleomagnetic data is a comparison of the angular dispersion of the sampled lava sequence with the database of *McFadden et al.* [1991]. They published global recordings of the secular variation as function of age and of latitude, observed from lava flows. For evaluating the cretaceous Site 1138, the time window 80-110 Ma is chosen from the global dataset for comparison. Figure 3.5 shows the angular dispersion of the directions of Site 1138 compared to the data of the databank. The angular dispersion is identical with the predicted virtual geomagnetic pole scatter for Site 1138. Hence, directional results at Site 1138 are reliable, and a paleolatitude can be calculated.

However, another problem in calculating paleosecular variation on lava flows is the sporadic nature of volcanic activity. During high activity it is possible that several flows are extruded within a very short period of time and therefore they record the same geomagnetic field (they are not time-independent). This serial correlation may lead to incorrect estimates of the angular dispersion. To avoid this problem similar directions

of consecutive flows are often combined in directional groups [e.g. *Laj et al.*, 1999]. On the other hand, since secular variation may be strongly variable in time, it is argued by *Love* [1998] that combining data using directional criteria may lead to incorrect estimates. From the overlapping of the α_{95} limits it could be inferred that the directions of units 3, 4, 5 and 6, 7 and 8, 9 and 10, 11 are possibly related. Forming four directional groups of these flows for calculating the angular dispersion about the spin axis and not taking flow 16 into account ($\alpha_{95} = 22.7^\circ$) results in only slightly different values (Table 3.3).

		N	S_B [°]	S_u [°]	S_l [°]	Inc [°]	k	α_{95} [°]
A.	all units	19	14.1	18.1	11.6	-62.3	62.8	4.2
B.	serial correlation	13	15.40	20.82	12.23	-62.0	53.4	5.7

Table 3.3: A: Values for the angular deviation and the upper and lower confidence limits as well as the related mean inclinations with precision parameter k and the α_{95} . B: Instead of all lava flows, 9 flows (units 3 - 11) have been combined to four directional groups and the same parameters calculated.

A geological argument for time passed between the single lava-events (and hence for monitored paleosecular variation in the lava flows) are the oxidized boundaries of units found in the lava flows of Site 1138. They suggest subaerial weathering between the eruptions, which only can take place if a considerable timespan passed. This is an evidence against the directions of the lava flows being related.

3.3.5 Paleolatitude of Site 1138

The mean inclinations of each lithologic unit from Site 1138 are plotted versus depth in Figure 3.6. The dashed line in Figure 3.6 gives the mean inclination for Site 1138.

Considering the averaging out of secular variation as discussed in section 3.3.4, it is allowed to convert the mean inclination of the site to a paleolatitude. The mean inclination without directional grouping (-62.3° ; max = -65.6° ; min = -57.3°) that takes all lava units into account is chosen for the calculation. The relationship $\tan I = 2 \tan \lambda$ results in the paleolatitude $\lambda = 43.6^\circ\text{S}$ (max.: 47.8°S ; min.: 37.9°S) as paleolatitude for the central Kerguelen Plateau.

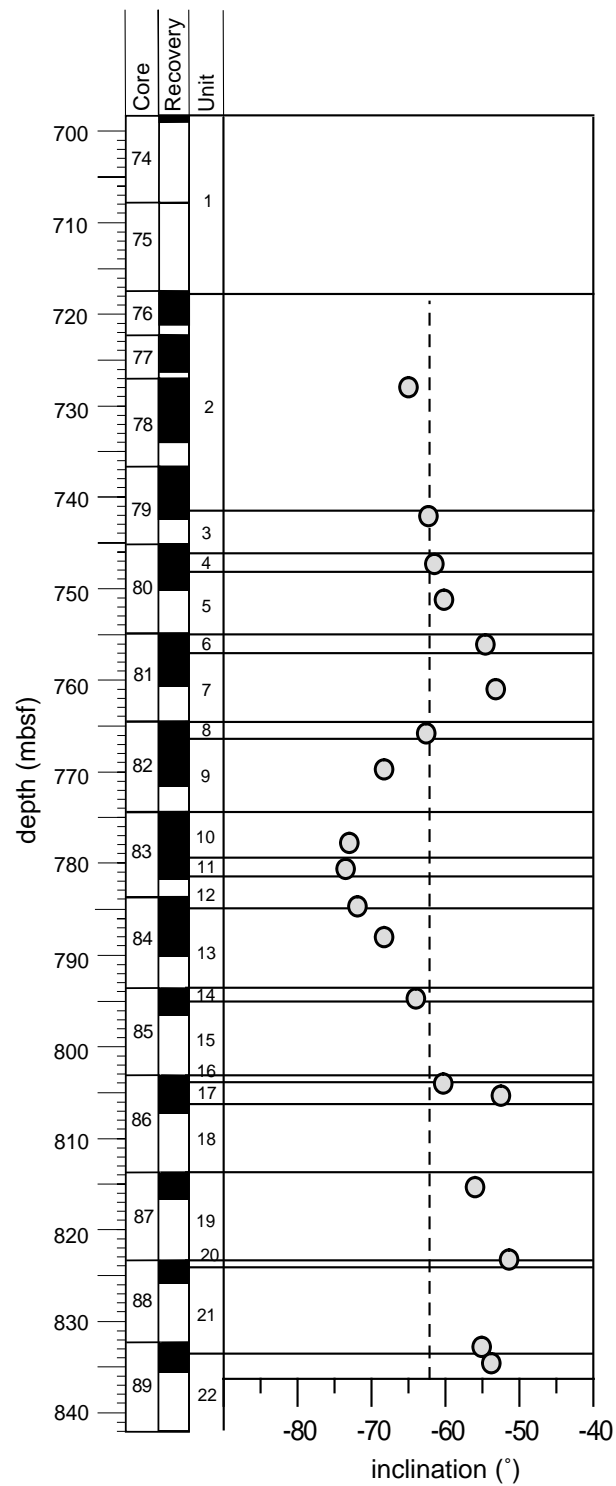


Figure 3.6: Inclination of basalts from Site 1138 versus depth. Mean inclinations for lava flows are represented by circles and the mean inclination of the site by the dashed vertical line (mean site inclination = -62.3° , $\alpha_{95}=4.2^\circ$). The variation of the inclination with depth results from secular variation.

3.4 The northern Kerguelen Plateau - Site 1140

Site 1140 lies on the northernmost Kerguelen Plateau, ~270 km north of the Kerguelen Archipelago. This site is the first to sample submarine igneous basement rocks of the northern Kerguelen Plateau. It is also the only site where lavas clearly formed in a submarine environment as pillow lavas. 81 discrete samples from the basement units have been stepwise demagnetized to determine the paleolatitude of the site using the inclination of the characteristic remanent magnetization.

3.4.1 Lithostratigraphy

Drilling at Site 1140 on the northernmost Kerguelen Plateau penetrated 87.9 m (with 49.1 m recovery) of basement rocks, which were divided into six units, five submarine basaltic flows (Units 1-3, 5, and 6) and a ~1-m-thick layer of dolomitized nannofossil chalk (Unit 4). Two other thin calcareous-dolomitic sedimentary interbeds are between basalt flows at the Unit 2/3 and Unit 5/6 boundaries (Figure 3.7).

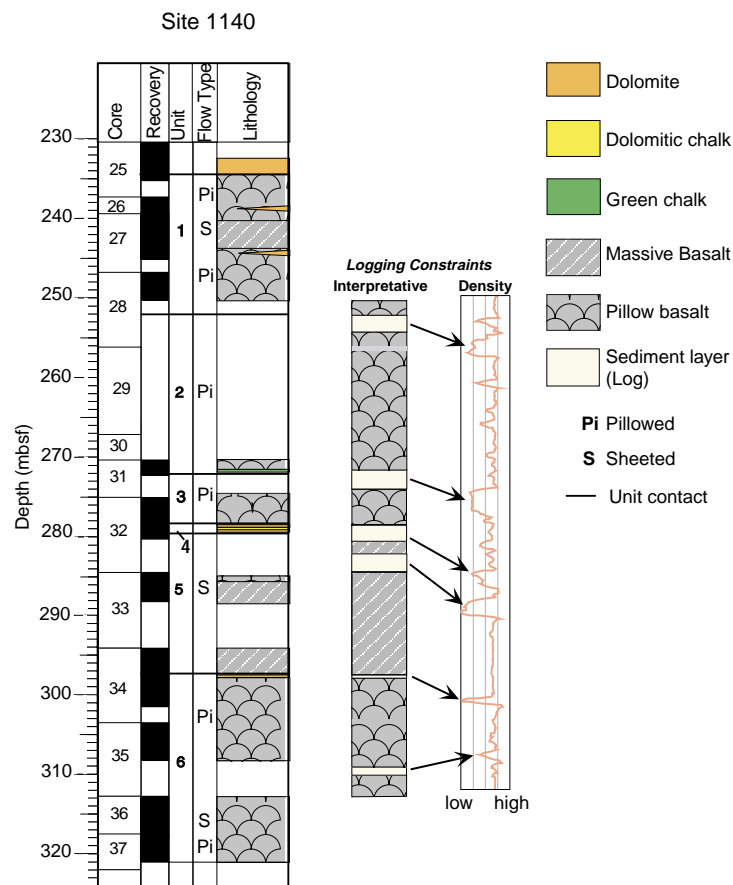


Figure 3.7: Lithology of basement of Site 1140. The interpretation of the logging data suggests more interbedded sediment layers than recovered.

Basement Units 1 and 6 each contain a ~ 5 -m-thick massive lobe in addition to ~ 30 small (50 to 100 cm) basaltic pillows. Only < 1 -m-diameter pillows were recovered from Units 2 and 3. Unit 5 contains similar pillows and a ~ 10 -m-thick massive lobe.

Site 1140 has been successfully logged after drilling, and logging results strongly suggest more interbedded sediment layers than recovered (Figure 3.7). Interbedded sediment layers indicate a time span of several hundreds of years for the formation of the basalt layers. This is an important assumption for a proper determination of the paleolatitude with respect to the averaging out of secular variation.

3.4.2 Rock magnetic studies

Analysis of the hysteresis measurements according to *Day et al.* [1977] indicates a grain size distribution dominated by pseudo-single-domain (PSD) particles. Strong field thermomagnetic curves $M_S(T)$ were obtained in order to determine the magnetic phases in the samples.

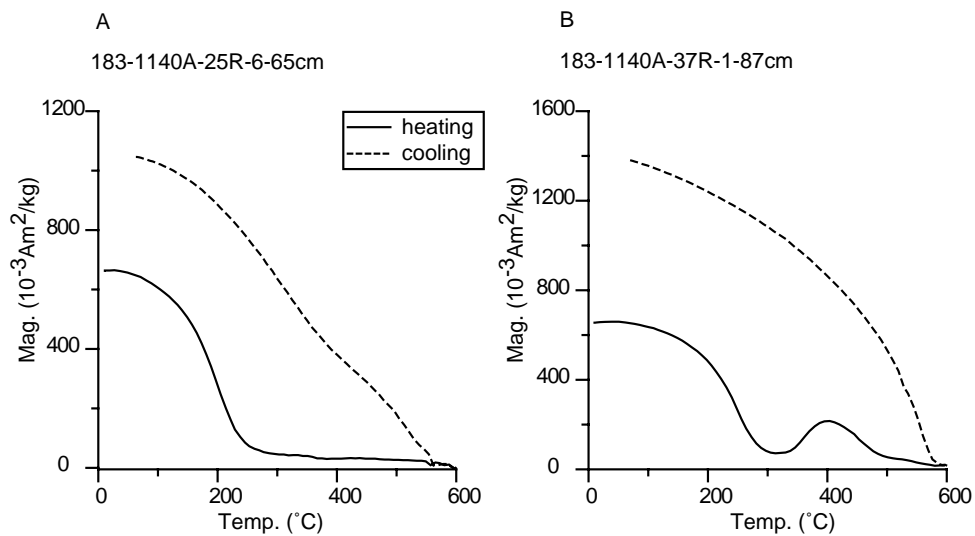


Figure 3.8: Thermomagnetic curves from basalts from Site 1140. Samples are characterized by Curie-temperatures between 200 - 300°C.

Curie temperatures between 200 - 300°C indicate titanomagnetite as magnetic carriers. A TM60-titanomagnetite with Curie temperatures in this range is typical for submarine basalts as drilled on Site 1140.

3.4.3 Demagnetization of the NRM

Thermal and alternating field results are consistent and equally effective in determining the ChRM. Typical demagnetization diagrams are shown in Figure 3.9. During both demagnetization techniques, most of the samples show a stable component, indicated

by straight tracks in the orthogonal projection pointing toward the origin in the higher temperature and AF range. The univectorial behavior during demagnetization allowed calculation of a characteristic remanence direction with principal component analysis.

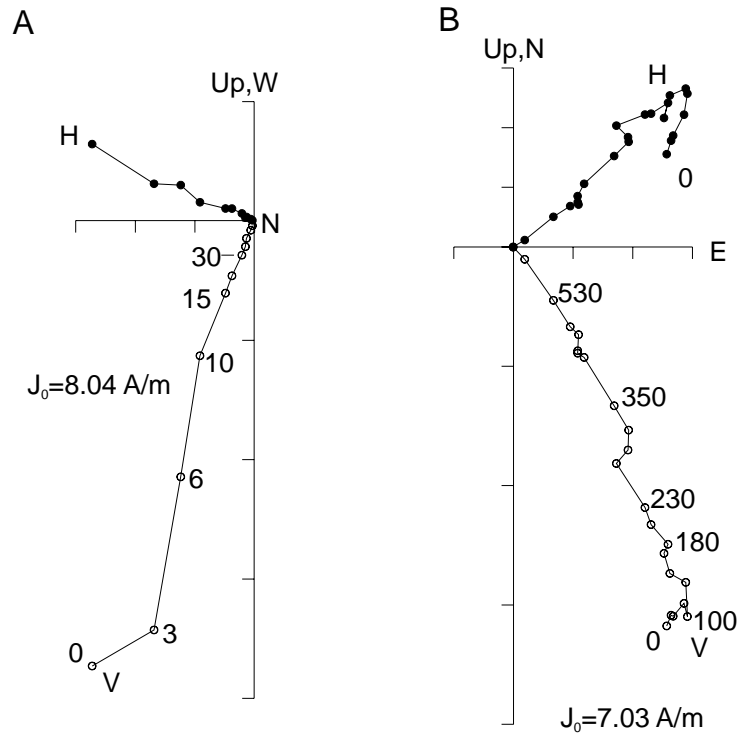


Figure 3.9: Characteristic behavior of samples of Site 1140 during alternating field and thermal demagnetization, respectively. The orthogonal vector diagrams [Zijderveld, 1967] show nearly univectorial decay to the origin after the removal of a small viscous overprint. Temperature steps and field steps are 50-25°C and 2-5 mT, respectively. A.: Alternating field demagnetization of sample 183-1140A-37R-4,16-18cm. B.: Thermal demagnetization of sample 183-1140A-33R-2,104-106cm, showing a larger viscous component, which, however, could be easily removed after heating to 120°C.

A magnetic reversal has been observed at the boundary between basement Units 1 and 2 of Site 1140, which are separated by two cored intervals from which there was no recovery (Cores 183-1140R-29R and 30R, Figure 3.7). Unit 1 is of normal polarity, and Units 2 through 6 are reversed. The negative inclinations of Site 1140 provide valuable information on the reliability of the magnetization which could be isolated. A common source of bias in paleomagnetic data derived from oceanic core material is a nearly vertical drilling-induced remanence. The negative inclinations argue against the presence of such an overprint because they are nearly opposite to the mean of the positive inclinations.

Lithologic unit 6, which consists of several pillow lava sequences, has been subdivided into four paleomagnetic subunits, based on directional grouping.

Table 3.4 lists the mean inclinations for every lava flow unit. Overall the within-flow scatter is small. The α_{95} values are $<5^\circ$ in all paleomagnetic flow units, associated with k values above 90, which underlines the high quality of the directional data (Table 3.2).

Unit number	N/n	Inc [°]	k	α_{95} [°]
1	15/13	-48.5	115	3.8
2	4/4	53.0	5466	1.6
3	8/8	50.2	532	2.5
4	4	–	–	–
5	13/7	49.4	1023	2.0
6a	15/14	65.9	90	4.1
6b	6/6	60.6	638	2.9
6c	8/7	49.1	334	3.5
6d	7/7	61.7	198	4.6
mean	81/66	55.3	69	7

Table 3.4: Paleodirectional results from the northern Kerguelen Plateau (Site 1140). For every sampled lava flow the mean inclination as well as the precision parameter k and the α_{95} are shown. Also given is the number of samples treated (N) versus the number of samples used (n) for calculating the mean direction.

A few samples with unstable directions were excluded from the directional analysis. The directions result in a mean site inclination of 55.3° with $\alpha_{95} = 7^\circ$ and $k = 69$.

3.4.4 Paleosecular variation record

The recording of paleosecular variation in the basalt sequence of Site 1140 must be analyzed, as discussed in section 3.3.4. Only if the paleosecular variation is properly averaged out in the mean inclination calculations for a site, a determination of the paleolatitude is possible. The same statistics are used as in section 3.3.4 to calculate the angular dispersion of the directional data. The total scatter S_T of the data has been corrected with the within-site scatter S_W to obtain the between-site scatter S_B . The between-site scatter results in $S_B = 11.98^\circ$. 95 per cent confidence limits have been determined after *Cox* [1969] and result in a upper limit $S_u = 17.72^\circ$ and a lower limit $S_l = 9.06^\circ$. This result for Site 1140 is compared to data of the global database of *McFadden et al.* [1991]. In Figure 3.10, the data of *McFadden et al.* [1991] are shown together with the angular dispersion data of Site 1140. From the database, data from the time window 22.5-45 Ma have been chosen, which includes the age of basalts from Site 1140 (34.3 ± 0.59 Ma).

Generally, the sampled lava flows have to be time-independent and must cover a time span of some thousands of years to obtain reliable paleomagnetic directions. Although for Site 1140 the dispersion is less than predicted by *McFadden et al.* [1991] and fits only within its error bars, the directional results are considered as reliable: An inversion of the magnetic field between Unit 1 and 3 allows on the one hand a certain directional control (a sort of reversal test) and points on the other hand to a considerable timespan, as several sediment layers in-between the pillows do. This strongly suggests that in the

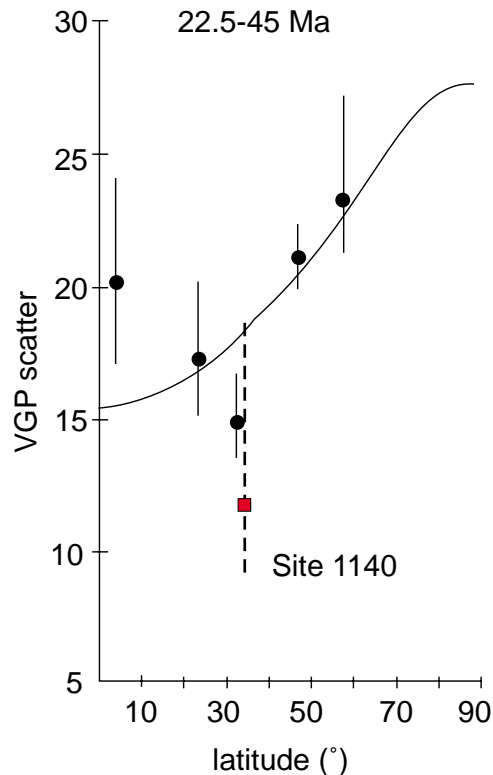


Figure 3.10: The dispersion of the mean direction of Site 1140 (square and dashed vertical line) is compared with the dispersion of data of similar latitude and age, taken from a global databank and calculated by *McFadden et al.* [1991] (dots and lines). Angular dispersion of Site 1140 is less than predicted by the model and the database.

northern Kerguelen Plateau basalt sequence secular variation is averaged out as well.

3.4.5 Paleolatitudes of Site 1140

In Figure 3.11 the mean inclinations of each unit from Site 1140 are plotted versus depth. The dashed line in Figure 3.11 indicates the mean inclination for Site 1140. Considering the averaging out of secular variation as discussed before, it is now possible to calculate the paleolatitudes for Site 1140 using the mean inclination of the site. For the northern Kerguelen Plateau a paleolatitude of -35.8° (max: -43.0° ; min.: -28.9°) is calculated, discordant from the estimated present-day latitude of the Kerguelen hotspot at -49° .

The relative large discrepancy between the paleolatitude of Site 1140 and the present-day latitude of the hotspot could be caused by ridge-plume interactions, as discussed in section 2.5. The Southeast Indian Ridge intersects the plume location at approximately 40 Ma, at the time the northern Kerguelen Plateau was formed, and subsequently migrated further north. A pipeline-like flow from the plume towards the ridge as proposed by *Morgan* [1978] could bias the location of the outcoming magma toward the north.

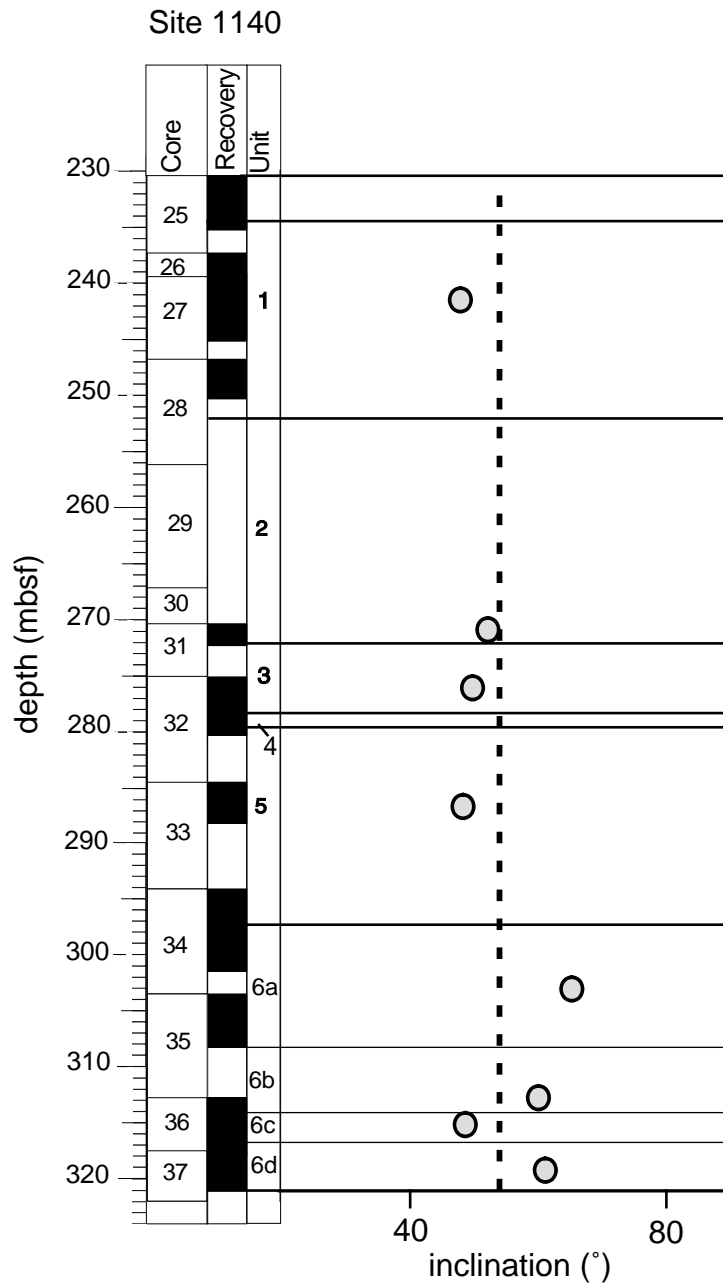


Figure 3.11: Inclination of basalts from Site 1140 versus depth. Mean inclinations for lava flow units are presented by circles and the mean inclination of the site by the dashed line (mean site inclination = 55.9° , $\alpha_{95} = 8.1^\circ$). See also legend of Figure 3.6.

3.5 Broken Ridge - Site 1142

Site 1142 is located on the Broken Ridge, ~ 1600 km north of the Kerguelen Plateau. This narrow oceanic plateau was separated during the Early Tertiary from the Kerguelen Plateau. At Site 1142, 50.9 m of basement penetration recovered six units. They include a diverse range of lithologies, including olivine-phyric basalt lava flows, possible pillow basalts, subaerial deeply weathered lavas, and volcanoclastic sediments. Some units are relatively massive, slightly altered basalt, whereas other volcanic units are variably brecciated by both volcanic and tectonic processes and have been completely altered to clay.

Inch-cores have been taken from the less altered parts of Site 1142. Hence, only lithologic unit 1 (2 m thick, slightly altered, massive, fine-grained basalt) and Unit 6 (10 m thick, fine-grained basalts with some alteration features) have been sampled, whereas units 2 to 5 have been excluded from sampling (completely altered basalt, claystone, breccia).

All basement rocks from Site 1142 are normally magnetized. Seismic reflection data indicate that to the north of the bathymetric crest of Broken Ridge, prebreakup sediment and igneous basement dip consistently to the north. As the real amount of dipping is unknown, it was not possible to interpret the characteristic remanent magnetization for paleolatitudes. No paleolatitude could be determined for the Broken Ridge. However, Table 3.5 lists mean inclination values from the two sampled lava flows from Site 1142, without tectonic corrections. Due to tectonic dipping, the inclinations are shallower than expected for basalts from the Broken Ridge, which at the time of its formation has been close to the central Kerguelen Plateau.

Unit number	N/n	Inc [°]	k	α_{95} [°]
1	6/5	-11.3	203	4.1
2	12/10	-23.0	114	3.8

Table 3.5: Paleodirectional results from the Broken Ridge. For the two sampled lava flows, the mean inclinations, as well as the precision parameter k and α_{95} is shown. Also given is the number of samples treated (N) versus the number of samples used (n) for calculating the mean direction.

3.6 Previous paleomagnetic investigations

So far, paleomagnetic investigations on basalts produced by the Kerguelen hotspot have been performed on the Kerguelen Island, on the Ninety-East Ridge during ODP Leg 121, on the southern Kerguelen Plateau during ODP Leg 120 and on the Rajmahal trap basalts

location	Kerguelen Island	Ninetyeast Ridge Site 756	Ninetyeast Ridge Site 758	Kerguelen Plateau Site 748	Kerguelen Plateau Site 749	Rajmahal Traps
age [Ma]	20-22 [⊕]	43.3 [⊕]	81.9 [⊕]	100 [♣]	100-115 ^{♣†}	117 [⊕]
inc	-65.5°	62.1°	-64°	-63°	-62°	-65°
inc _{max}	-69.9°	66°	-66.9°		-66°	-67.5°
inc _{min}	-61.1°	57.8°	-59.6°		-58°	-62.5°
n	59	8	22	1	5	48
α_{95}	4.4°		3.7°		4°	2.5°
k	17.4		69		353	85
palat	47.7°	43.4°	45.8°	44.5°	43.2°	47°
palat _{max}	53.8°	48.3°	49.5°		48.3°	50.4°
palat _{min}	42.2°	38.5°	40.4°		38.7°	43.8°
reference	Henry and Plessard (1997)	Klootwijk et al. (1991)	Klootwijk et al. (1991)	Inokuchi and Heider (1992)	Inokuchi and Heider (1992)	Klootwijk (1971)

Table 3.6: Summary of paleolatitudes determined from characteristic inclinations of basaltic lava flows in previous studies for the Kerguelen Plateau, the Rajmahal traps and the Ninetyeast Ridge. n: Number of flows or sites; inc: inclination; paleolat: paleolatitude; k: precisions-parameter; palat: paleolatitude. Ages determined with $^{40}\text{Ar}/^{39}\text{Ar}$ ([⊕]), K/Ar ([♣]) or with biostratigraphy ([†]).

in northeastern India. Table 3.6 summarizes the paleodirectional information obtained in these previous studies.

The most recent paleolatitude estimate for the position of the Kerguelen hotspot around 21 Ma comes from Kerguelen Island. *Henry and Plessard* [1997] investigated 32 dated lava flows paleomagnetically and combined their results with previously published data from Kerguelen Island. For the mean direction from 59 lava flows with ages between 20 and 22 Ma they obtain an inclination $I = -65.5^\circ$ with $\alpha_{95} = 1.6^\circ$. The corresponding paleolatitude is $\lambda = 47.7^\circ\text{S}$.

During Leg 121 of the Ocean Drilling Program basaltic basement was drilled along the Ninetyeast Ridge. Eight basalt flows (total thickness of 78 m) were sampled at Site 756 in the southern part of the Ridge which have an age of 43 Ma and a mean inclination of $I = +62.1^\circ$ [*Klootwijk et al.*, 1991], corresponding to a paleolatitude of $\lambda = 43.4^\circ\text{S}$. Site 758 lies at the northern end of the Ninetyeast Ridge and drilled basement consists of 81.9 Ma old basalts. From the ChRM of the 22 drilled basalt flows (total thickness of 182 m), a mean inclination of -64° was determined, which corresponds to a paleolatitude of $\lambda = 45.8^\circ\text{S}$.

Four basement sites were drilled during ODP Leg 120 on the Kerguelen Plateau. The mean directions of the characteristic remanent magnetization of Sites 747-750 were determined by *Inokuchi and Heider* [1992]. The mean inclination from 13 lava flows of Site 747 is -51° which is 11° shallower than the inclinations at Sites 748 and 749. This shallow inclination is most likely due to north-ward tilting of the basement at Site 747, which can

be seen in the seismic reflection profiles [Munschy *et al.*, 1992]. The mean inclination of 5 basalt flows from Site 749 on the southern Kerguelen Plateau is -62° which translates into a paleolatitude of 43.2°S ($+5.1^\circ, -4.5^\circ$). This result is supported by one lava flow of similar age at Site 748 which yields a paleolatitude of 44.5°S . The paleomagnetic samples from the two flows at Site 750 had unstable magnetizations and the few that could be interpreted had been remagnetized in the present field [Inokuchi and Heider, 1992].

Klootwijk [1971] carried out a detailed paleomagnetic investigation on basalts of the Rajmahal trap and obtained a well constrained mean direction. He combined his results with the data of McDougall and McElhinny [1970] and Radhakrishnamurthy [1970] from the Rajmahal traps and arrived at a mean inclination of -65° (paleolatitude 47°S , max: 50.4°S , min: 43.8°S) based on 48 Sites.

3.7 Implications on the paleolatitudes of the Kerguelen hotspot

The main stimulation for the paleomagnetic investigations of the basalts from the Kerguelen Plateau came from the question about hotspot motion. If a hotspot does not move with time relative to the spin axis of the Earth, all paleolatitudes of its products should mirror the present-day and ancient latitude of the hotspot's position. As the Kerguelen Plateau is a product of the Kerguelen hotspot, its paleolatitude should mirror the latitude of the Kerguelen hotspot, which is at 49°S .

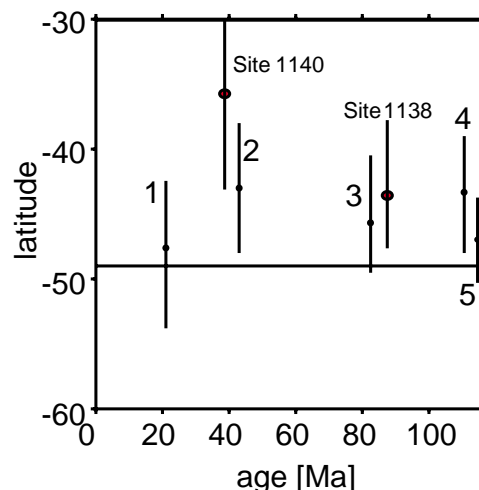


Figure 3.12: Overview over the paleomagnetically determined paleolatitudes for the Kerguelen hotspot versus age. The horizontal line at 49° represents the present-day latitude of the Kerguelen hotspot. Dots are paleolatitudes from paleomagnetic investigations, vertical lines show their error bars. 1: Kerguelen Island; 2, 3: Ninetyeast Ridge; 4: southern Kerguelen Plateau; 5: Rajmahal traps.

Figure 3.12 shows previous paleomagnetic investigations (section 3.6) and new ob-

tained paleolatitudes for the central Kerguelen Plateau (section 3.3) and northern Kerguelen Plateau (section 3.4), compared to the 49°S of the actual position of the Kerguelen hotspot.

For the most recent paleolatitude of the Kerguelen hotspot at approximately 20 Ma, 49°S is clearly within the error bar of the paleolatitude. The α_{95} limit from the paleolatitude of Site 758 from the Ninetyeast Ridge and from the Rajmahal traps also intersect with the present-day position of the Kerguelen hotspot. All the other paleomagnetically obtained paleolatitudes lie (even outside the α_{95} limit) further north at slightly shallower southerly latitudes than the present-day position of the hotspot at 49°S. The difference is between four and ten degrees. If the present-day position of the hotspot is assumed to be underneath Heard Island (latitude 52.5°S), the discrepancy even increases.

In the following two chapters (chapter 4 and chapter 5) two explanations for the discrepancy between present-day position of the hotspot and the paleomagnetic data are presented. True polar wander and hotspot motion will be introduced and their effect on the paleolatitudes of hotspots will be discussed.

Chapter 4

Paleolatitudes of the Kerguelen hotspot: True polar wander

True polar wander (TPW) is generally understood as the drift of the Earth's mantle as a whole (or some reference frame fixed in the Earth) with respect to the spin axis. TPW changes the position of the Earth's mantle (with the hotspots) relative to the rotation axis (which coincides with the dipole axis of the Earth's magnetic field when averaged over several thousand years). In this way, TPW will affect the paleolatitudes of hotspots. There are different opinions about the magnitude of TPW during the last 200 Ma. In this chapter, TPW and reference frames will be introduced, the TPW discussion summarized and possible effects of TPW on the position of the Kerguelen hotspot shown.

4.1 True polar wander and reference frames

Assuming stationary hotspots with respect to the Earth's mantle, the volcanic traces left by hotspots in the lithosphere record the histories of plate motions over the lower mantle. This *mantle reference frame* is independent of the *paleomagnetic reference frame*, which is defined by the dipole or spin axis of the Earth. Differential motion between the mantle and the spin axis can be determined by comparing plate motions recorded in these two reference frames. Such motion has been termed true polar wander [e.g. *Duncan and Richards*, 1991; *Courtilot and Besse*, 1987]. True polar wander may have its origin in redistribution of mass within the Earth through processes such as mantle convection and plate motions, which can change the Earth's moments of inertia [*Goldreich and Toomre*, 1969].

Generally, TPW can be determined by comparison of plate motion in the paleomagnetic reference system and plate motion in the hotspot-based mantle reference system. This has been done by several authors, most recently by *Prévot et al.* [2000], *Besse* [2000] and *Besse and Courtilot* [1991]. In a first step, they transferred worldwide reliable paleo-

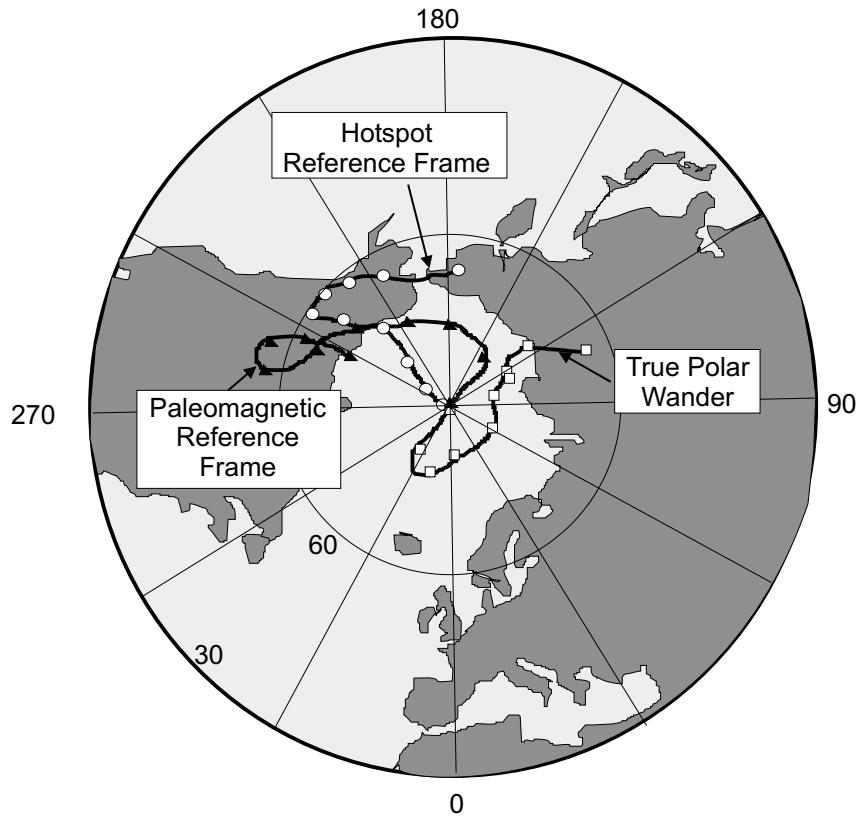


Figure 4.1: Comparison of the paleomagnetic apparent polar wander path (black triangles, which are paleomagnetic pole positions for all plates rotated to the African plate) with the path deduced from the hotspot reference frame (white circles). True polar wander (white squares) is calculated by subtracting one from the other; this represents global motion of the mantle with respect to the Earth's spin axis. Points on each curve are 20 Ma increments, from 200 Ma to the present. Confidence intervals of 95% (not shown) are of the order of 4° (from *Courtillot and Besse* [1987] and *Besse and Courtillot* [1991]).

magnetic data from all continents onto one single plate, usually the African plate. For the transfer, poles of relative plate rotation, determined from marine magnetic anomalies, are used. This results in the apparent motion of the geomagnetic pole with respect to an observer on the African plate. The apparent motion of the hotspot reference frame with respect to Africa can also be described by a polar wander path. The differences of these two paths, which is defined as true polar wander, can be obtained by subtracting one curve from the other (Figure 4.1). *Besse and Courtillot* [1991] determined a global true polar wander curve for the last 200 Ma from a comparison of plate motion in the two different reference systems. Figure 4.1 shows their results: the path indicated by triangles represents the motion of the magnetic pole relative to Africa; the path indicated by circles represents the motion of a hypothetical hotspot at the pole relative to Africa (or the motion of the hotspot reference frame relative to Africa); while finally the path indicated by squares represents the difference between the two previous paths, which is the motion of a hotspot relative to the pole and, hence, the true polar wander path.

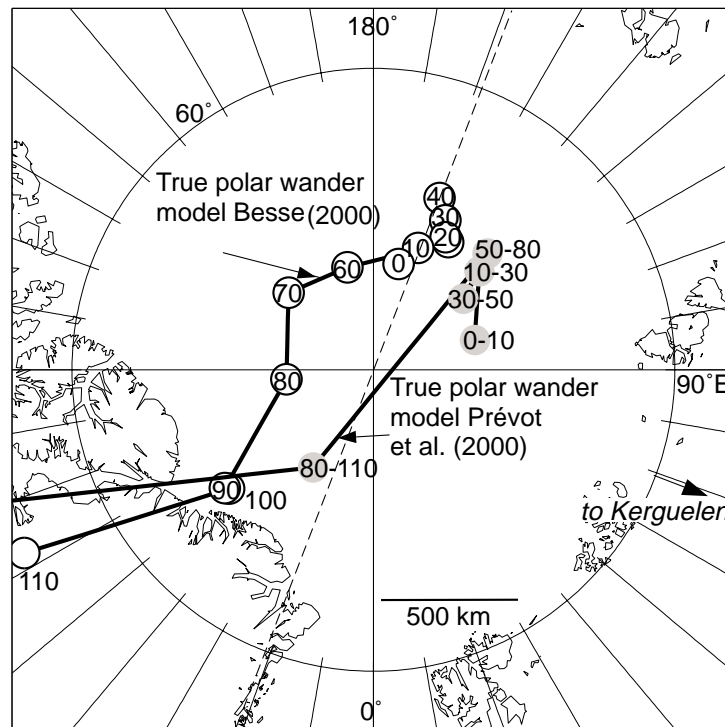


Figure 4.2: Polar wander in the hotspot reference frame from the data of *Besse* [2000] and *Prévot et al.* [2000]. An arrow pointing toward the direction of Kerguelen and a dashed line at a right angle to that arrow is shown. The distances between this dashed line and the polar wander curves approximately give the contributions of polar motion to changes in the hotspot's paleolatitudes. Confidence intervals of 95% are not shown but in the order of 4° . This Figure differs from Figure 4.1 in so far that here the motion of the pole relative to the hotspot reference system is shown. This explains the rotation of 180° compared to the true polar wander path of Figure 4.1.

The determination of true polar wander is based on the assumption of hotspot fixity. Preliminary calculations [*Steinberger, 2000a*] have, however, shown that taking into account moving hotspots does not fundamentally change the true polar wander curves.

Besse [2000] recently revised their TPW curve (Figure 4.2). His new TPW curve is roughly consistent in shape and magnitude with the one from *Prévot et al.* [2000], who used a new rigorously selected paleomagnetic database gathering only directions obtained from magmatic rocks. However, *Besse* [2000] presents his true polar wander curve with gradual motion, while *Prévot et al.* [2000] suggests a sudden motion of the pole. Both authors find that TPW has been less than $\sim 5^\circ$ for the last 80 Ma (Figure 4.2). They also suggest a period of shifting between 80 and approximately 150 Ma (and therefore at the time of the formation of the southern and central Kerguelen Plateau), representing a 18° shift of the entire Earth.

Instead, *Tarduno and Smirnov* [2001] examined Cretaceous data from North America derived from granitic rocks. These were excluded in the analysis of *Prévot et al.* [2000]. Their analysis suggest that the time-averaged position of the spin axis has deviated by

no more than $\sim 5^\circ$ over the last 130 Ma. In this case, there would be no significant contribution of TPW to changes in paleolatitudes of a hotspot.

4.2 Effects of true polar wander on the Kerguelen hotspot

Assuming stationary hotspots and the absence of true polar wander, mantle plumes do not move with respect to the geomagnetic (or spin) axis. On the contrary, true polar wander would change the paleolatitude of the hotspot with time relative to the spin axis.

The effect of true polar wander on the paleolatitudes of the Kerguelen hotspot can be determined from the TPW paths: in Figure 4.2, an arrow is pointing in direction of the Kerguelen hotspot. A perpendicular line to this arrow as approximation of the great circle through pole and position of the Kerguelen hotspot is shown. The distances between this line and the polar wander curve gives approximately the contribution of polar motion to changes in the paleolatitudes of the Kerguelen hotspot.

Figure 4.3 shows the exactly determined effect of TPW on the paleolatitudes of the Kerguelen hotspot for the different TPW paths. The horizontal line in Figure 4.3 gives the present-day latitude of the hotspot (49°S). The dashed lines represent the latitude of the hotspot versus time, with consideration of the TPW effect. The vertical signs indicate the paleomagnetically determined paleolatitudes for the Kerguelen hotspot, that are discussed in chapter 3.

The dataset from *Besse and Courtillot* [1991] would result in paleolatitudes for the Kerguelen hotspot further north for 0-60 Ma and in paleolatitudes further south for 60-110 Ma compared to the present-day latitude of the hotspot. The two recent TPW curves [*Besse*, 2000; *Prérot et al.*, 2000] consist mostly of one dominant TPW event at approximately 100 Ma, that results in a shifting of $\sim 10^\circ$ for the paleolatitudes of the Kerguelen hotspot. All three datasets, however, are consistent in so far that the latitudes in the early phase of the hotspot activity at approximately 110 Ma ago are further south than the present-day latitude (55°S - 61°S compared to 49°S). Paleomagnetic results from the parts of the Kerguelen Plateau formed at that time (southern and central Kerguelen Plateau) should therefore give paleolatitudes which are further south than the present-day position of the hotspot. Instead, as can be seen in Figure 4.3, paleomagnetic data indicate paleolatitudes that are further north. The discrepancy between paleomagnetic results and effects of TPW is greatest with the data of *Besse and Courtillot* [1991].

Clearly, the difference between present-day position and paleomagnetic result cannot be explained with the TPW paths. Taking TPW as suggested by *Besse and Courtillot* [1991], *Besse* [2000] and *Prérot et al.* [2000] into account, the difference even increases. This leads to the following possible conclusions:

(1) The TPW paths as determined by *Besse and Courtillot* [1991], *Besse* [2000] and *Prévot et al.* [2000] are not correct and a correct true polar wander path would be just opposite to their determined path so that the difference between present-day position and paleomagnetic results could be explained. However, an independent study by *Steinberger and O'Connell* [1997] confirms the paleomagnetically obtained true polar wander paths. *Steinberger and O'Connell* [1997] calculate the true polar wander back in time with numerical models for the redistribution of mass in the mantle of the Earth.

(2) there must be another explanation for the difference of paleolatitudes and present-day position of the Kerguelen hotspot. This puzzle could be resolved by *hotspot motion*, which is discussed in the following chapter. If TPW is not significant, as suggested by *Tarduno and Smirnov* [2001] hotspot motion could be the only reason for the difference.

(3) Hotspot motion can occur together with true polar wander and their overlapping effect could bias the latitude of the hotspot.

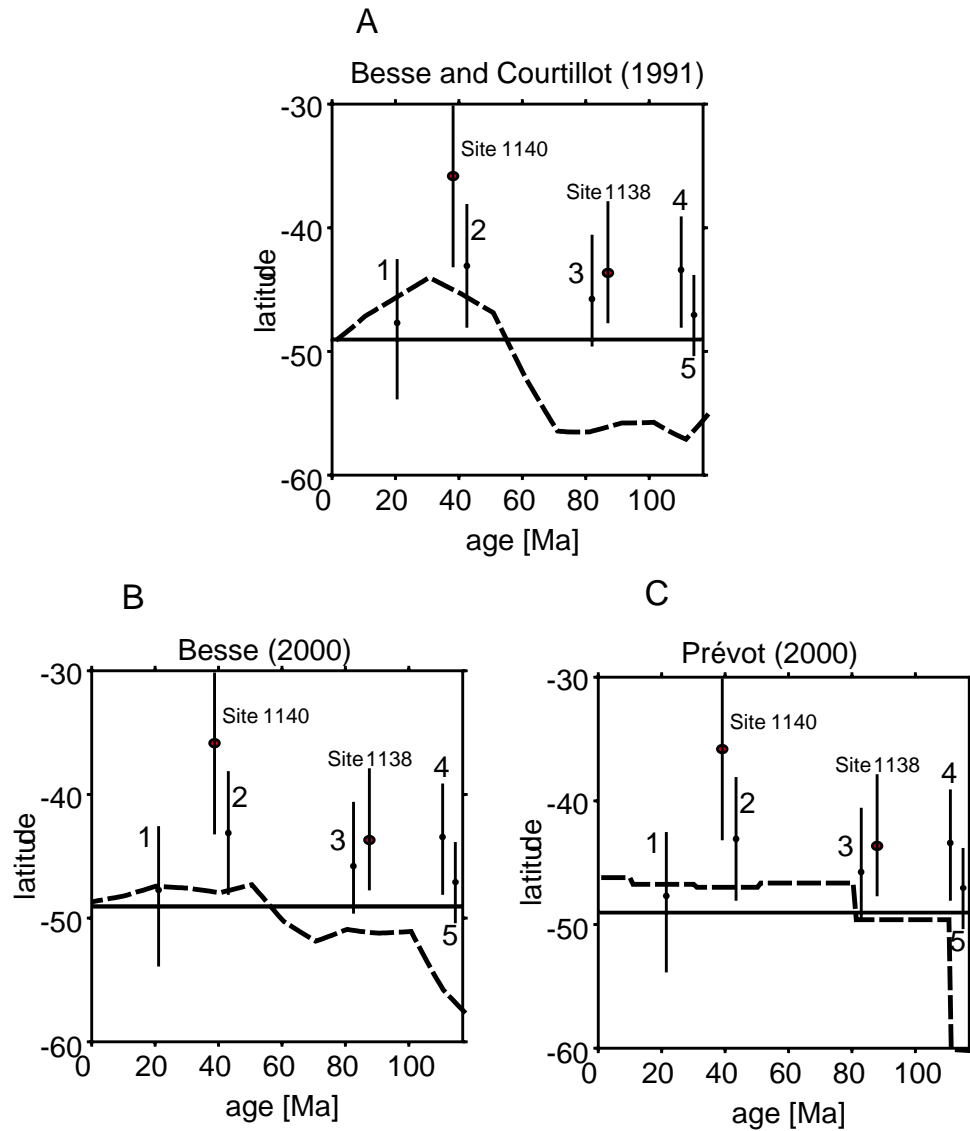


Figure 4.3: The effect of TPW on the paleolatitude of the Kerguelen hotspot versus time is shown for the different TPW paths (dashed lines). The horizontal solid line at 49°S indicates the present-day latitude of the Kerguelen hotspot, dots and vertical lines represent paleomagnetic paleolatitudes as discussed in chapter 3. A.: Effects due to TPW from *Besse and Courtillot* [1991], B.: effects due to TPW from *Besse* [2000], C.: effects due to TPW from *Prévot et al.* [2000]. Paleomagnetic data from 1: Kerguelen Island; 2, 3: Ninetyeast Ridge; 4: southern Kerguelen Plateau; 5: Rajmahal Traps; and from Sites 1140 and 1138.

Chapter 5

Paleolatitudes of the Kerguelen hotspot: hotspot motion and modeling results

In the previous chapters, paleolatitudes from the Kerguelen Plateau were determined using paleomagnetic data (chapter 3) and prediction of paleolatitudes of the Kerguelen hotspot were made using true polar wander paths (chapter 4). Paleolatitudes of a hotspot could also be biased by hotspot motion. The drift of hotspots in a convecting mantle will be discussed in this chapter. The possible motion of the Kerguelen hotspot since its origin approximately 117 Ma ago will be modeled and the resulting hotspot drift will be used to predict the hotspot's paleolatitudes.

5.1 Hotspot motion or hotspot stability?

Wilson [1965] was the first to recognize that certain chains of volcanic islands such as Hawai'i show a progressive increase in age in the direction of plate motion and seem to be tracks originating from localized hotspots in the mantle beneath the plate. He stated that these volcanic island chains are formed when the plate moves across such a hotspot. *Morgan* [1971] recognized that the various hotspot tracks on the Pacific plate can be explained by assuming that the hotspots are fixed relative to one another. He introduced the concept of deeply anchored mantle plumes. Since then, hotspots are commonly seen as fixed points to which absolute plate motion can be referred and they are used as a reference frame for plate reconstructions.

However, a direct test of moving hotspots has first been made by *Molnar and Stock* [1987]. They show results of a detailed comparison between the tracks of Hawai'i and hotspots in other oceans with their predicted tracks, calculated using the fixity assumption and relative plate motions. They found systematic displacements between Hawai'i and

the other hotspots (Iceland and Tristan de Cunha in the Atlantic; Reunion, St Paul's and Kerguelen in the Indian Ocean). The results indicate a southwards drift of the Hawai'ian hotspot. This southward drift is furthermore consistent with paleomagnetic results of *Sager and Bleil* [1987] and *Tarduno and Cottrell* [1997]. These paleomagnetic studies give paleolatitudes from the Hawai'ian seamounts, that are too far north for the present-day position of the hotspot, indicating a southward motion and, hence, agree with the results of *Molnar and Stock* [1987].

Hotspots are thought to have their origin deep in the lower mantle, probably above the core-mantle boundary in the D'' layer. According to the fixed hotspot hypothesis, the mantle conduit of the hotspot would rise with constant shape and would be stationary through the convecting mantle of the Earth. However, much of the return convective flow that balances plate motion is thought to occur in the lower mantle. It can therefore not be the immobile basic layer through which fixed plumes rise. *Steinberger and O'Connell* [1998] calculated a global mantle-circulation model for the past, using buoyancy forces inferred from seismic tomographic anomalies and taking the present and past plate motions as boundary conditions. Then, they inserted plume conduits and calculated how these conduits are advected by the mantle. In the following, their concept will be applied to calculate the motion of the Kerguelen hotspot.

5.2 Methods and theory

Aim of this study is to calculate the motion of the Kerguelen hotspot using numerical methods. The method has been developed by *Steinberger and O'Connell* [1998] and has been extended and advanced in this thesis. Here it will be applied specifically for calculation of the Kerguelen hotspot motion. Supplementary to *Steinberger and O'Connell* [1998], several new density models and a new viscosity model for the Earth's mantle as well as a new viscosity structure for the rising plume will be used for the calculations of the hotspot drift. Figure 5.1 summarizes the proceeding for calculation of the hotspot motion, which is described in the following.

In a first step, a large-scale flow field for the Earth's mantle must be calculated. Seismic tomography models for the Earth's mantle are used as input to obtain the flow fields (Figure 5.1A - B). First, the seismic s-wave velocity anomalies ($\delta v_s/v_s$) are converted into density heterogeneities ($\delta\rho/\rho$). For the tomographic models, a conversion factor $(\delta\rho/\rho)/(\delta v_s/v_s) = 0.2$ from seismic velocity to density heterogeneities has been used. This value is inferred from geoid modeling [e.g. *Forte et al.*, 1993] and from laboratory experiments [*Karato*, 1993]. Then, the method of *Hager and O'Connell* [1979, 1981] is used to obtain a flow field: the internal driving forces (hot mantle material is rising, cold material is sinking) are inferred from the density heterogeneities and provide the flow field (Figure 5.1B - C). Different seismic tomographic models provide different density

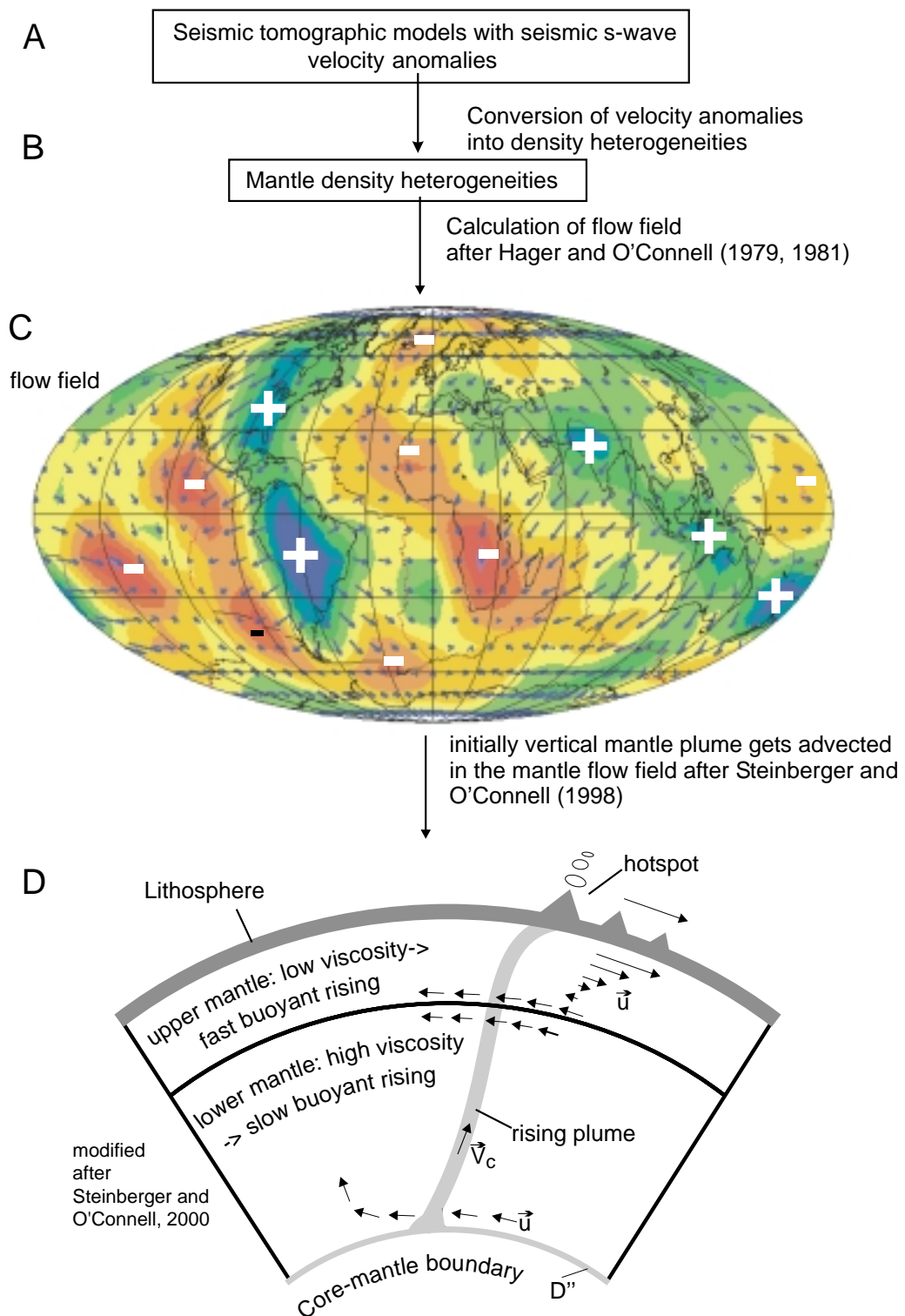


Figure 5.1: The proceeding for modeling the hotspot motion. A: first, the anomalies of a seismic tomographic model are converted into density heterogeneities (B). The internal driving forces inferred from the density heterogeneities provide a flow field for the Earth's mantle, represented schematically by arrows for a depth just above the D'' layer. "+" indicates positive density anomalies, "-" indicates negative density anomalies (C). D: finally, an initially vertical mantle plume with its origin at the core-mantle boundary is inserted, and its advection in the convecting mantle calculated. This results -on the Earth's surface- as a hotspot motion.

models for the Earth's mantle, and hence several mantle flow fields are available for the calculation of the plume advection. The flow fields also depend on the viscosity structure of the mantle. Two different viscosity structures will be used here for comparison.

The mantle flow that can be calculated after conversion of the seismic velocity into density anomalies is time-dependent. First, plate motion changes with time, and as the plate motion is a boundary condition for the model, it influences the mantle flow with time. Second, the flow field carries the internal density anomalies to new positions. Hence, the flow field can be used to advect the density field backward in time [*Steinberger and O'Connell*, 1998, 1997].

Finally, an initially vertical plume conduit is inserted in the calculated large-scale mantle flow. The assumption of an initially vertical plume can be justified because the large head of a plume rising from D'' would rise much faster than the narrow conduit [*Steinberger*, 2000a]. For the Kerguelen hotspot, the Rajmahal Traps and the southern Kerguelen Plateau are the oldest products associated with the hotspot. Hence, their age of approximately 117 Ma is chosen as the age of the initial vertical conduit. The conduit is then advected and distorted in the mantle's flow field (Figure 5.1D). The advection of the conduit in the convecting mantle results on the Earth's surface as a hotspot motion.

In this simplified model, the rising mantle conduit is advected in large-scale mantle flow (flow velocity \vec{u}), and the conduit elements rise buoyantly through the surrounding viscous mantle (buoyant Stokes rising speed \vec{v}_c). The total velocity of each conduit element is the vector sum of flow velocity \vec{u} and rising velocity \vec{v}_c .

The viscosity structure of the mantle which is needed for the calculation of hotspot motion is usually inferred from models of postglacial rebound and the geoid. However, none of these methods can constrain details of mantle viscosity structure so that considerable uncertainties remain. For some of the calculations for the Kerguelen hotspot, the viscosity model as in *Steinberger and O'Connell* [1998] has been used. Another viscosity model [*Steinberger and Calderwood*, 2001] is able to explain the geoid with a variance reduction of 72% for a density field based on the tomography model of *Masters et al.* [2000]. This new model differs only in the lowermost mantle significantly from the one used in *Steinberger and O'Connell* [1998]. Both viscosity models have been used for the calculations of the Kerguelen hotspot drift. However, the results when using the two different viscosity structures do not differ significantly (Figure 5.2).

The anomalous mass flux B of a plume conduit is defined as volume flux times difference of density inside and outside the conduit. B is needed for the modeling of a rising mantle conduit and has been determined for various hotspots based on the magnitudes of associated topographic swells. The uncertainty of B for the Kerguelen hotspot is large [*Sleep*, 1990]; in this work an arithmetic mean of determinations by *Sleep* [1990], *Davies* [1988] and *Schilling* [1991] that provides a value $B = 0.9 \cdot 10^3 \text{kg/s}$ has been used. However, variation of B does not significantly bias the calculated hotspot motion, as shown in sec-

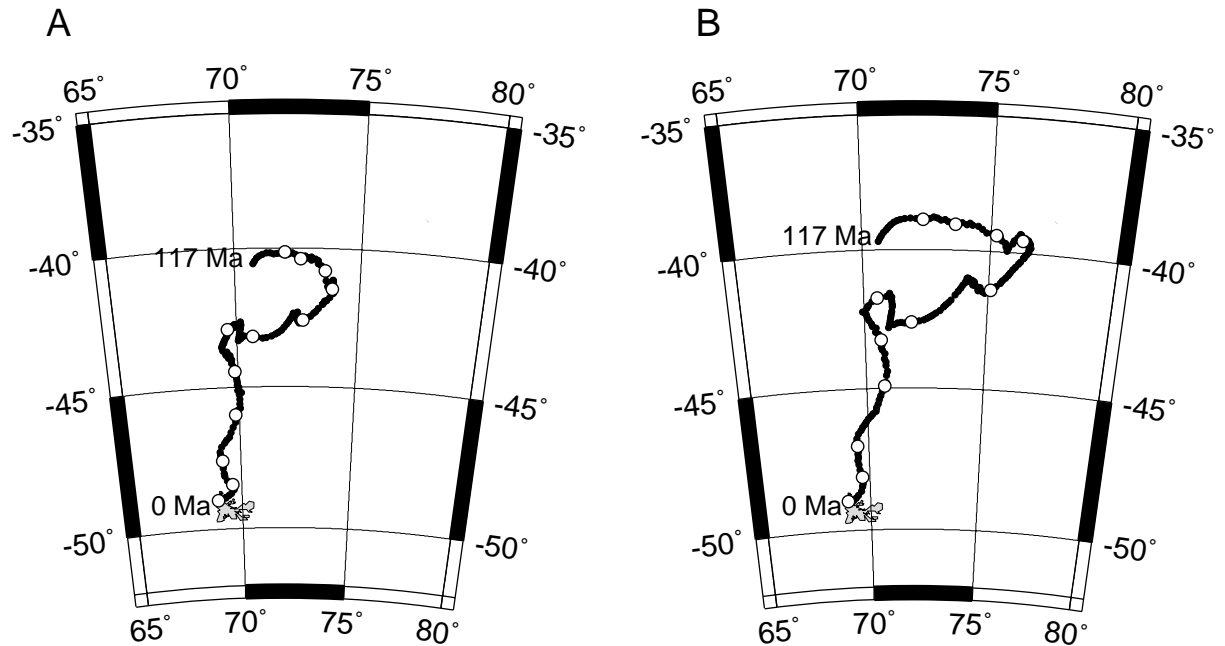


Figure 5.2: Motion of the Kerguelen hotspot using the tomographic model of *Masters et al.* [2000] and the viscosity structure for the Earth's mantle of A: as in *Steinberger and O'Connell* [1998]; B: *Steinberger and Calderwood* [2001]. The present-day hotspot position (0 Ma) is underneath Kerguelen Island at 49°S, 69°E. The motion is calculated for the last 117 Ma. White circles are set every 10 Ma. Resulting hotspot motion is very similar for both viscosity structures.

tion 5.6. For comparison, the Hawai'ian hotspot is the largest hotspot with an anomalous mass flux of $B = 8 \cdot 10^3 \text{kg/s}$.

5.3 A new viscosity structure for the rising plume

One problem when modeling the rising of a plume in a convecting mantle is the change of viscosity within the plume. The calculations of hotspot motion with the program of *Steinberger and O'Connell* [1998] use a constant viscosity in the rising plume. It was not accounted for pressure- and temperature-dependent viscosity inside the plume conduit and heat loss to the surrounding mantle during the rising of the plume. Viscosity is temperature-dependent and increases with decreasing temperature at constant pressure.

With increasing distance from the core-mantle boundary, the temperature difference from the plume to the surrounding mantle (ΔT) will decrease, and hence, the difference in viscosity from plume to mantle will decrease. Because the radius of the rising plume is depending on the viscosity inside the conduit, it will also change with depth. A mantle plume with larger radius is behaving more stable in the flowing mantle, it will rise faster which means that the advection by the mantle will play a less important role compared to the buoyant rising. For taking this effect into account, the program of *Steinberger and*

O'Connell [1998] was supplemented with a subroutine, that accounts for the changes of viscosity with temperature.

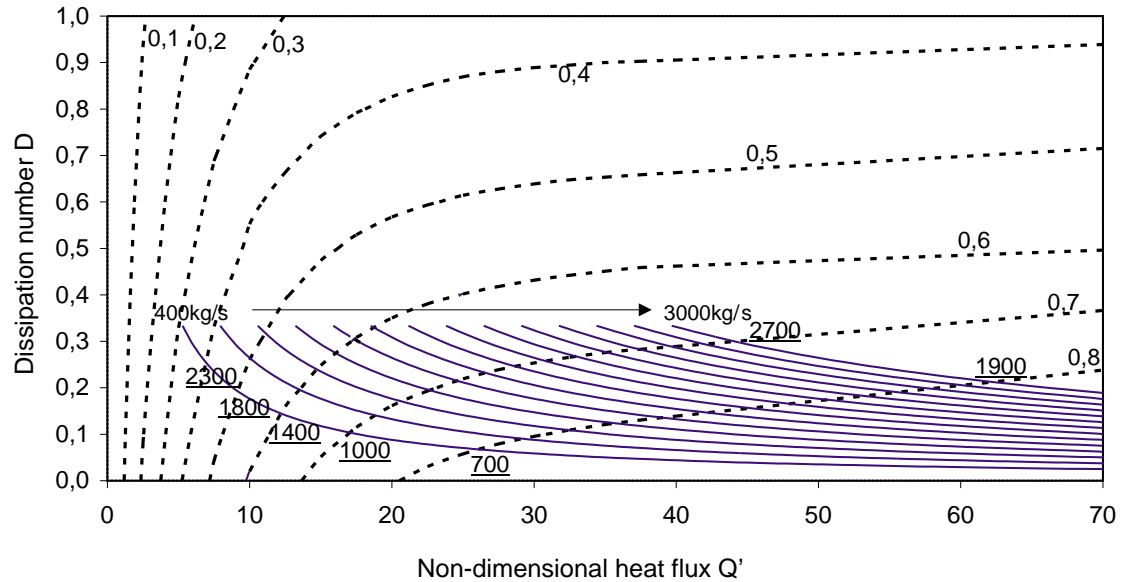


Figure 5.3: Dotted lines: variation of the temperature within a plume relative to the initial temperature anomaly at the core-mantle boundary ($\Delta T/\Delta T_{CMB}$) as function of the non-dimensional heat flux $Q' = Q/(\rho c_p \kappa h \Delta T)$ and of the dissipation number $D = \alpha g h / c_p$ (from *Albers and Christensen* [1996]). Indices for the dotted lines indicate the relative variation in temperature. Standard values are used for the remaining parameters. Solid lines: Variation of Q and D as function of depth for different anomalous mass fluxes (from 400 kg/s to 3000 kg/s in 200 kg/s - steps). Underlined numbers indicate the height above the core-mantle boundary (km) for the mass fluxes of 400 and 3000 kg/s, where a relative variation in temperature anomaly has been reached.

$\alpha = 1.5 \cdot 10^{-5} \text{K}^{-1}$	thermal expansivity
$\kappa = 0.1 \cdot 10^{-5} \text{m}^2/\text{s}$	thermal diffusivity
$\rho = 4500 \text{kg}/\text{m}^3$	density
$c_p = 1260 \text{J}/(\text{kg} \cdot \text{K})$	thermal conductivity
$g = 10 \text{m}/\text{s}^2$	gravity acceleration

Table 5.1: Standard values for model parameters, according to *Olson et al.* [1993], *Osako and Ito* [1991] and *Loper and Stacey* [1983].

The first step in the subroutine is the determination of the temperature anomaly in the plume (or the temperature difference between plume and surrounding mantle) ΔT as a function of depth. The variation of the temperature in a rising plume is independent from the variation of viscosity or other material parameters [*Albers and Christensen*, 1996]. It is, however, determined by the initial temperature anomaly at the core-mantle boundary

ΔT_{CMB} , by the heat flux Q in the plume and by the dissipation number D [Albers and Christensen, 1996].

The influence of these parameters are summarized in Figure 5.3. The dotted lines in Figure 5.3 represent the relative decrease of an initial temperature anomaly. At the same time these relative temperature decreases are a function of D and Q . The relationship between D , Q and relative temperature decrease $\Delta T/\Delta T_{CMB}$ is independent from the height h above the core-mantle boundary [Albers and Christensen, 1996]. However, the non dimensional heat flux $Q' = Q/\rho c_p \kappa h \Delta T$ and the dissipation number $D = \alpha g h / c_p$ are both, besides of the parameters shown in Table 5.1, a function of the height h above the core-mantle boundary. In addition, Q can be written as $Q = B c_p / \alpha$.

With these relationships and the standard parameters listed in Table 5.1, Q and D are determined as function of the height h and of the anomalous mass flux B . In Figure 5.3, the solid lines show this relation for several mass fluxes B (from 400 kg/s to 3000 kg/s in 200 kg/s - steps). Following one of these lines from right to left, the distance to the core-mantle boundary increases and the temperature anomaly in the plume decreases. These relations are used in the subroutine to determine the temperature anomaly of the plume as a function of height.

Next, the ratio between viscosity within the plume and outside the plume is calculated. The following estimation has been applied:

The viscosity law for a Newtonian flow is [e.g. Turcotte and Schubert, 1982]:

$$\eta = A \exp\left(\frac{E + pV}{RT}\right) \quad (5.1)$$

Hence, the ratio between viscosities within the plume (η_{in}) and outside the plume (η_{out}) is:

$$\frac{\eta_{in}}{\eta_{out}} = \exp\left(\frac{E + pV}{R(\Delta T + T)} - \frac{E + pV}{RT}\right) \quad (5.2)$$

After a transformation and an approximation using a Taylor-development follows:

$$\frac{\eta_{in}}{\eta_{out}} = \exp\left(-\frac{E + pV}{RT^2} \Delta T\right) \quad (5.3)$$

In the adiabatic case, the ratio between viscosity inside and outside the plume is assumed to be constant:

$$const = \frac{\eta_{in,ad}}{\eta_{out,ad}} = \exp\left(-\frac{b}{T^2} \Delta T_{ad}\right), \quad (5.4)$$

with $b = \frac{E + pV}{R}$.

For the non-adiabatic case follows:

$$\frac{\eta_{in}}{\eta_{out}} = \exp\left(-\frac{b}{T^2}\Delta T\left(\frac{\Delta T_{ad}}{\Delta T_{ad}}\right)\right) = \text{const}\left(\frac{\Delta T}{\Delta T_{ad}}\right) \quad (5.5)$$

The temperature anomaly for the adiabatic case ΔT_{ad} can be approximately obtained using a very large mass flux and the relationship shown in Figure 5.3. ΔT results from the previous calculations.

The constant (the ratio between the viscosities for an adiabatic case) can be estimated using the behavior of a very large plume like the Hawai'ian plume. The magnitude of the constant is estimated to be of the order of 10^{-3} [Steinberger, 2000a]. However, the estimation is rather uncertain, hence for the calculation of the plume radius (Figure 5.4) and the hotspot motion (section 5.6), different extreme values have been used to test their influence on the results.

Considering the viscosity structure of the mantle that is used for the hotspot motion modeling, it is now possible to calculate the viscosity in the plume depending on the height above the core-mantle boundary.

Next, the radius of the plume depending on the height above the core-mantle boundary can be determined. The estimate for the conduit radius r_c can be made from Poiseuille's formula for a flow in a pipe, which is written as [e.g. Turcotte and Schubert, 1982]:

$$r_c = \left(\frac{8B\eta_{in}}{\pi\Delta\rho dp/dz}\right)^{1/4} \quad (5.6)$$

$\Delta\rho$, the density difference between plume and surroundings, is due to the temperature contrast between plume and surroundings and estimated to be 30 kg/m^3 [Sleep, 1992]. The pressure gradient dp/dz can be estimated assuming that the conduit would be "strangulated", if pressure inside and outside the plume differs strongly. It is not well constrained, but less than a pressure gradient obtained when using the hydrostatic approximation $dp/dz = \Delta\rho g$. This approximation is, however, used for the modeling procedure, but at the same time a balancing *factor for pressure gradient* "fpg" is introduced into the denominator of equation 5.6 to account for a smaller dp/dz . Variation of *fpg* and the effect on the hotspot motion is shown in section 5.6.

The depth-depending radius is shown in Figure 5.4. The radius of a plume does not change significantly when different initial temperature anomalies are assumed, but the assumed viscosity contrast at the base of the conduit is left unchanged. It is, however, stronger dependent on the anomalous mass flux of the plume and on the viscosity contrast on the core-mantle boundary between plume and mantle. The influence of these parameters on the calculated hotspot drift will be shown in section 5.6. The depth-depending radius can now be included in the calculation of the hotspot drift instead of the constant radius that has been used before.

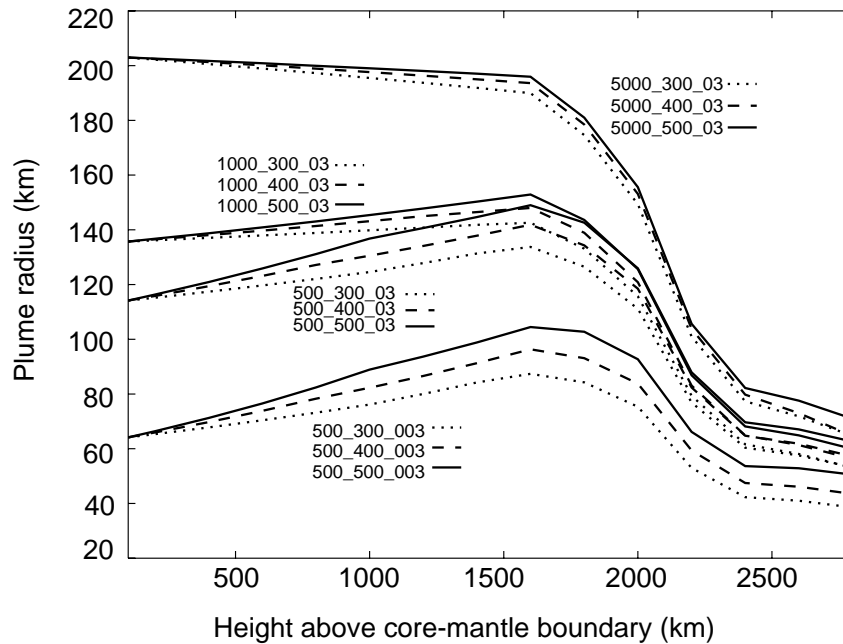


Figure 5.4: Radius of a plume as function of the height above the core-mantle boundary. The radii are calculated for different anomal mass fluxes (first index), different starting temperature anomalies at the core-mantle boundary (second index) and different viscosity contrasts on the core-mantle boundary (third index). For the calculation, the viscosity structure as in *Steinberger and O'Connell* [1998] is used.

In Figure 5.5, the result for hotspot motion for the Kerguelen hotspot based on the tomographic model of *Masters et al.* [2000] and the viscosity model for the mantle of *Steinberger and Calderwood* [2001] is shown. It is a representative example to show the effect of a depth-dependent plume radius on hotspot drift. For the calculation presented in Figure 5.5A, a constant viscosity within the rising plume with a consequently constant plume radius is used. Figure 5.5B shows the result of exactly the same calculation except the viscosity in the plume: here variations of viscosity within the rising plume are assumed. The hotspot motion does not change significantly its mean direction and magnitude. With the new viscosity structure in the plume, however, the shape of the hotspot motion track is affected and shows small changes.

5.4 Results for the Kerguelen hotspot motion and predictions for paleolatitudes

For the calculation of the Kerguelen hotspot motion, the Kerguelen hotspot is assumed to be underneath Kerguelen Island at 49°S and 69°E. The present-day position of the hotspot is possibly farther south underneath Heard Island or underneath the seamounts between Kerguelen and Heard Island [*Coffin and Antretter*, 2001] (see section 5.5). However, when choosing the most northern position of the hotspot (at 49°S), the (then still existing)

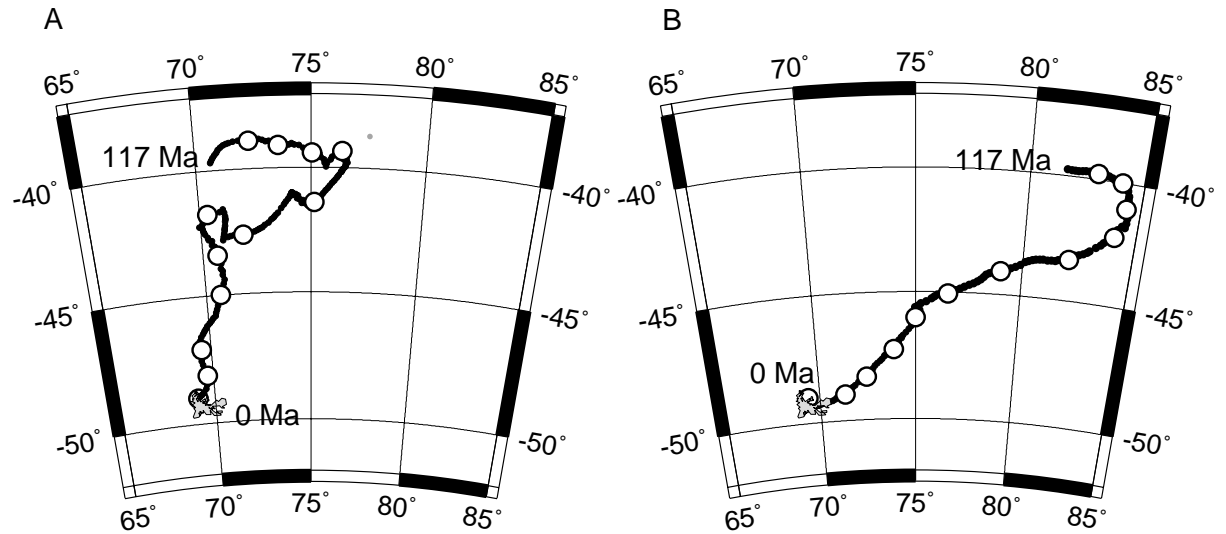


Figure 5.5: A: The motion for the Kerguelen hotspot from 117 Ma ago to the present, calculated with a constant radius in the rising plume and using the tomographic model of *Masters et al.* [2000] and the viscosity model for the mantle of *Steinberger and Calderwood* [2001]. B: The same calculation as in A but with variable viscosity in the rising plume. Input parameters: Starting temperature anomaly $\Delta T_{CMB} = 300^\circ\text{K}$; viscosity contrast at the base $\eta_{in}/\eta_{out} = 0.001$; factor for pressure gradient $fp_g = 0.05$. White circles are set every 10 Ma.

difference between the paleomagnetic data and the present latitude is kept as small as possible.

Several seismic tomographic models have been used to calculate a flow field for the Earth's mantle. The more models are calculated and the more results can be compared, the better is the control over the reliability of the results. For the calculation of the Kerguelen hotspot motion the following tomographic models have been used:

Su et al. [1994]

Li and Romanowicz [1996]

Grand [2001]

Ritsema and Van Heijst [2000]

Mégnin and Romanowicz [2000]

Masters et al. [2000]

Furthermore, one density model has been used that is obtained directly from the slab-distribution within the mantle (slab-model):

Steinberger [2000b]

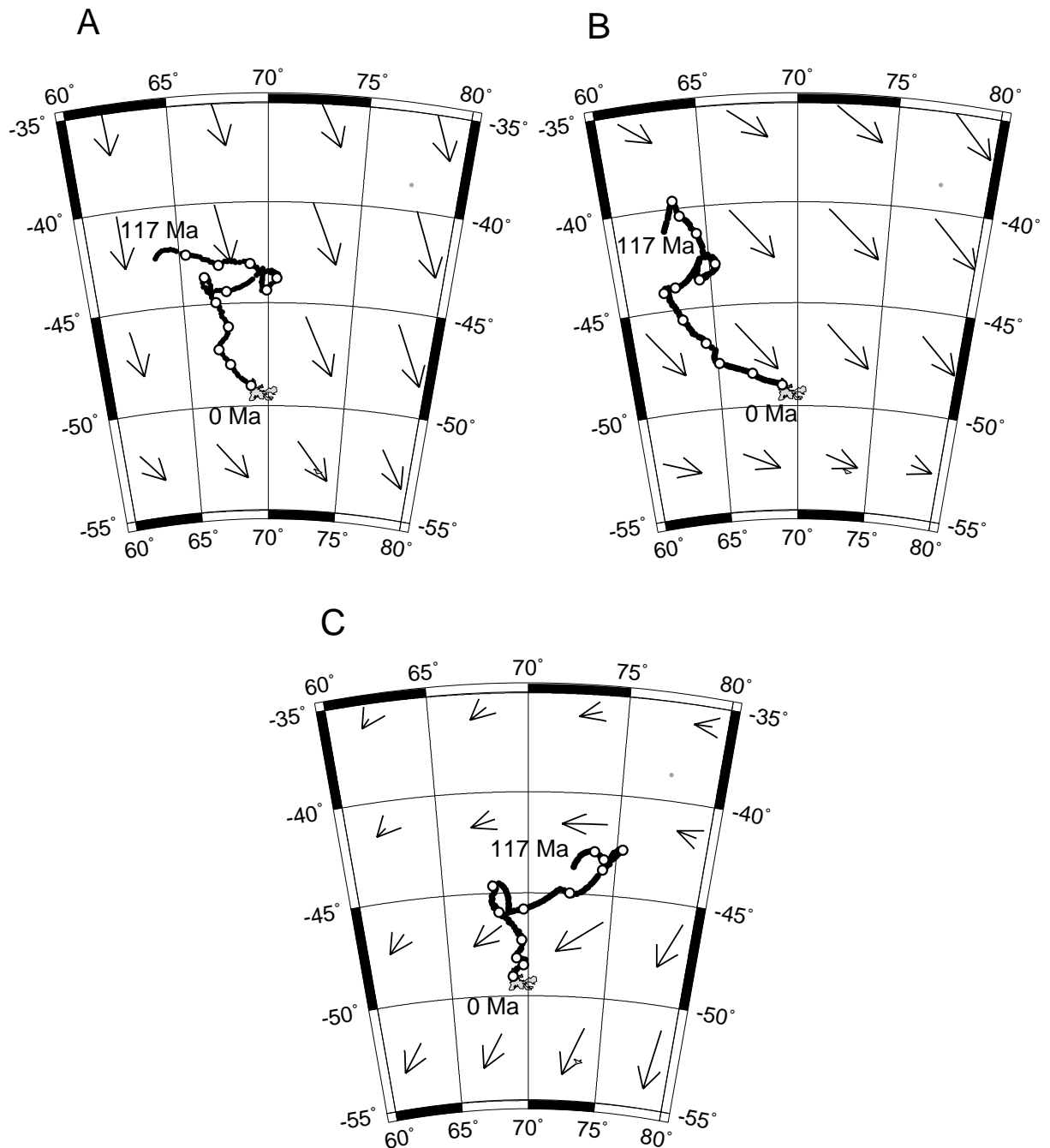


Figure 5.6: Examples for the calculated drift of the Kerguelen hotspot since its origin 117 Myr ago. For the calculation, an initially vertical mantle plume is advected in the velocity field of a convecting mantle *Steinberger and O'Connell [1998]*. The velocity field is calculated from a density model of the mantle. 1 degree arrow length = 1 degree / 40 Ma horizontal flow velocity. Arrows represent the present-day flow at a depth of 670 km. The density models can be obtained due to converted seismic tomographic models (A: *Li and Romanowicz [1996]*; B: *Su et al. [1994]*) or directly due to slab distribution (C: *Steinberger [2000b]*). The calculated position of the hotspot 117 Ma ago is shown in dark color, the supposed present-day position in light color, tick marks are made every 10 Ma. All calculations indicate a southward motion of the Kerguelen hotspot. The amounts are 8° for the slab dependent density model *Steinberger [2000b]* and the tomographic model of *Li and Romanowicz [1996]* and 10° for the tomographic model of *Su et al. [1994]*.

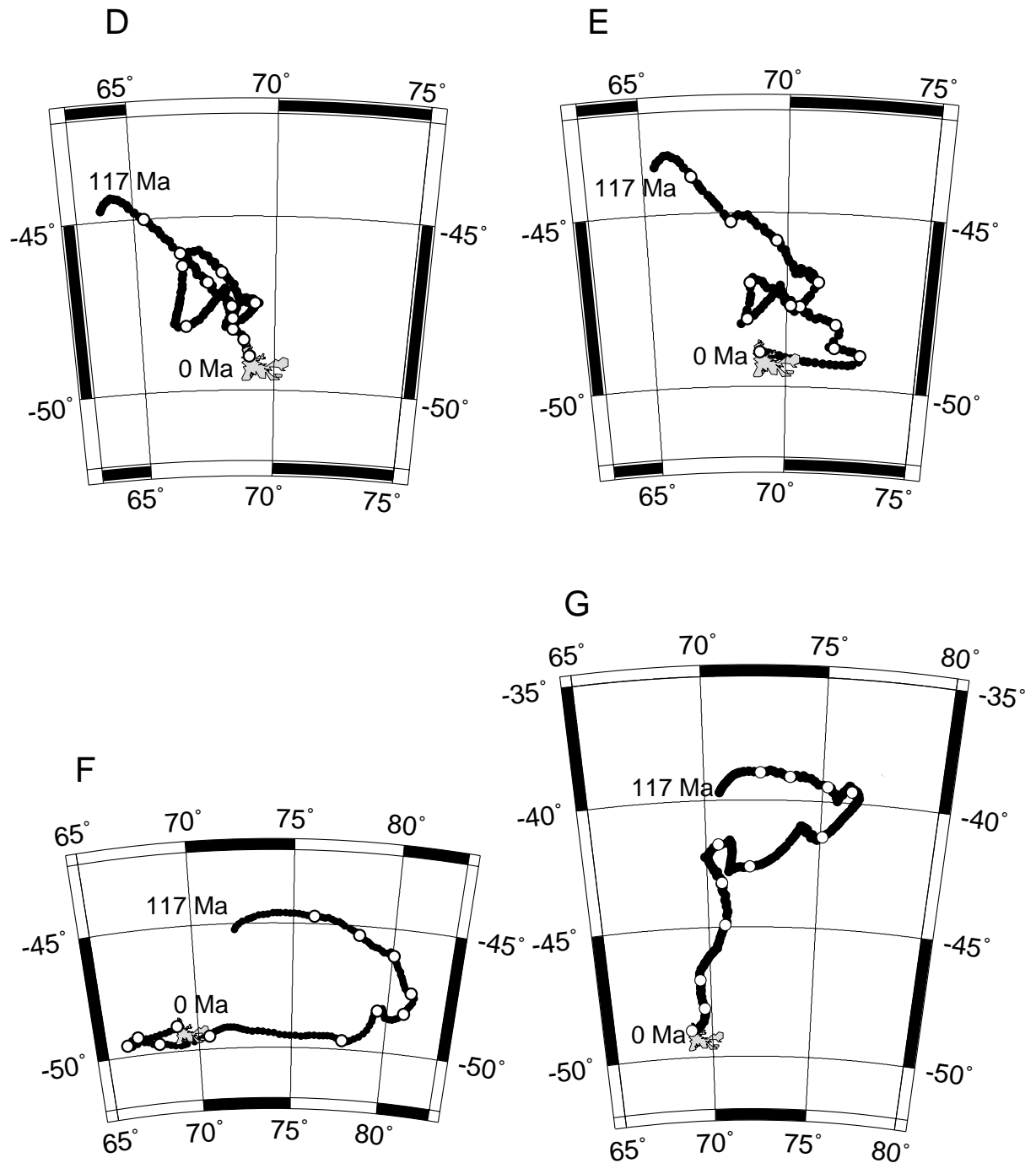


Figure 5.6 (continuation). D: *Grand* [2001]; E: *Ritsema and Van Heijst* [2000]; F: *Mégnin and Romanowicz* [2000] and G: *Masters et al.* [2000]. All calculations result in a southward motion of the Kerguelen hotspot. The amount of motion is approximately 5° for D, E, F and 10° for G.

The plate motion histories of *Müller et al.* [1993] in the Indian and Atlantic Ocean and of *Gordon and Jurdy* [1986] and *Lithgow-Bertelloni and Richards* [1998] in the Pacific have been used as boundary conditions for the calculation of the flow fields. These plate motion models are based on the assumption of hotspot fixity, which apparently contradicts the assumption of hotspot motion made here. Preliminary calculations [*Steinberger*, 2000a] have, however, shown that taking into account the predicted hotspot motions does not fundamentally alter the plate motion models. The plate motion model only marginally influences mid mantle flow at relevant depths (and hence predicted hotspot motion), because the plates are somewhat decoupled by a zone of low viscosity from the flow at deeper level. The calculated hotspot motion reflects the mantle flow in the mid mantle zone, which is represented in Figure 5.6 by arrows. Therefore, there is no circular reasoning in the approach adopted.

Similarly, the true polar wander curves of chapter 4 were constructed in a "fixed hotspot" reference frame and thus, strictly speaking, would have to be modified in order to account for hotspot motions. Again, preliminary calculations indicate that such a modification only leads to small changes in the polar wander curves, less than error margin, and thus it was not implemented [*Steinberger*, 2000a].

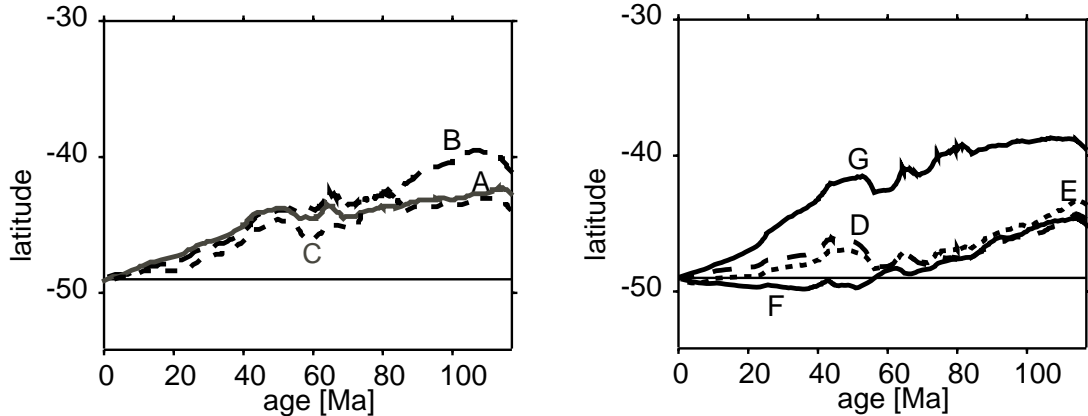


Figure 5.7: Resulting paleolatitudes versus time for the Kerguelen hotspot due to hotspot motion using different mantle flows (A: *Li and Romanowicz* [1996]; B: *Su et al.* [1994]; C: *Steinberger* [2000b]; D: *Grand* [2001]; E: *Ritsema and Van Heijst* [2000]; F: *Mégnin and Romanowicz* [2000] and G: *Masters et al.* [2000]). The assumed present-day latitude is indicated by a horizontal line at 49°S .

Results for the Kerguelen hotspot motion with the tomographic models from *Su et al.* [1994] and *Li and Romanowicz* [1996] and with the slab-model from *Steinberger* [2000b] are shown in Figure 5.6A-C. The three calculations indicate a southward motion of the Kerguelen hotspot between 8 to 10 degrees during the past 110 Ma, depending on the model used.

The mid mantle zone is characterized by a south-eastward mantle flow for the tomographic models and by a south-westward mantle flow for the slab-model shown in Figure

5.6A-C. Qualitatively, this can be explained as follows: for the tomographic models a main feature is a large upwelling beneath Africa that causes a material outflux; this outflux is coupled with the outflux from the subduction zone beneath Indonesia and causes the south-eastward flow. On the contrary, the slab-model is characterized only by the outflux from the subduction zone beneath Indonesia and hence by a south-westward flow.

The results for the hotspot motion with the models of *Grand* [2001], *Ritsema and Van Heijst* [2000], *Mégnin and Romanowicz* [2000] and *Masters et al.* [2000] are shown in Figure 5.6D-G. Again, all calculations result in a southward motion for the Kerguelen hotspot. The amount is $\sim 5^\circ - 10^\circ$.

Figure 5.7 shows the paleolatitudes for the Kerguelen hotspot since its origin approximately 120 Ma ago based on the calculated hotspot motion. For all calculated models the Kerguelen hotspot was further north at the time of its origin than at present time.

5.5 Where is the Kerguelen hotspot?

For the calculation of the hotspot motion as well as for the interpretation of the paleomagnetically determined paleolatitudes (chapter 3) and the effect of true polar wander (chapter 4) it was assumed that the present-day position of the Kerguelen hotspot is underneath Kerguelen Island, at 49°S and 69°E . However, the present-day position of the hotspot is possibly further south underneath Heard Island or under the seamounts between Kerguelen and Heard Island [*Coffin and Antretter*, 2001]. In this section, it is briefly argued why the assumption of the present-day position of the hotspot underneath Kerguelen Island at 49°S is reasonable for our study, using the modeling procedure described above.

Both Kerguelen and Heard Island show a volcanic history from approximately 40 Ma ago to the present. In the following, the motion for the Kerguelen hotspot for the last 40 Mio years is calculated, depending on the present-day position of the Kerguelen hotspot. It was assumed that the Kerguelen hotspot is on or inbetween the Kerguelen Island and Heard Island. Five different possible present-day positions have been chosen, with the first and the fifth on Kerguelen Island (approx. long.: 69° , lat.: -49°) and Heard Island (approx. long.: 74° , lat.: -53°) itself, respectively, and three more possible locations inbetween ($71^\circ/-51^\circ$, $72^\circ/-52^\circ$, $73^\circ/-52.5^\circ$). The hotspot motion has then been calculated; representative examples for two different mantle flow fields [*Li and Romanowicz*, 1996; *Steinberger*, 2000b] and three hotspot positions are shown in Figure 5.8.

In section 5.4, hotspot motion was calculated since the origin of the Kerguelen hotspot approximately 117 Mio years ago. The calculations get less precise going back in time, and therefore results for the different tomographic models differ for more than 80 Mio years back in time. However, for the last 40 Mio years, results obtained from the different models

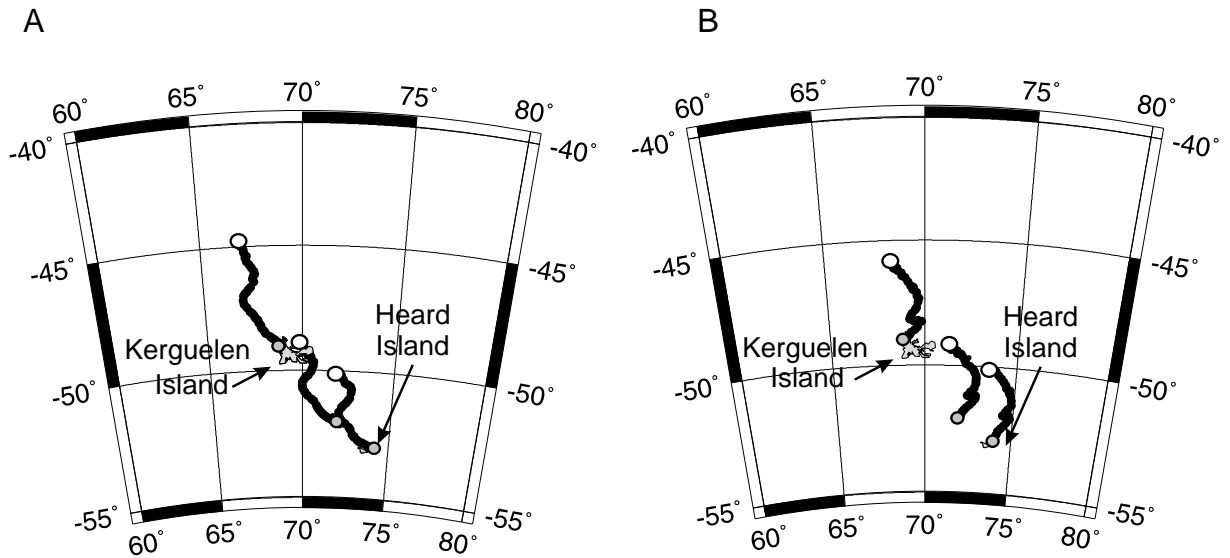


Figure 5.8: Hotspot motion was calculated with different present-day positions for the Kerguelen hotspot and for different tomographic models. Here, results for three present-day hotspot positions ($69^\circ/-49^\circ$, $72^\circ/-52^\circ$ and $74^\circ/-53^\circ$) and two tomographic models (A: *Li and Romanowicz* [1996]; B: *Steinberger* [2000b]) are shown. The assumed position of the hotspot is indicated by grey dots, the calculated positions 40 Ma ago by white dots.

agree very well. The calculations result in a southward hotspot motion of approximately 4° . The shape of the hotspot motion does not change significantly between the different tomographic models or between the assumed different present-day hotspot positions.

Assuming a present-day position for the hotspot at (or close to) Heard Island, it would have been close to the present position of Kerguelen Island 40 Mio years ago when allowing for hotspot motion. For a present-day position at Kerguelen Island, the hotspot would have been about 4° further north at a latitude of approximately 45°S . The paleomagnetic studies on ~ 35 Mio year old basalt samples from the northern Kerguelen Plateau (ODP Site 1140, chapter 3) give a paleolatitude of 35.8°S (max: 43.0°S , min: 28.9°S). To keep the discrepancy between paleomagnetic and modeling results as small as possible, the present-day hotspot position in this study is assumed to be as far north as possible and hence underneath Kerguelen Island. If the present-day position is in fact underneath Heard Island, that discrepancy would increase by approximately four degrees.

5.6 The influence of input-parameters on the hotspot motion results

In the previous section it has been shown that the results for the Kerguelen hotspot motion are not strongly dependent on the present-day location of the plume. In this section other relatively poorly known input parameters are varied and the results are

compared. The results obtained from the tomographic model by *Masters et al.* [2000] have been chosen for the comparison, because it is characterized by hotspot motion of large amount and hence might be more sensible to variations of input parameters. Also, the new viscosity structure for the plume that has been presented in section 5.3 is applied. For these calculations, the anomalous mass flux B , the initial temperature anomaly at the core-mantle boundary ΔT_{in} , the factor of pressure gradient fpg and the ratio of viscosity plume/mantle at the core-mantle boundary are needed to model the hotspot motion but are not well constrained.

Variation of the anomalous mass flux B The anomalous mass flux B is poorly known for the Kerguelen hotspot [*Sleep, 1990*]. For the previous calculations, an arithmetic mean of determinations by *Sleep* [1990], *Davies* [1988] and *Schilling* [1991] that provides a value $B = 0.9 \cdot 10^3$ kg/s has been used. Figure 5.9 shows the results for the motion for an anomalous mass flux $B = 0.2, 0.9$ and $2.0 \cdot 10^3$ kg/s. Results do not change significantly.

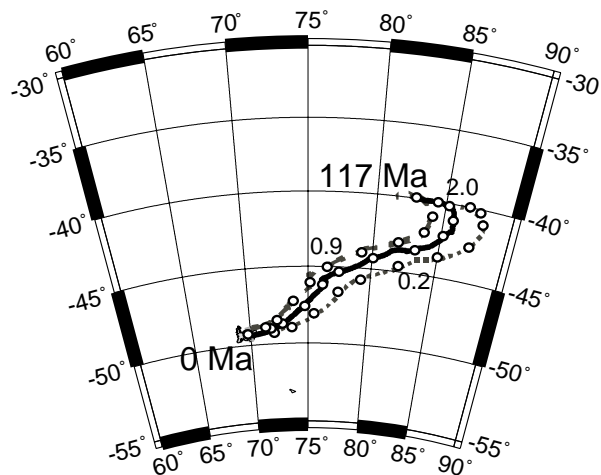


Figure 5.9: The Kerguelen hotspot motion for different anomalous mass fluxes B (dotted line: $B = 0.2 \cdot 10^3$ kg/s; dashed line: $B = 0.9 \cdot 10^3$ kg/s; solid line: $B = 2.0 \cdot 10^3$ kg/s.)

Variation of the initial temperature anomaly at the core-mantle boundary ΔT_{CMB} The initial temperature anomaly ΔT_{CMB} in the plume is fairly well constrained. For the hotspot motion calculation, a $\Delta T_{CMB} = 300^\circ$ K has been used. In Figure 5.10 hotspot motion is shown for 300° K and 500° K, and it is evident that both curves give fairly similar results.

Variation of the pressure gradient dp/dz The vertical pressure gradient dp/dz is estimated under the assumption that a large difference in pressure inside and outside the

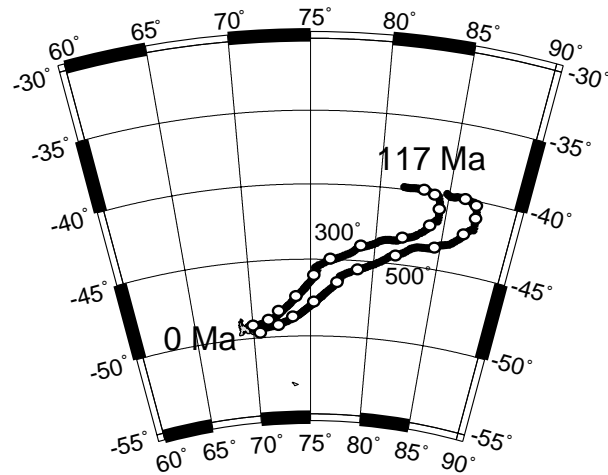


Figure 5.10: The Kerguelen hotspot motion for different initial temperature anomalies $\Delta T_{CMB} = 300^\circ$ and 300° .

conduit would “strangulate” it. dp/dz is therefore constrained to be less than expected when considering an hydrostatic case. Here it is varied using the factor for pressure gradient fpg , that has been introduced in section 5.3. Figure 5.11 shows the variation of the hotspot motion curve depending on fpg . For standard calculations, $fpg = 0.05$ has been used. No significant change in calculated hotspot motion occurs when changing fpg to 0.1 or 0.01.

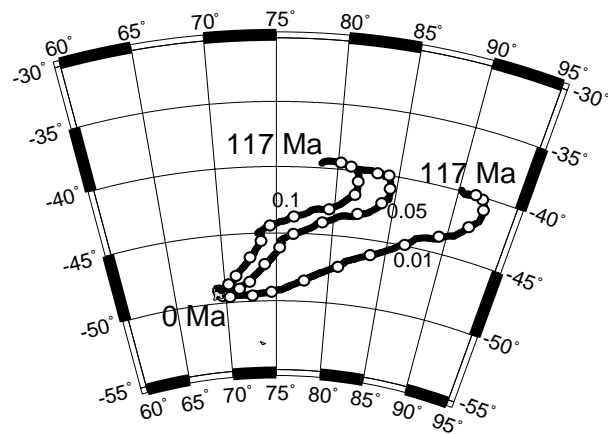


Figure 5.11: The Kerguelen hotspot motion for different pressure gradients. The pressure gradient is varied using the factor for pressure gradient fpg , that has been introduced in section 5.3. Results for $fpg = 0.05$, $fpg = 0.01$ and $fpg = 0.1$ are shown.

Variation of the ratio of viscosity plume/mantle at the core-mantle boundary

The ratio between the viscosity inside and outside the plume at the core-mantle boundary is not well constrained, but estimated to be of the order of 10^{-3} . Figure 5.12 shows the

calculated hotspot motion for a viscosity ratio of 0.001 as well as of 0.01 and 0.0001. Even the variation of an order of magnitude does not significantly change the hotspot path.

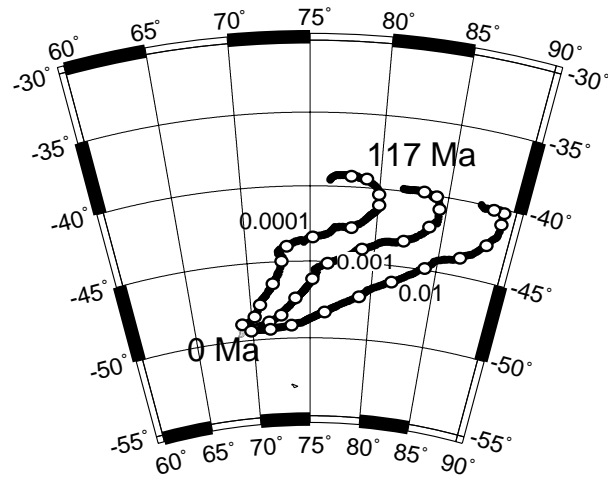


Figure 5.12: The Kerguelen hotspot motion for different viscosity ratios between plume and mantle viscosity at the core-mantle boundary 0.001, 0.01 and 0.0001.

5.7 Paleolatitudes of the Kerguelen hotspot: Summary

The results of the paleomagnetic study of the paleolatitudes of the Kerguelen hotspot (chapter 3) and the prediction for the paleolatitudes when taking true polar wander (chapter 4) and hotspot motion (chapter 5) into account are summarized in Figure 5.13.

In order to distinguish effects of polar motion and hotspot motion, each plot in Figure 5.13 contains three curves, showing changes in latitude due to polar motion (chapter 4), due to the motion of hotspots (chapter 5), and due to a combination of both. Seven mantle-density models as input for hotspot motion calculations, and two recent determinations of true polar wander are used.

The horizontal lines at 49°S in each diagram represent the assumed present-day latitude of the Kerguelen hotspot. Also shown are paleomagnetically obtained paleolatitudes with error bars (vertical lines). Two of them (Site 1138 and 1140) are new paleomagnetic results presented in chapter 3. It was shown that paleosecular variation is averaged out and therefore paleolatitudes are reliable. The other paleomagnetic data are taken from previous paleomagnetic studies on the Kerguelen Island, the southern Kerguelen Plateau and the Ninetyeast Ridge. They are also summarized in chapter 3.

Paleomagnetic results and numerical modeling are in good agreement for the Kerguelen hotspot in all calculated models. The paleolatitudes that we obtained with paleomagnetic studies on basalts from the northern and central Kerguelen Plateau confirm previous results and are further north than the present hotspot position. True polar wander [Besse, 2000; Prévot *et al.*, 2000] cannot explain the discrepancy between paleomagnetic results and present-day hotspot position. The true polar wander results would suggest paleolatitudes which are further south than the present-day hotspot position 110 Ma ago, in contrast to the paleomagnetic results. A southward hotspot motion is required to explain the observed paleolatitudes. All models that have been used in chapter 5 for the calculation of the hotspot motion yield a southward motion of roughly the amount that is necessary to explain the discrepancy.

The agreement between paleomagnetically obtained paleolatitudes and modeled hotspot motion strongly suggests that the Kerguelen hotspot has in fact moved south since its origin approximately 117 Ma ago. The magnitude of the motion is probably at least 5 and up to 10 degrees. Hotspot motion as found here on the example of the Kerguelen hotspot indicates that the hypothesis of a fixed hotspot reference frame does not hold.

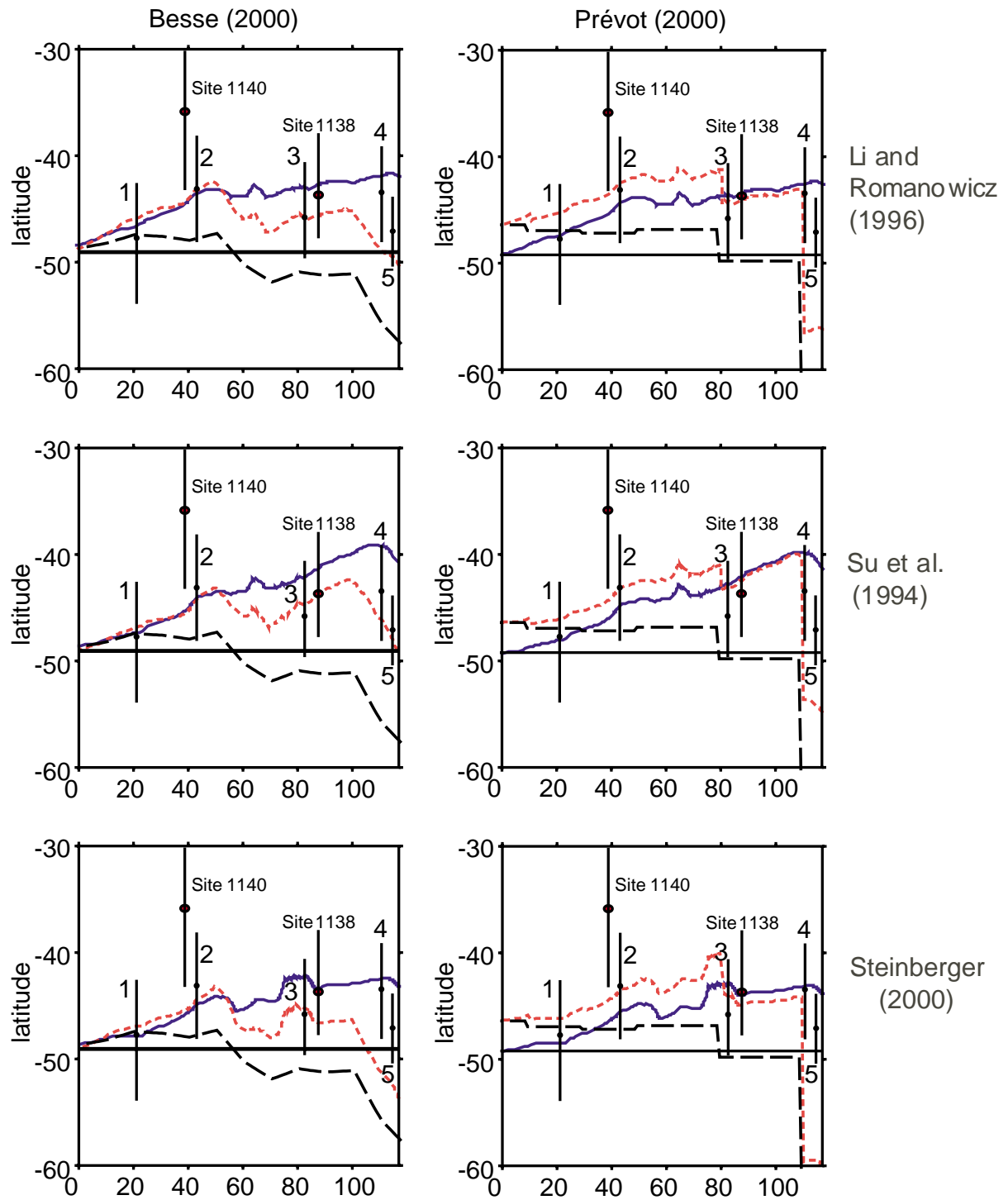


Figure 5.13: Predicted and paleomagnetically determined paleolatitudes of the Kerguelen hotspot versus time for the last 117 Ma. The horizontal line at 49°S in each of the diagrams represents the present-day latitude of the hotspot. Vertical black lines show paleolatitudes obtained in previous paleomagnetic investigations and the new paleolatitudes of the central Kerguelen Plateau (Site 1138) and the northern Kerguelen Plateau (Site 1140), presented in chapter 3. The solid lines show the modeling results for the hotspot motion from chapter 5. The dashed lines represent the change in latitude with time due to true polar wander (chapter 4). Diagrams in the left column use the TPW path of *Besse* [2000], diagrams in the right column the TPW path of *Prévot et al.* [2000]. The dotted line represents the combination of both hotspot motion and true polar wander.

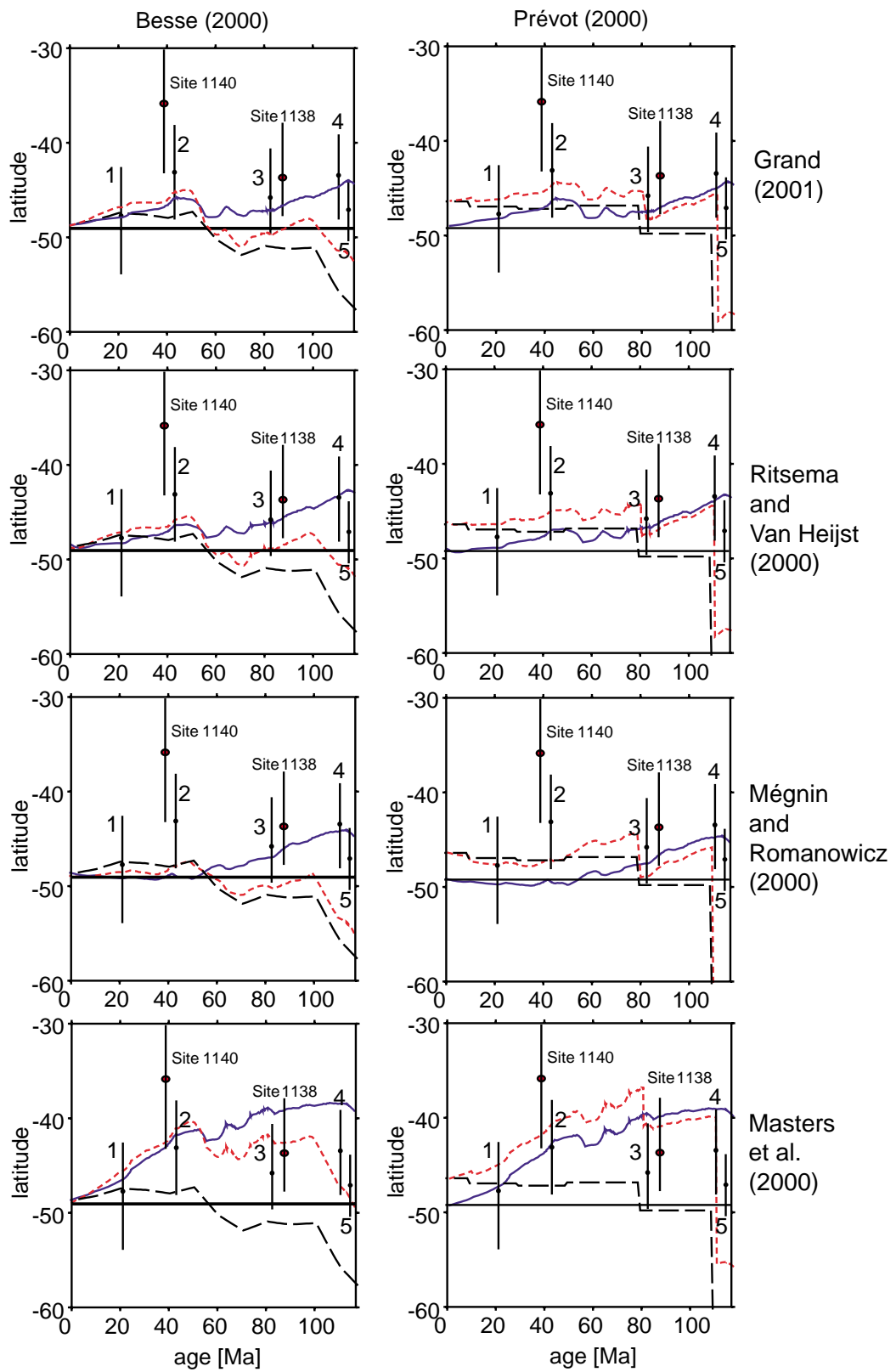


Figure 5.13 (continuation).

Chapter 6

Was the Ontong Java Plateau formed by the Louisville hotspot?

The Ontong Java Plateau, a large igneous province in the western Pacific, was thought to be formed by a rising plume head in the initial stage of the Louisville hotspot, approximately 120-125 Ma ago. However, a recent plate reconstruction suggests that the plateau was formed well to the north of the current location of this hotspot. The motion of the Louisville hotspot for the last 120 Mio years is modeled in this chapter and compared to previous paleomagnetic results from the Ontong Java Plateau and to the plate reconstruction. It is shown that -taking the drift of the Louisville hotspot into account- a formation of the plateau by the Louisville hotspot is possible.

6.1 Background

The Alaska-sized Ontong Java Plateau in the western Pacific is the largest of the LIPs. Most current models ascribe oceanic plateaus to the initial "plume-head" stage of hotspot development [e.g. *Richards, 1991*]. *Richards [1991]*, *Tarduno et al. [1991]* and *Mahoney et al. [1983]* all favored the starting plume head of the Louisville hotspot (now at $\sim 51^\circ\text{S}$, 138°W) as the source of the Ontong Java Plateau, but a recent plate reconstruction suggests that the plateau was formed well to the northeast of the current location of this hotspot [*Neal et al., 1997*]. According to this reconstruction, the center of the Ontong Java Plateau at approximately 125 Ma was at 42°S , 159°W and therefore 9° north and 21° west of the Louisville hotspot (Figure 6.1). Paleomagnetic data for basement and basal sediments at Site 289 from the Deep Sea Drilling Program yield a paleolatitude of $30\text{-}35^\circ\text{S}$ [*Hammond et al., 1975*]; a similar paleolatitude is indicated by basement lavas at Site 807 from the Ocean Drilling Program, although the basement there may have been tilted around the time of emplacement [*Mayer and Tarduno, 1993*].

No hotspot is known to exist today in the vicinity of the location of the plateau in

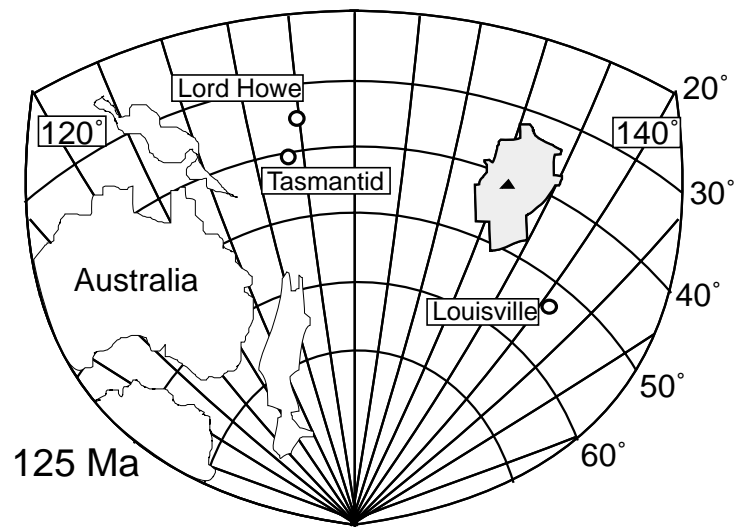


Figure 6.1: Approximate location of the Ontong Java Plateau at 125 Ma after the plate reconstruction from *Neal et al.* [1997]. Shading represents postulated extent of 122 Ma volcanism. Several present-day hotspots are shown as circles. The triangle represents the inferred location of the Ontong Java Plateau plume center beneath the crest of the high plateau. The reconstruction uses the Pacific Plate Euler poles of *Kroenke and Wessel* [1997]. (After *Neal et al.* [1997]).

the 125 Ma reconstruction at about 42°S (Figure 6.1). This location is approximately 1600 km distant from the Louisville hotspot, which, as noted above, has been suggested by several workers to be linked to the Ontong Java Plateau.

The plate reconstruction model [*Neal et al.*, 1997] as well as the previous paleomagnetic investigations [*Mayer and Tarduno*, 1993] are inconsistent with the model of the Plateau being formed by a stationary Louisville hotspot, because paleomagnetically determined paleolatitudes on basalts produced by hotspots should always be identical with the latitude of the hotspot itself, assuming stationary mantle plumes. However, there are two explanations for a change of the latitude of a hotspot with time, as discussed in the previous chapters:

1. One possibility for a change in paleolatitudes is true polar wander (TPW). TPW is the relative motion between the mantle (with the hotspots) and the rotational axis of the Earth (see chapter 4).
2. The second possibility is a motion of the hotspot in the convecting mantle as discussed in chapter 5.

6.2 Modeled motion of the Louisville hotspot

Calculations for the drift of the Louisville hotspot have been conducted with the method described in chapter 5. The results are shown in Figure 6.2 and 6.3. In Figure 6.2, the tomographic model of *Su et al.* [1994] and the slab model of *Steinberger* [2000b] together

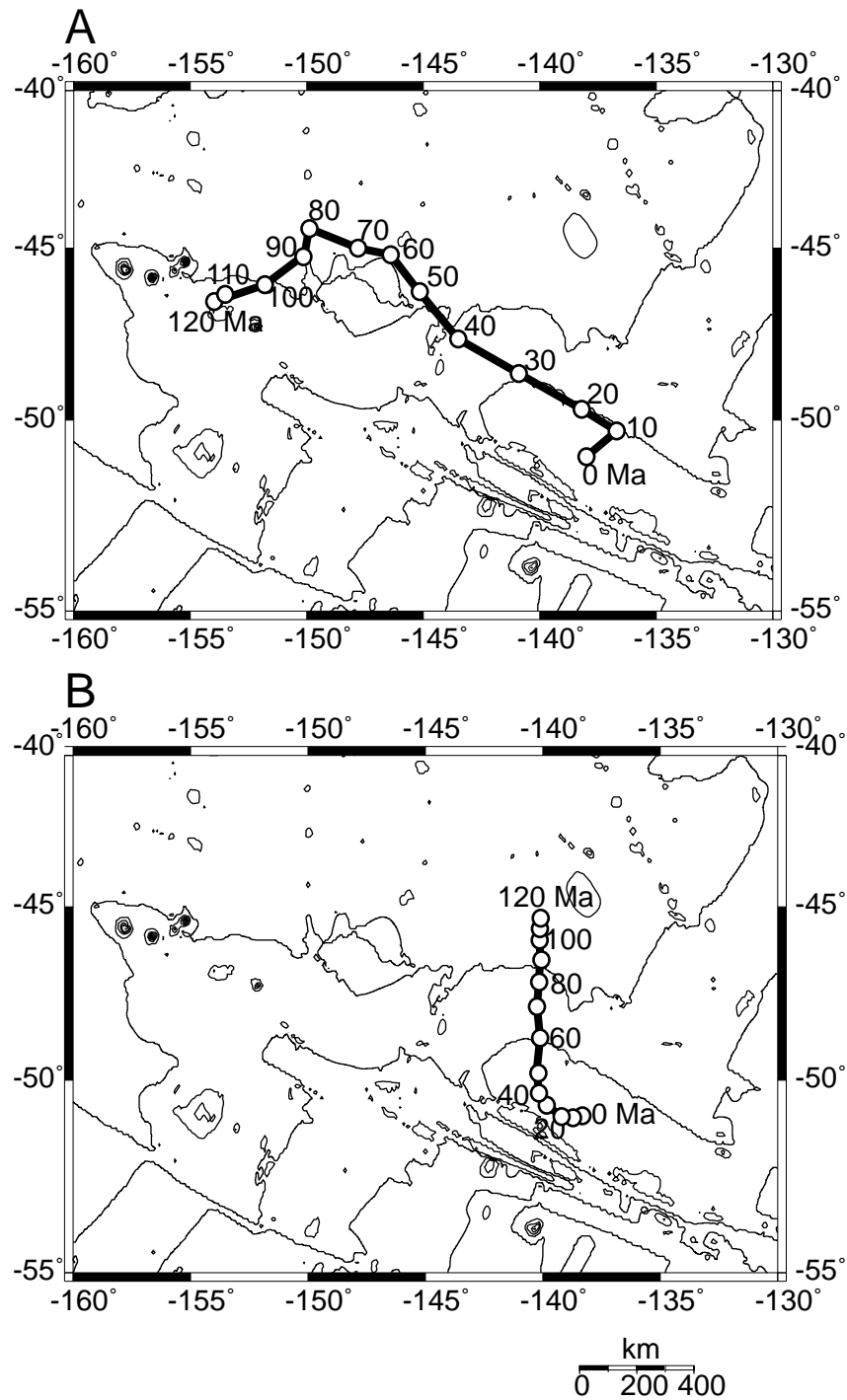


Figure 6.2: Drift of the Louisville hotspot since its first occurrence approximately 120 Mio years ago. The dots give the position of the hotspot every 10 Mio years, the age is indicated also by numbers. The present-day position of the Louisville hotspot is at 51°S . To calculate the mantle flow field we used the tomographic model from *Su et al.* [1994] (A) and the slab model of *Steinberger* [2000b] (B) as well as the viscosity structure for the mantle as in *Steinberger and O'Connell* [1998]. For both cases we found a southward drift of the hotspot of 5° and 6° for model A and B, respectively.

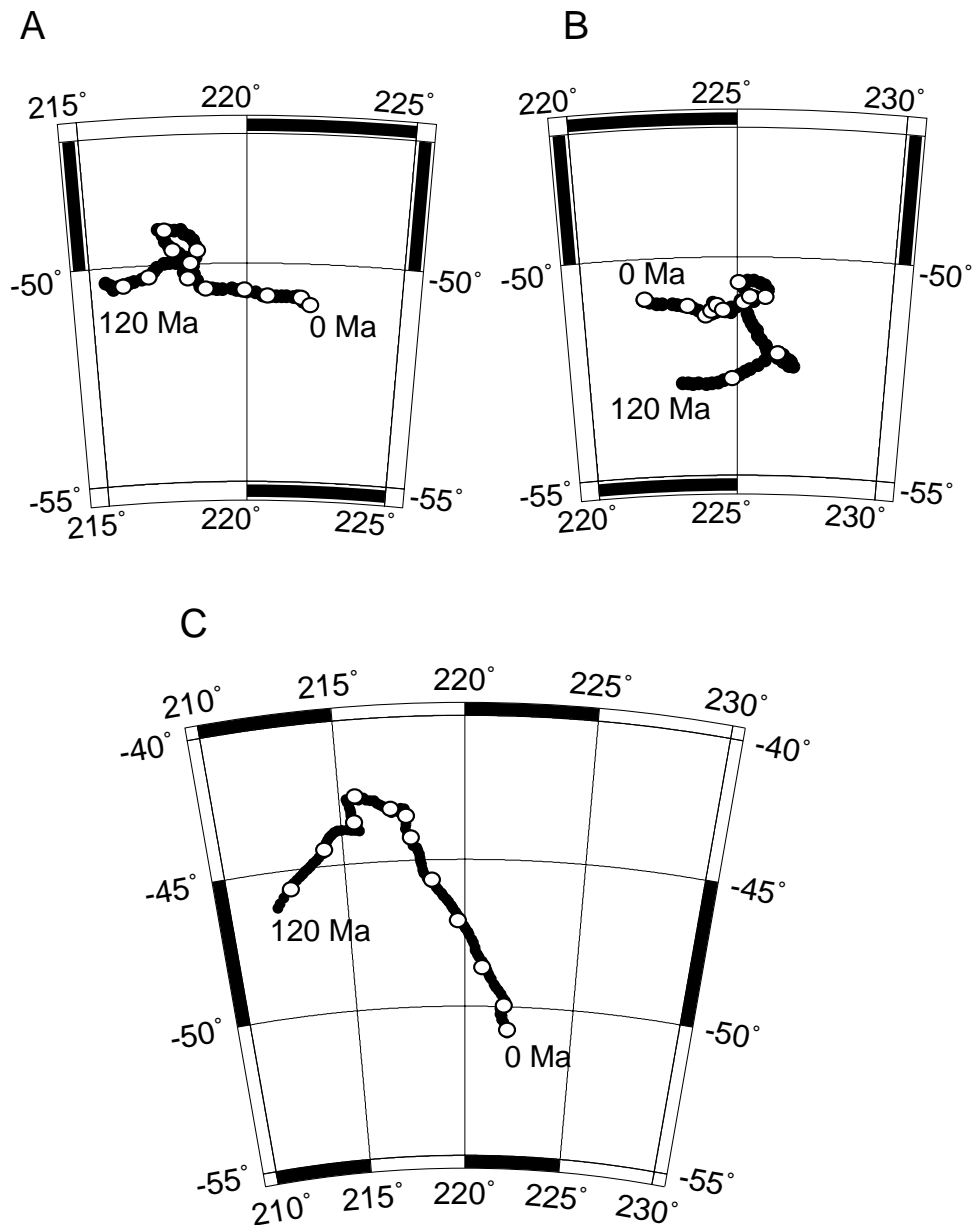


Figure 6.3: Drift of the Louisville hotspot since its first occurrence approximately 120 Mio years ago. The calculated position of the hotspot is shown with white dots every 10 Ma. The present-day position of the Louisville hotspot is at 51°S. To calculate the mantle flow field we used the tomographic models from *Grand* [2001] (A), *Ritsema and Van Heijst* [2000] (B) and *Masters et al.* [2000] (C) as well as the mantle viscosity model from *Steinberger and Calderwood* [2001]. In A the hotspot drifts approximately 5° to the east, in B it drifts approximately 2° to the north, while in C the hotspot drifts southeast with a latitudinal component of approximately 10° and a longitudinal component of the same amount.

with the mantle viscosity model as in *Steinberger and O'Connell* [1998] have been used to obtain a mantle flow field in which the rising mantle plume is advected. Results indicate a southward motion of 5° and 6° for the model of *Su et al.* [1994] and *Steinberger* [2000b], respectively, since the first occurrence of the hotspot approximately 120 Ma ago. The calculation with the tomographic model of *Su et al.* [1994] provides in addition an eastward motion of approximately 20° . This indicates a position of the hotspot at 46°S and 155°W 120 Ma ago, which is very close to the center of the Ontong Java Plateau at the same time, provided by the plate reconstruction after *Neal et al.* [1997]. Figure 6.3 shows the results for the hotspot motion with the tomographic models of *Grand* [2001], *Ritsema and Van Heijst* [2000] and *Masters et al.* [2000] and the viscosity model of *Steinberger and Calderwood* [2001]. Again, for the *Masters et al.* [2000]-model, a southeastward motion is obtained. However, the hotspot remains fairly stable using the model of *Grand* [2001] and even drifts northward by approximately 2° using the tomographic model of *Ritsema and Van Heijst* [2000].

In contrast to the calculations in chapter 5, where all models provided a southward drift for the Kerguelen hotspot, results for the Louisville hotspot are not that consistent. However, most of the calculations result in a motion roughly towards the south or south-east, with a latitudinal component of approximately 6° - 10° southward. Figure 6.4 shows the paleolatitudes for the Louisville hotspot versus time based on the calculation that provide a southward hotspot drift. For comparison, the horizontal dashed line indicates the center of the Plateau 125 Ma ago, as suggested by *Neal et al.* [1997]. A southward motion of the hotspot can explain the discrepancy between plate reconstruction and Louisville hotspot latitude. This indicates that indeed the Ontong Java Plateau could have been formed by a moving Louisville hotspot.

6.3 Influence of TPW

The inclination of magnetization in basalts which are produced by a (now assumed to be fixed) hotspot can be influenced by true polar wander. True polar wander is defined as the rotation between the mantle and the rotation axis of the Earth (chapter 4). The most recent true polar wander curves were determined by *Besse and Courtillot* [1991], *Besse* [2000] and *Prévot et al.* [2000]. The influence of these true polar wander curves for basalts from the Louisville hotspot is predicted and shown in Figure 6.5.

For the last 40 Mio years, true polar wander does almost not affect the paleolatitudes. Before that time, true polar wander provides paleolatitudes for the Louisville hotspot, which are about 5° and up to 11° further north than the present-day hotspot position (Figure 6.5). True polar wander can reduce the discrepancy between the present-day latitude of the hotspot and the paleomagnetic results from *Hammond et al.* [1975] and *Mayer and Tarduno* [1993] but is not sufficient to completely explain the difference, as

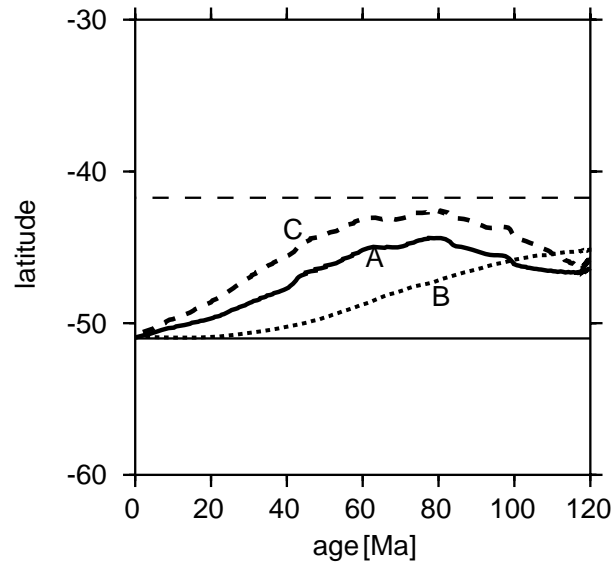


Figure 6.4: Paleolatitudes versus time for the Louisville hotspot due to hotspot motion using different mantle flows (A: *Su et al.* [1994], B: *Steinberger* [2000b] and C: *Masters et al.* [2000]). The present-day position of the Louisville hotspot as well as the center of the Ontong Java Plateau suggested after *Neal et al.* [1997] are indicated by a solid and dashed horizontal line, respectively.

shown in Figure 6.5. Only a combination of southward motion for the Louisville hotspot and of the (southward) effect of TPW could, however, completely explain the discrepancy.

However, the paleomagnetically obtained paleolatitudes that are so far available for the Ontong Java Plateau are based on only two sites, one of them has probably been tilted tectonically.

The formation of the Ontong Java Plateau by the Louisville hotspot is an example that hotspot drift is important for plate reconstructions. Hotspots are commonly taken as fixed points on the Earth and have been used as reference frame for tectonic reconstructions. In a hotspot reference frame, the formation of the Ontong Java Plateau by the Louisville hotspot is not possible. It is possible, however, when taking hotspot motion into account.

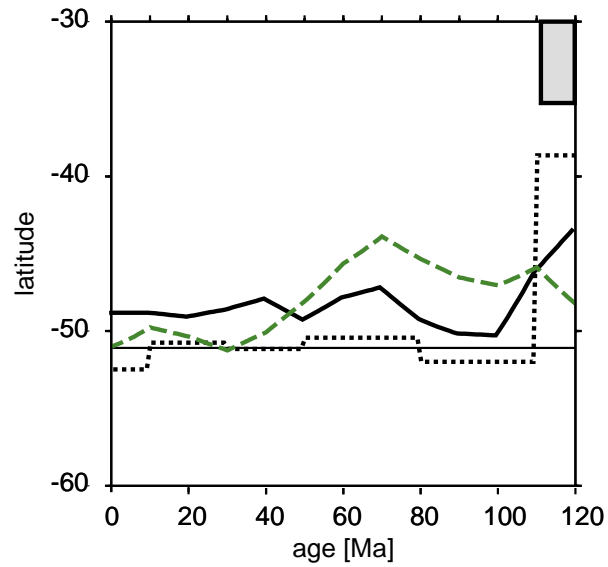


Figure 6.5: The effect of TPW on the paleolatitude of the Louisville hotspot versus time is shown for three different TPW paths (dashed line: *Besse and Courtillot* [1991]; solid line: *Besse* [2000] and dotted line: *Prévoit et al.* [2000]). Paleomagnetic results from the Ontong Java Plateau point to a paleolatitude between 30° and 35° at 120 Ma, indicated by a grey filled rectangle. The paleolatitudes that are predicted when true polar wander is taken into account are further north than the present-day latitude of the hotspot (51°S). However, the discrepancy between paleomagnetic data and present-day position is too large to be completely explained by the effect of true polar wander.

Chapter 7

Conclusion

Are hotspots fixed or do they move in a convecting mantle?

In this work, several arguments have been discussed to clarify this question for the Kerguelen hotspot in the southern Indian Ocean. Paleolatitudes from paleomagnetic studies are compared to the present-day position of the hotspot, true polar wander is used to predict changes in latitudes and, finally, hotspot motion is modeled back in time.

The Kerguelen hotspot is located in the southern Indian Ocean, probably underneath the Kerguelen Island at a latitude of 49°S and a longitude of 69°E. It is active since approximately 117 Ma and since then produced the Kerguelen Plateau in the southern Indian Ocean, the Broken Ridge, now approximately 1600 km north of the Kerguelen Plateau, the Ninetyeast Ridge (the seamount chain attributed to the Kerguelen hotspot) and the Rajmahal Traps in India.

Basalts from the central and northern Kerguelen Plateau, that have been drilled during ODP Leg 183 in December 1998 to February 1999, have been used to determine paleolatitudes for the Kerguelen Plateau. Discrete basalt samples have been stepwise demagnetized, and the inclination of characteristic remanent magnetization was determined. The mean-site inclinations have been converted into paleolatitudes of Site 1138 for the central Plateau (100 Ma) and of Site 1140 for the northern Plateau (35 Ma). The dispersion in the directions helped to judge whether paleosecular variation is properly averaged out. While in Site 1138 the dispersion in direction and alternated rims of lava units indicate a complete recording of paleosecular variation, in Site 1140 sediment layers inbetween the pillow groups and non overlapping α_{95} -limits suggest that the paleomagnetic units allow to determine a reliable paleolatitude. Comparison of the present-day latitude of the Kerguelen hotspot with the results from both sites as well as from several previous paleomagnetic studies indicate that the Kerguelen hotspot has been further north in the past. Previous studies have been conducted on the Ninetyeast

Ridge, on the southern Kerguelen plateau and on the Rajmahal Traps in India that have probably been formed in the initial phase of the hotspot.

True polar wander is defined as the shift between the Earth's mantle (with the hotspot) versus the rotation (or magnetic dipole) axis of the Earth. If true polar wander occurs it affects the latitudes of a hotspot. Three independently obtained true polar wander paths indicate that at the time of its formation the Kerguelen hotspot should have produced basalts with paleolatitudes further south than at present. This prediction is contrary to the paleomagnetic results. Because the shape and magnitude of the three true polar wander paths is also supported by a numerical calculation of the shift of the mantle due to changes of moments of inertia, they shall be deemed to be reliable. The discrepancy between predicted paleolatitudes by true polar wander, paleomagnetic results and present-day latitude might, however, be explained by hotspot motion.

The drift of the Kerguelen hotspot since its origin approximately 117 Ma ago has been modeled. Seven different density models of the Earth's mantle have been used to calculate mantle flow fields. In each of these flow fields an initially vertical plume has been advected back in time. This procedure results in seven hotspot paths at the Earth's surface. All seven results, although obtained from independent density models, indicate a southward motion for the Kerguelen hotspot. Indeed, this southward motion resolves the discrepancy between paleomagnetic results and the present-day hotspot position. True polar wander can occur together with hotspot motion, and this combination is in agreement with the results as well. The calculations for the hotspot motion are depending on several parameters, for example the present-day hotspot position, the anomalous mass flux, the viscosity in the mantle, and others. Variation of these parameters showed that the drift results are stable and do not strongly change with the input parameters. The variation of the hotspot position is important for the choice of the present-day position of the hotspot. For this thesis it was assumed to be underneath the volcanically active Kerguelen Island. More precisely, it is possibly located underneath Heard Island or under the seamounts inbetween Kerguelen and Heard Island. The calculation of hotspot drift with different present-day positions indicate that with the assumption of the hotspot to be under Kerguelen Island the discrepancy is kept as small as possible.

It is shown that hotspot motion in combination with or without true polar wander explains the paleolatitudes of the Kerguelen hotspot, while true polar wander alone does not. A southward drift of the Kerguelen hotspot by 5 to 10 degrees, which is also supported by the modeling of hotspot motion, fits the paleomagnetic results and balances the effect of true polar wander.

Morgan [1971] claimed the Kerguelen hotspot to be the least fixed of the hotspots, and the results presented in this work confirm his statement.

The Ontong Java Plateau, a large igneous province in the western Pacific, was thought to be formed by the Louisville hotspot approximately 120 Ma ago. A recent plate reconstruction, however, suggests that the plateau was formed far north of the present-day position of the Louisville hotspot. Therefore, recently it was doubted, whether the formation of the Ontong Java Plateau by the Louisville hotspot was possible.

In this thesis, the drift of the Louisville hotspot since its origin 120 Ma ago has been modeled with the method used before for the Kerguelen hotspot. Again, seven hotspot paths at the Earth's surface have been calculated from seven different mantle flow fields. Most of the hotspot paths indicate a southward motion of the Louisville hotspot. Therefore, allowing for hotspot motion, the Louisville hotspot might have been located underneath the Ontong Java Plateau at the time of its formation, and could have been responsible for its formation. However, no reliable paleomagnetic results from the Ontong Java Plateau exist, but are needed to confirm or reject the modeling results. Maria Antretter participated on ODP Leg 192 to the Ontong Java Plateau (September - November 2000), and obtained suitable basement rock samples to determine paleolatitudes for the Ontong Java Plateau. These new paleolatitudes will help to clarify the Ontong Java Plateau - Louisville hotspot relation.

In July 2001, the ODP Leg 197 is planned to drill basement rocks from the Hawai'ian-Emperor seamount chain. This chain is the best example of a change in plate motion recorded in a fixed-hotspot frame of reference. Alternatively, the bend might primarily record differences in motion of the Hawai'ian hotspot relative to the Pacific lithosphere.

Main objective of Leg 197 is to test the hypothesis of motion of the Hawai'ian hotspot. This points to the broad scientific interest in the question about hotspot motion and this thesis with the studies about the motion of the Kerguelen and Louisville hotspot gives important contributions to that discussion.

Bibliography

- Albers, M. and U. R. Christensen, The excess temperature of plumes rising from the core-mantle boundary, *Geophys. Res. Lett.*, *23*, 3567–3570, 1996.
- Berggren, W. A., D. V. Kent, C. C. Swisher, and M. P. Aubry, A Revised Cenozoic geochronology and chronostratigraphy, in *Geochronology Time Scales and Global Stratigraphic Correlation*, edited by W. A. Berggren, D. V. Kent, M. P. Aubry, and J. Hardenobl, vol. 54, pp. 129–212, Soc. Econ. Paleontol. Mineral., 1995.
- Besse, J., pers. comm., 2000.
- Besse, J. and V. Courtillot, Revised and Synthetic Apparent Polar Wander Paths of the African, Eurasian, North American and Indian Plates, and True Polar Wander Since 200 Ma, *J. Geophys. Res.*, *96*, 4029–4050, 1991.
- Coffin, M. and M. Antretter, Where is the Kerguelen Hotspot?, *Geology*, *in preparation*, 2001.
- Coffin, M. and O. Eldholm, Large igneous provinces: crustal structure, dimensions and external consequences, *Rev. Geophys.*, *32*, 1–36, 1994.
- Coffin, M. F., Heard on the Kerguelen Plateau, *JOI/USSAC Newsletter*, *11*, 1998.
- Coffin, M. F., H. L. Davies, and W. F. Haxby, Structure of the Kerguelen Plateau province from SEASAT altimetry and seismic reflection data, *Nature*, *324*, 134–136, 1986.
- Coffin, M. F. and O. Eldholm, Scratching the surface: Estimating dimensions of large igneous provinces, *Geology*, *21*, 515–518, 1993.
- Coffin, M. F., F. A. Frey, P. J. Wallace, and scientific crew Leg 183, Kerguelen Plateau–Broken Ridge, Sites 1135 – 1142, in *Proc. ODP, Init. Repts.*, edited by M. F. Coffin, F. A. Frey, P. J. Wallace, and scientific crew Leg 183, vol. 183, Texas A& M University, College Station, TX 77845-9547, 2000.
- Coffin, M. F., M. Munsch, J. B. Colwell, R. Schlich, H. L. Davies, and Z. G. Li, Seismic stratigraphy of the Raggatt Basin, southern Kerguelen Plateau: tectonic and paleo-oceanographic implications, *Geol. Soc. Am. Bull.*, *102*, 563–589, 1990.

- Courillot, V. and J. Besse, Magnetic field reversal, polar wander, and core-mantle coupling, *Science*, 237, 1140–1147, 1987.
- Cox, A., Confidence Limits for the Precision Parameter κ , *Geophys. J. R. astr. Soc.*, 18, 545–549, 1969.
- Davies, G. F., Ocean bathymetry and mantle convection, 1. Large-scale flow and hotspots, *J. Geophys. Res.*, 93, 10467–10480, 1988.
- Day, R., M. D. Fuller, and V. A. Schmidt, Hysteresis properties of titanomagnetites: Grain size and composition dependence, *Phys. Earth Planet. Inter.*, 13, 260–266, 1977.
- Duncan, R. A. and M. A. Richards, Hotspots, mantle plumes, flood basalts, and true polar wander, *Rev. Geophys.*, 29, 31–50, 1991.
- Duncan, R. A. and M. Storey, The life cycle of Indian Ocean hotspots, in *Synthesis of results from scientific drilling in the Indian Ocean*, *Geophys. Monogr.*, edited by R. A. Duncan, D. K. Rea, R. B. Kidd, U. von Rad, and J. K. Weissel, vol. 70, pp. 91–103, Am. Geophys. Union, 1992.
- Forte, A. M., A. M. Dziewonski, and R. L. Woodward, Aspherical structure of the mantle, tectonic plate motions, nonhydrostatic geoid, and topography of the core-mantle boundary, in *Dynamics of the Earth's Deep Interior and Earth Rotation*, *Geophys. Mon. Ser.*, edited by J.-L. Le Mouél, D. E. Smylie, and T. Herring, pp. 135–166, AGU, Washington, DC., 1993.
- Fröhlich, F. and E. Wicquart, Upper Cretaceous and Paleogene sediments from the northern Kerguelen Plateau, *Geo-Marine Letts.*, 9, 127–133, 1989.
- Giret, A. and J. Lameyre, A study of Kerguelen plutonism; petrology, geochronology and geological implications, in *Antarctic earth science; fourth international symposium*, edited by R. L. Oliver, P. R. James, and J. B. Jago, pp. 646–651, Cambridge Univ. Cambridge, United Kingdom, 1983.
- Goldreich, P. and A. Toomre, Some remarks on polar wandering, *J. Geophys. Res.*, 74, 2555–2567, 1969.
- Gordon, R. G. and D. Jurdy, Cenozoic global plate motions, *J. Geophys. Res.*, 91, 12389–12406, 1986.
- Gradstein, F. M., F. P. Agterberg, J. G. Ogg, J. Hardenbol, P. Van Veen, J. Thierry, and Z. Huang, A Triassic, Jurassic and Cretaceous time scale, in *Geochronology Time Scales and Global Stratigraphic Correlation*, edited by W. A. Berggren, D. V. Kent, M. P. Aubry, and J. Hardenobl, vol. 54, pp. 95–128, Soc. Econ. Paleontol. Mineral., 1995.

- Grand, S. P., Updated tomographic model based on Grand et al. (1997), <ftp://amazon.geo.utexas.edu/outgoing/steveg/>, 2001.
- Hager, B. H. and R. J. O'Connell, Kinematic models of large-scale mantle flow, *J. Geophys. Res.*, *84*, 1031–1048, 1979.
- Hager, B. H. and R. J. O'Connell, A simple global model of plate dynamics and mantle convection, *J. Geophys. Res.*, *86*, 4843–4867, 1981.
- Hammond, S. R., L. W. Kroenke, and F. Theyer, Northward motion of the Ontong Java Plateau between 110 and 30 m.y.: A paleomagnetic investigation of DSDP Site 289, *Init. Repts. Deep Sea Drill. Proj.*, *30*, 415–418, 1975.
- Henry, B. and C. Plessard, New palaeomagnetic results from the Kerguelen Islands, *Geophys. J. Int.*, *128*, 73–83, 1997.
- Inokuchi, H. and F. Heider, Paleolatitude of the southern Kerguelen Plateau inferred from the paleomagnetic study of upper Cretaceous basalts, *Proc. ODP Sci. Results*, *120*, 89–96, 1992.
- Karato, S., Importance of anelasticity in the interpretation of seismic tomography, *Geophys. Res. Lett.*, *20*, 1623–1626, 1993.
- Klootwijk, C. T., Palaeomagnetism of the - upper Gondwana- Rajmahal traps, northeastern India, *Tectonophys.*, *12*, 449–467, 1971.
- Klootwijk, C. T., J. S. Gee, J. W. Peirce, and G. M. Smith, Constraints on the India-Asia convergence: Paleomagnetic results from Ninetyeast ridge, *Proc. ODP Sci. Results*, *121*, 777–882, 1991.
- Kroenke, L. W. and P. Wessel, Pacific plate motion between 125 and 90 Ma and the formation of the Ontong Java Plateau (abstract), *Chapman Conf. On Global Plate Motions*, 1997.
- Laj, C., H. Guillou, N. Szeremeta, and R. Coe, Geomagnetic paleosecular variation at Hawaii around 3 Ma from a sequence of 107 lava flows at Kaena Point (Oahu), *Earth Planet. Sci. Lett.*, *170*, 365–376, 1999.
- Larson, R. L., Geological consequences of superplumes, *Geology*, *19*, 963–966, 1991.
- Leclaire, L., Y. Bassias, M. Denis-Clochiatti, H. L. Davies, I. Gautier, B. Gensous, P.-J. Giannesini, P. Patriat, J. Segoufin, M. Tesson, and J. Wannesson, Lower Cretaceous basalt and sediments from the Kerguelen Plateau, *Geo-Mar. Lett.*, *7*, 169–176, 1987.

- Li, X. D. and B. Romanowicz, Global Mantle Shear-Velocity Model Developed Using Nonlinear Asymptotic Coupling Theory, *J. Geophys. Res.*, *101*, 22,245–22,272, 1996.
- Lipman, P. W., Declining growth of Mauna Loa during the last 100 000 years: rates of lava accumulation vs. gravitational subsidence, *Geophys. Monogr.*, *92*, 45–80, 1995.
- Lithgow-Bertelloni, C. and M. A. Richards, The dynamics of Cenozoic and Mesozoic plate motions, *Rev. Geophys.*, *36*, 27–78, 1998.
- Loper, D. E. and F. D. Stacey, The dynamical and thermal structure of deep mantle plumes, *Phys. Earth Planet. Inter.*, *33*, 304–317, 1983.
- Love, J. J., Paleomagnetic volcanic data and geometric regularity of reversals and excursions, *J. Geophys. Res.*, *103*, 12435–12452, 1998.
- Mahoney, J. J., J. D. McDougall, G. W. Lugmair, and K. Gopalan, Kerguelen hot spot source for the Rajmahal traps and Ninetyeast Ridge?, *Nature*, *303*, 385–389, 1983.
- Markl, R. G., Further evidence for the Early Cretaceous breakup of Gondwanaland off Southwestern Australia, *Mar. Geol.*, *26*, 41–48, 1978.
- Masters, G., G. Laske, H. Bolton, and A. Dziewonski, The relative behaviour of shear velocity, bulk sound speed, and compressional velocity in the mantle: implications for chemical and thermal structure, in *Geophys. Monogr. Ser.: Seismology and Mineral Physics*, edited by S. Karato, vol. 117, pp. 63–87, AGU, Washington, D. C., 2000.
- Mayer, H. and J. A. Tarduno, Paleomagnetic investigation of the igneous sequence, Site 807, Ontong Java Plateau, and a discussion of Pacific true polar wander, in *Proc. ODP, Sci. Results*, edited by W. H. Berger, L. W. Kroenke, L. A. Mayer, and scientific crew, vol. 130, College Station TX (Ocean Drilling Program), 1993.
- McDougall, I. and M. W. McElhinny, The Rajmahal traps of India - K-Ar ages and palaeomagnetism, *Earth Planet. Sci. Lett.*, *9*, 371–378, 1970.
- McElhinny, M. W. and R. T. Merrill, Geomagnetic Secular Variation Over the Past 5 m.y., *Rev. Geophys. Space Phys.*, *13*, 687–708, 1975.
- McFadden, P. L., R. T. Merrill, M. W. McElhinny, and S. Lee, Reversals of the Earth's Magnetic Field and Temporal Variations of the Dynamo Families, *J. Geophys. Res.*, *96*, 3923–3933, 1991.
- McFadden, P. L. and A. B. Reid, Analysis of palaeomagnetic inclination data, *Geophys. J. R. astr. Soc.*, *69*, 307–319, 1982.

- Mégnin, C. and B. Romanowicz, The shear velocity structure of the mantle from the inversion of body, surface and higher modes waveforms, *Geophys. J. Int.*, *143*, 709–728, 2000.
- Molnar, P. and J. Stock, Relative motions of hotspots in the Pacific, Atlantic and Indian oceans since late Cretaceous time, *Nature*, *327*, 587–591, 1987.
- Morgan, W., Convection plumes in the lower mantle, *Nature*, *230*, 42–43, 1971.
- Morgan, W. J., Rodriguez, Darwin, Amsterdam,..., a second type of hotspot island, *J. Geophys. Res.*, *83*, 5355–5360, 1978.
- Morgan, W. J., Hotspot tracks and the opening of the Atlantic and Indian Oceans, in *The oceanic lithosphere*, edited by C. Emiliani, pp. 443–487, Wiley, New York, 1981.
- Müller, R. D., J.-Y. Royer, and L. A. Lawver, Revised plate motions relative to the hotspots from combined Atlantic and Indian Ocean hotspot tracks, *Geology*, *21*, 275–278, 1993.
- Munsch, M., J. Dymant, M. O. Boulanger, D. Boulanger, J. D. Tissot, R. Schlich, Y. Rotstein, and M. F. Coffin, Breakup and seafloor spreading between the Kerguelen Plateau - Labuan Basin and the Broken Ridge - Diamantina Zone, *Proc. ODP Sci. Results*, *120*, 931–944, 1992.
- Mutter, J. C. and S. C. Cande, The early opening between Broken Ridge and Kerguelen Plateau, *Earth Planet. Sci. Lett.*, *65*, 369–376, 1983.
- Neal, C. R., J. J. Mahoney, L. W. Kroenke, R. A. Duncan, and M. G. Pettersen, The Ontong Java Plateau, in *Large Igneous Provinces*, *Geophys. Monogr.*, edited by J. J. Mahoney and M. F. Coffin, vol. 100, pp. 183–216, Am. Geophys. Union, 1997.
- Nicolaysen, K., F. A. Frey, K. V. Hodges, D. Weis, and A. Giret, ^{40}Ar - ^{39}Ar geochronology of flood basalts from the Kerguelen Archipelago, southern Indian Ocean; implications for Cenozoic eruption rates of the Kerguelen plume, *Earth Planet. Sci. Lett.*, *174*, 313–328, 2000.
- Olson, P., G. Schubert, and C. Anderson, Structure of axisymmetric mantle plumes, *J. Geophys. Res.*, *98*, 6829–6844, 1993.
- Osako, M. and E. Ito, Thermal diffusivity of MgSiO_3 perovskite, *Geophys. Res. Lett.*, *18*, 239–242, 1991.
- Prévot, M., E. Mattern, P. Camps, and M. Daignières, Evidence for a 20° tilting of the Earth's rotation axis 110 million years ago, *Earth Planet. Sci. Lett.*, *179*, 517–528, 2000.

- Pringle, M. S., M. Storey, and J. Wigbrans, ^{40}Ar - ^{39}Ar geochronology of mid-Cretaceous Indian ocean basalts: constraints on the origin of large flood basalt provinces, *EOS, Trans. Amer. Geophys. Union*, 75, 728, 1994.
- Radhakrishnamurthy, C., Laboratory studies for ascertaining the suitability of rocks for palaeomagnetism, in *Palaeogeophysics*, edited by S. K. Runcorn, pp. 235–241, Academic Press, London, 1970.
- Richards, M. A., Hotspots and the case against a uniform viscosity composition mantle, in *Glacial Isostasy, Sea Level and Mantle Rheology*, edited by R. Sabadini and K. Lambeck, pp. 571–587, Kluwer Academic Publishers, Dordrecht, 1991.
- Richards, M. A., R. A. Duncan, and V. E. Courtillot, Flood basalts and hot spot tracks, *Science*, 246, 103–107, 1989.
- Ritsema, J. and H. J. Van Heijst, Seismic imaging of structural heterogeneity in Earth's mantle: Evidence for large-scale mantle flow, *Science Progress*, 83, 243–259, 2000.
- Rotstein, Y., R. Schlich, M. Munsch, and M. F. Coffin, Structure and tectonic history of the southern Kerguelen Plateau (Indian Ocean) deduced from seismic reflection data, *Tectonics*, 11, 1332–1347, 1992.
- Royer, J.-Y. and N. Rollet, Plate tectonic setting of the Tasmanian region, *Aust. J. Earth Sci.*, 44, 543–560, 1997.
- Sager, W. and U. Bleil, Latitudinal shift of Pacific hotspots during the late Cretaceous and early Tertiary, *Nature*, 6112, 488–490, 1987.
- Schaming, M. and Y. Rotstein, Basement reflectors in the Kerguelen Plateau, south Indian Ocean: Implications for the structure and early history of the plateau, *Geol. Soc. Amer. Bull.*, 102, 580–592, 1990.
- Schilling, J.-G., Fluxes and excess temperatures of mantle plumes inferred from their interaction with migrating mid-ocean ridges, *Nature*, 352, 397–403, 1991.
- Sleep, N., Hotspots and mantle plumes: Some phenomenology, *J. Geophys. Res.*, 95, 6715–6736, 1990.
- Sleep, N. H., Time dependence of mantle plumes; some simple theory, *J. Geophys. Res.*, 97, 20007–20019, 1992.
- Stagg, H. M. J. and J. B. Willcox, A case for Australia-Antarctica separation in the Neocomian (ca. 125 Ma), *Tectonophysics*, 210, 21–32, 1992.

- Stein, M. and A. W. Hofmann, Mantle plumes and episodic crustal growth, *Nature*, *373*, 63–68, 1994.
- Steinberger, B., Plumes in a convecting mantle; models and observations for individual hotspots, *J. Geophys. Res.*, *105*, 11127–11152, 2000a.
- Steinberger, B., Slabs in the lower mantle - results of dynamic modelling compared with tomographic images and the geoid, *Earth Planet. Sci. Lett.*, *118*, 241–257, 2000b.
- Steinberger, B. and A. R. Calderwood, Mineral Physics Constraints on Viscous Flow Models of Mantle Flow, *J. Conf. Abs.*, *6*, 2001.
- Steinberger, B. and R. J. O’Connell, Changes of the Earth’s rotation axis owing to advection of mantle density heterogeneities, *Nature*, *387*, 169–173, 1997.
- Steinberger, B. and R. J. O’Connell, Advection of plumes in mantle flow: implications for hotspot motion, mantle viscosity and plume distribution, *Geophys. J. Int.*, *132*, 412–434, 1998.
- Storey, M., M. S. Pringle, M. F. Coffin, and J. Wijbrans, Geochemistry of Kerguelen Plateau basalts: results from ODP Legs 119 and 120, *EOS, Trans. Amer. Geophys. Union*, *77*, W123, 1977.
- Su, W.-J., R. L. Woodward, and A. M. Dziewonski, Degree 12 model of shear velocity heterogeneity in the mantle, *J. Geophys. Res.*, *99*, 6945–6980, 1994.
- Tarduno, J. A. and R. D. Cottrell, Paleomagnetic evidence for motion of the Hawaiian hotspot during formation of the Emperor seamounts, *Earth Planet. Sci. Lett.*, *153*, 171–180, 1997.
- Tarduno, J. A. and A. V. Smirnov, Stability of the Earth with respect to the spin axis for the last 130 million years, *Earth Planet. Sci. Lett.*, *184*, 549–553, 2001.
- Tarduno, W. V., J. A. Sliter, L. W. Kroenke, M. Leckie, J. J. Mahoney, R. J. Musgrave, M. Storey, and E. L. Winterer, Rapid formation of the Ontong Java Plateau by Aptian mantle plume volcanism, *Science*, *254*, 399–403, 1991.
- Thellier, E. and O. Thellier, Recherches géomagnétiques sur des coulées volcaniques d’Auvergne, *Ann. Géophys.*, *1*, 37–52, 1944.
- Turcotte, D. L. and G. Schubert, *Geodynamics. Application of continuum physics to geological problems*, Wiley, New York, 1982.

- Weis, D., W. M. White, F. A. Frey, R. A. Duncan, J. Dehn, M. Fisk, J. Ludden, A. Saunders, and M. Storey, The influence of mantle plumes in generation of Indian oceanic crust, in *Synthesis of results from scientific drilling in the Indian Ocean, Geophys. Monogr.*, edited by R. A. Duncan, D. K. Rea, R. B. Kidd, U. von Rad, and J. K. Weissel, vol. 70, pp. 58–89, Am. Geophys. Union, 1992.
- Weissel, J. K. and G. D. Karner, Flexural uplift of rift flanks due to mechanical unloading of the lithosphere during extension, *J. Geophys. Res.*, *94*, 13,919–13,950, 1989.
- Wilson, J., Evidence from oceanic islands suggesting movement in the earth, *Phil. Trans. R. Soc.*, pp. 145–167, 1965.
- Yale, M. M. and J. Phipps Morgan, Asthenosphere flow model of hotspot–ridge interactions: a comparison of Iceland and Kerguelen, *Earth Planet. Sci. Lett.*, *161*, 45–56, 1998.
- Zijderveld, J. D. A., AC demagnetization of rocks: analysis of results, in *Methods in Palaeomagnetism*, edited by D. W. Collinson, K. M. Creer, and S. K. Runcorn, pp. 254–287, Elsevier, New York, 1967.

Acknowledgments

Initially, I would like to thank my supervisors Franz Heider, Bernhard Steinberger and Heinrich Soffel for their patient advise. I thank Heinrich Soffel for the thorough reading of the manuscript, Bernhard Steinberger for his advise in the theoretic part of the thesis and Franz Heider for organizing my first participation on an ODP cruise.

I would farther like to thank Nikolai Petersen for his advice and suggestions on true polar wander.

I thank the crews of ODP Leg 183 and 192 for the collaboration, helpful discussions and good times at sea. Especially I would like to thank the CoChiefs Mike Coffin, Fred Frey, John Mahoney and Godfrey Fitton and the Staff Scientist Paul Wallace for their guidance and organization of the cruises. I thank my shipboard teammates Hiroo Inokuchi and Xixi Zhao for the good collaboration. I scientifically and humanly benefited from the collaboration with Dietmar Müller, Bob Duncan and Mike Fuller.

I gratefully acknowledge the supply of unpublished data by Bob Duncan, Malcolm Pringle and Jean Besse.

I acknowledge several people for their help with the laboratory equipment: O. Bühler, H. Reichl, A. Mayer, H. Khek, A. Hornung and H. Spitzfaden. I would like to thank Manuela Weiss for her help and company in the paleomagnetic laboratory.

I would also like to thank some of my friends from the institute: Roman Leonhardt, Valerian Bachtadse, Christoph Heunemann, David Krása, Jürgen Matzka, Betty Scheu, Michael Winklhofer and Alex Zwing.

Financial support by ODP-Germany, DFG Projects He1814/10-1, So72/63-2 and So72/63-3 is gratefully acknowledged.

Appendix A

Rock magnetic and paleomagnetic study on sediments from Sites 1138 and 1140

Studies of the rock magnetic and paleomagnetic properties of sediments from the Kerguelen Plateau have been conducted with the aim of generating a magnetostratigraphy. In combination with biostratigraphic data a constrain on the minimum age of the underlying basalts could be made prior to $^{40}\text{Ar}/^{39}\text{Ar}$ age-dating of the basement. Dating of the different lithological units found in the sedimentary sections of the holes was done. Also, an estimation of the sedimentation rate with time was made. Analyses of magnetic properties provided information on the nature of the remanence and the minerals responsible for stable remanence.

A.1 Methods

During Leg 183 of the Ocean Drilling Program in the Southern Indian Ocean, approximately 465 m of sedimentary core material was recovered from the Holes 1138A (central Kerguelen Plateau) and 1140A (northern Kerguelen Plateau) (see Figures 2.2 and 2.6). All this material was obtained by drilling with a "rotary core barrel" (RCB). Consequently, all cores were neither oriented with respect to geographic north nor intact. Instead, much of the sampled sedimentary material was available as 2- to 5-cm-thick disk-shaped pieces whose azimuthal orientation was randomized by the coring process. However, as both sites are located at relatively high latitudes, the magnetic inclinations provide reasonable information for detecting reversals of the geomagnetic field recorded in the sediments.

The paleomagnetic data presented here are of two different types: those obtained using the shipboard pass-through magnetometer and those derived from conventional analysis of discrete sediment samples. Shipboard measurements were routinely taken on archive core

sections in 5 cm steps before and after stepwise alternating-field (AF) demagnetization up to at least 20 mT. Discrete samples from soft material were taken by pressing 6-cm³ plastic sample boxes into the working half of the cores. The harder sediments were cut with a sharp stainless steel spatula before sampling with a plastic cube. Typically, we obtained two samples per 1.5-m core section when the sediment was not disturbed. A scribe mark on the cubes was oriented relative to the vertical axis of the core. Discrete samples were subjected to progressive alternating-field (AF) demagnetization upon return to Munich. Paleomagnetic measurements were carried out in the Paleomagnetism Laboratory of the Universität München with a cryogenic magnetometer. All samples were stepwise AF-demagnetized in three directions. Approximately 600 samples from Holes 1138A and 1140A were AF-demagnetized in at least five steps up to at least 60 mT in order to isolate their characteristic remanence components.

Magnetozones were defined from shipboard measurements by selected directional data from the cryogenic magnetometer. Typical selection criteria were: (1) intensity of remanent magnetization after AF demagnetization at 20 mT is stronger than 2×10^{-4} A/m and hence above the noise level of the magnetometer in a condition of rough sea, (2) inclination is greater $\pm 30^\circ$, (3) at least two consecutive values (which corresponds to 10 cm length of split core, respectively) is of the same polarity, (4) no significant core disturbance is observed. Positive and negative inclinations are defined as reversed and normal magnetic polarities, respectively. The magnetic polarity stratigraphy, with constraints from the biostratigraphic data, was interpreted using the timescales of *Berggren et al.* [1995] and *Gradstein et al.* [1995] for Cenozoic and Mesozoic polarity boundaries, respectively. The measurements on discrete samples upon return to Munich were used to confirm or change the magnetozones.

Twenty-one sediment samples were selected from different lithotypes from Sites 1138 and 1140 for rock magnetic studies. Isothermal remanent magnetization (IRM), back-field, hysteresis curves and thermomagnetic curves were measured using a Variable Field Translation Balance (VFTB).

At Site 1136, no magnetostratigraphy could be obtained due to high disturbances and low recovery of the sedimentary core. At Site 1142 on the Broken Ridge, the last site of Leg 183, no sediments were recovered from the drilled interval because the material was washed out.

A.2 Lithologies of Sites 1138 and 1140

The lithologies of Sites 1138 and 1140 and ages of units are presented. Ages of the stratigraphic sections were determined due to biostratigraphic and magnetostratigraphic correlation. Magnetostratigraphic results are shown in section A.3.

Hole 1138A was drilled on the central Kerguelen Plateau in a water depth of 1153 m

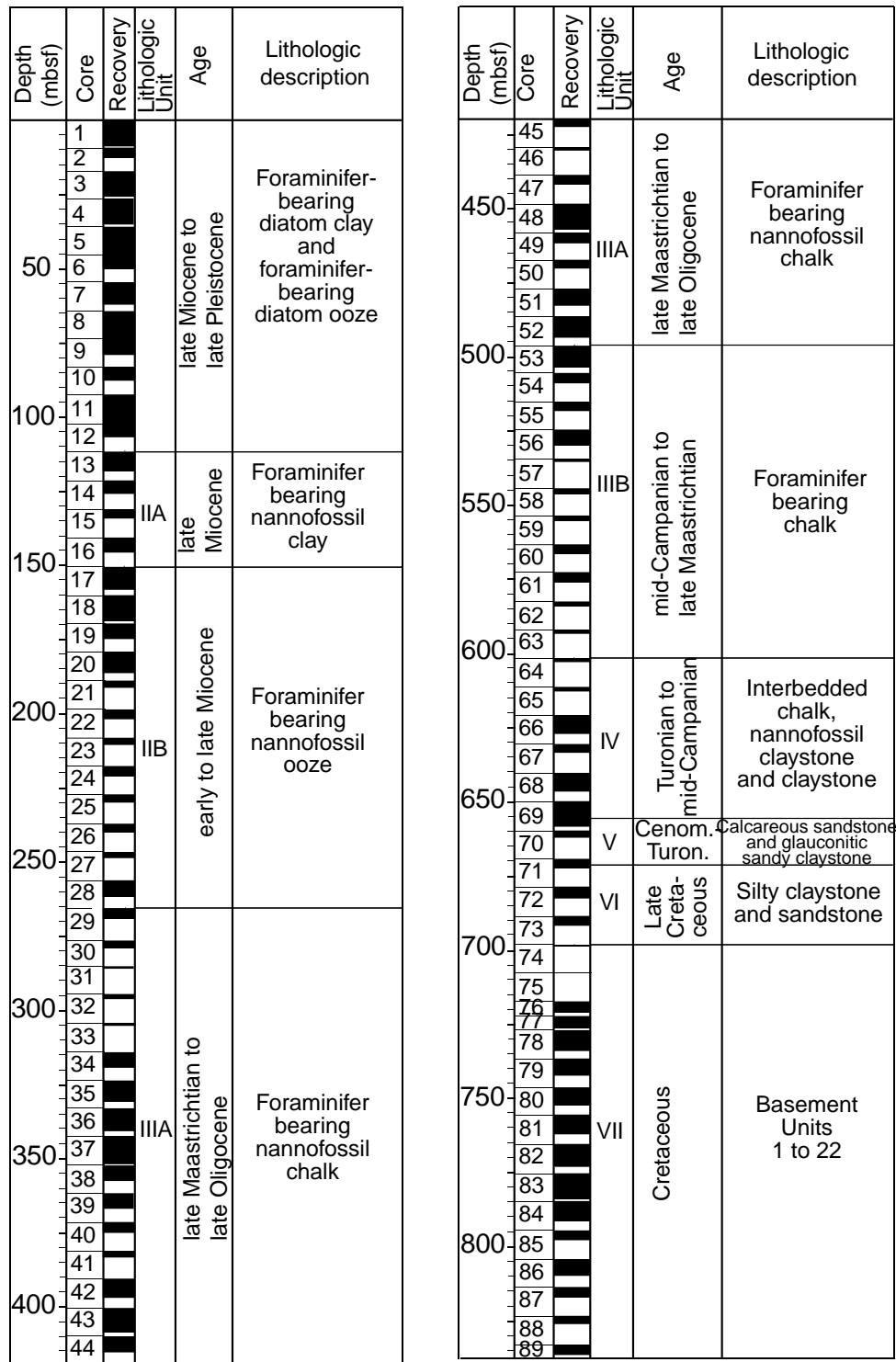


Figure A.1: Composite stratigraphic section for Site 1138 showing core recovery, lithologic unit boundaries, ages of units and names of lithologies. After Coffin *et al.* [2000].

down to a depth of 842.7 mbsf. 144 m of basalts were overlaid by 698 m of sediments, of which 343 m have been recovered. For an overview over the drilled stratigraphic section see Figure A.1 [Coffin *et al.*, 2000]. Seven lithologic units were recognized in Hole 1138A. Units I - VI are sedimentary rocks resting unconformably on the volcanic basement (Unit VII). The upper 650 m of sediment is biosiliceous and carbonate pelagic ooze, of which the top 110 m section comprises a relatively complete and expanded sequence of Quaternary and Pliocene biosiliceous sediments. The lower \sim 50 m of the sedimentary section consists of Upper Cretaceous shallow-marine and terrestrial sediments.

Unit I (0 - 112.0 mbsf) consists of foraminifer-bearing diatom clay with interbedded foraminifer-bearing diatom ooze in the upper portion. Few volcanic ash layers were found in this upper Pleistocene to upper Miocene unit. Unit II (112.0 - 265.9 mbsf) is composed of foraminifer-bearing nannofossil clay (Subunit IIA) that overlies foraminifer-bearing nannofossil ooze (Subunit IIB). Volcanic material is disseminated in the sediment as well as in rare distinct tephra layers. Unit III (265.9 - 601.8 mbsf) is late Oligocene to mid-Campanian in age. It consists of foraminifer-bearing chalk and contains scattered chert nodules in its lower part. The Cretaceous/Tertiary boundary near the base of Subunit IIIA (Core 183-1138A-52R) is possibly complete, but lithologies do not change across it. Unit IV (601.8 - 655.6 mbsf), of mid-Campanian to Cenomanian age, consists of cyclic alternations of foraminifer-bearing chalk with intervals of nannofossil claystone. Unit V (655.57 - 671.88 mbsf) consists predominantly of glauconitic calcareous sandstone of Turonian-Cenomanian age deposited in a neritic environment. Unit VI (671.88 - 698.23 mbsf) consists of Upper Cretaceous fossil rich silty claystone with interbedded sandstone of fluvial or shallow-marine origin. At the bottom of Unit VI, silty claystone rests upon volcanic basement rocks (Unit VII, see chapter 3).

In Site 1140 on the northern Kerguelen Plateau, the sedimentary section above igneous basement rocks consists entirely of pelagic ooze and chalk and appears to rest unconformably on the underlying submarine basalt flows [Coffin *et al.*, 2000]. Only one sedimentary unit (lithologic Unit I) overlying volcanic basement rocks was recognized (Figure A.2). Unit I (0 - 234.5 mbsf) consists predominantly of foraminifer-bearing nannofossil ooze and nannofossil chalk. Biostratigraphic data and interpretation of reversed and normal magnetic Chrons indicate that lithologic Unit I is middle Miocene to early Oligocene or latest Eocene in age. This unit was divided into two subunits (IA and IB). Subunit IA (0 - 10.0 mbsf) consists of white diatom nannofossil ooze with interbeds of dark brown silty diatom ooze. Subunit IB (10.0 - 234.5 mbsf) comprises most of the sedimentary section and is predominantly nannofossil ooze, which contains middle Miocene nannofossil and planktonic foraminifer species of warm-water affinity not found elsewhere on the Kerguelen Plateau.

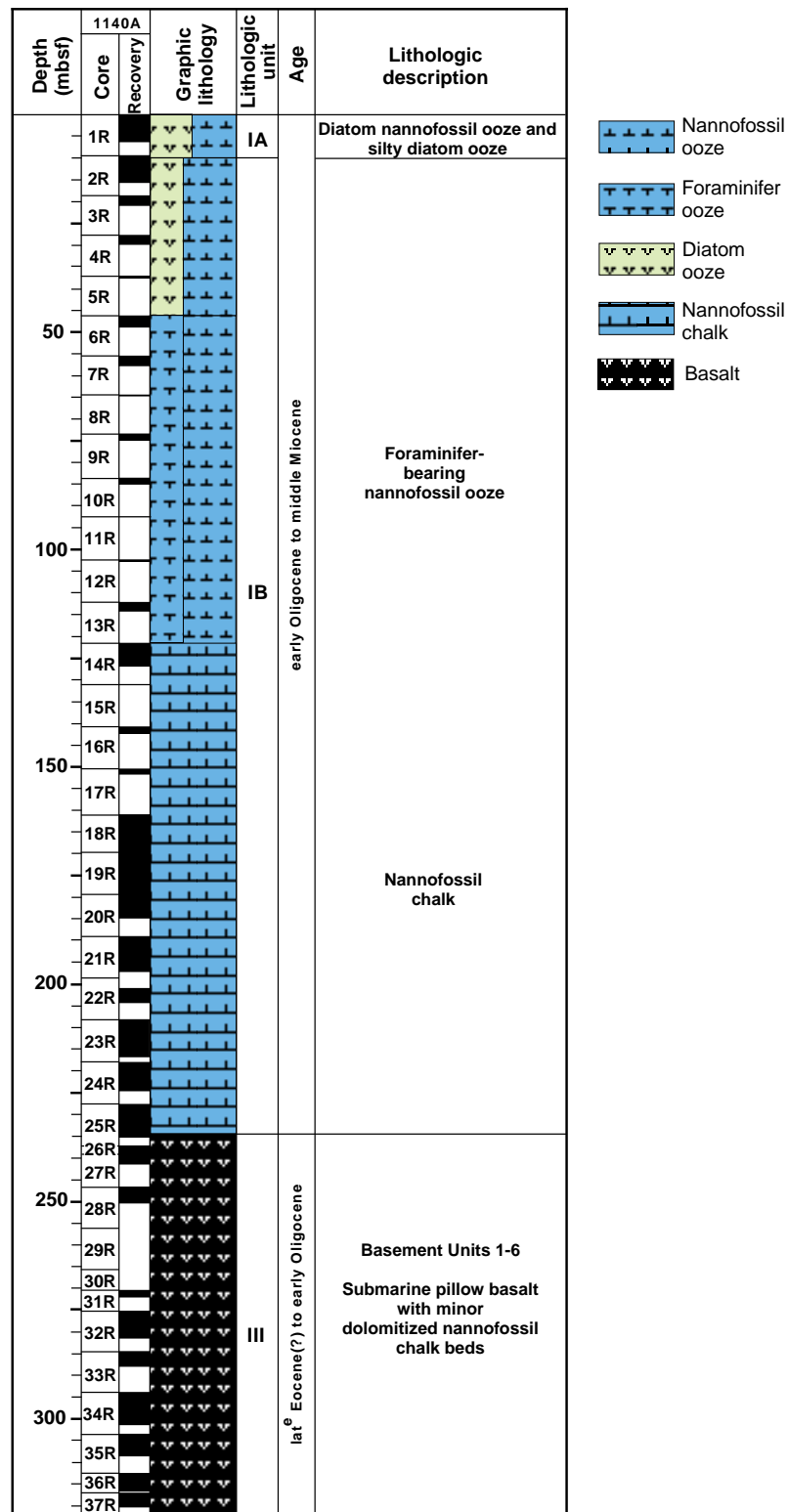


Figure A.2: Composite stratigraphic section for Site 1140 showing core recovery, a simplified summary of lithology, lithologic unit boundaries, ages of units and names of lithologies. After Coffin et al. [2000].

A.3 Magnetostratigraphy

Magnetic polarities in the sediment sections of Sites 1138 and 1140 have been determined. Biostratigraphic data from the sediments have been correlated with the magnetozones for identification of the magnetozones in the timescale. Finally, the magnetostratigraphy has been correlated with the drilling depth for determining the sedimentation rates.

A.3.1 Site 1138

The analysis of the 450 discrete samples, that have been taken from the working halves of Site 1138, indicate a different behavior during demagnetization. Characteristic examples are shown in Figure A.3.

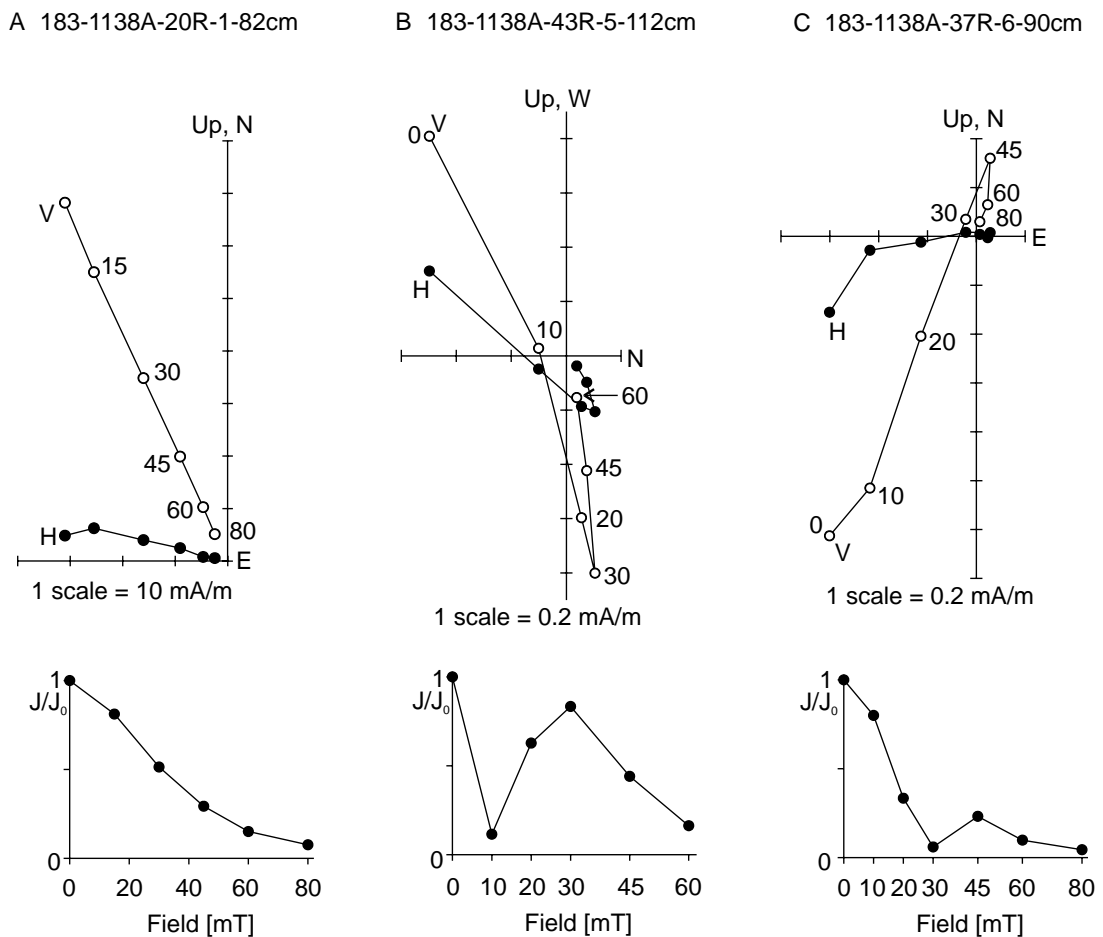


Figure A.3: Zijderveld-diagrams of sediments from Site 1138.

Samples with normal and reversed polarity without overprint or with a small overprint in direction or in opposite direction of the characteristic remanence were found in most parts of the site (Figure A.3A). These overprints which may be due to storing in the present magnetic field or due to drilling effects, have been destroyed at a demagnetization

level of 5-10 mT. Hence the overprint of these parts of the site has been easily destroyed after shipboard demagnetization at 20 mT of the archive halves and the analysis of the discrete samples onshore could confirm the previously found polarities. In Figure A.3B an example of another type of sample is shown. The normal overprint over the reversed characteristic remanence is completely removed at 30 mT. A two component analysis shows that the normal overprint corresponds to the direction of the actual earth magnetic field. Figure A.3C shows the Zijderfeld plot and the decay curve of a sediment sample with normal characteristic remanence and reversed overprint. Only after demagnetization at 45 mT the overprint has been removed. A steep reversed overprint of samples with normal polarity could be due to drilling effects. The standard shipboard demagnetization at 20 mT was not enough to obtain the accurate direction of the characteristic magnetization. Hence, in the parts of the site where that behavior was found, magnetic polarity had to be corrected after the analysis of the discrete samples. These parts are in core 17, 18, 37, 48, 51 and 53.

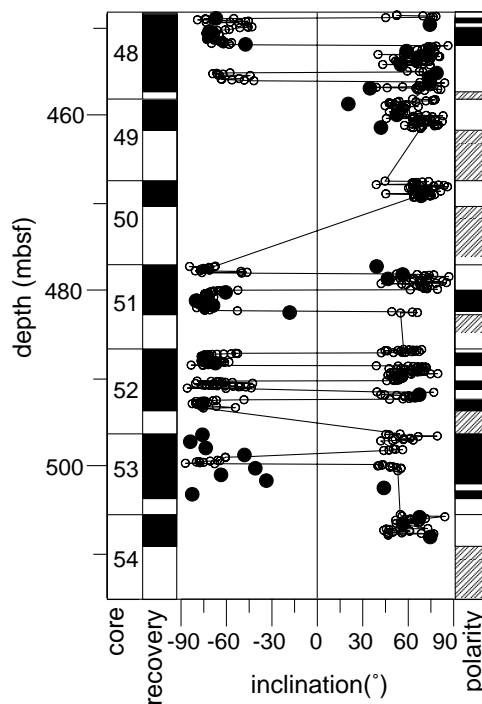


Figure A.4: Inclination data for sediments from Site 1138. Small circles represent shipboard continuous measurements, black dots represent results from demagnetization of discrete samples. The black and white bars in the right hand column indicate normal and reverse polarity, respectively. Shaded bars are zones without recovery or with unreliable inclination data, which have not been interpreted. Data from discrete samples have been used to confirm or to correct the continuous measurements. For example, sections in core 51 and 53 had to be corrected.

An example where the continuous measurements had to be corrected is shown in Figure A.4, together with an example for the magnetostratigraphic record determined from the shipboard inclination data and the characteristic inclinations of single sample cubes. The

complete record for sediments of Site 1138 is shown in Appendix B.

For sites on the southern hemisphere negative inclinations correspond to normal polarity of the Earth's magnetic field, and positive inclinations to reversed polarity. The inclinations obtained from the discrete samples confirm in most cases the results obtained during Leg 183 from the archive halves cores. An interpretation of the inclination record in terms of normal and reversed polarity is shown by black and white bars, respectively. Magnetic polarity chrons could be identified by correlating our results to a standard magnetic time scale and by considering biostratigraphic results. The combined magnetostratigraphic and biostratigraphic results have been correlated with drilling depth to obtain a sedimentation rate for Site 1138. This sedimentation rate is available on the CD of Appendix C.

A.3.2 Site 1140

In Figure A.5, representative examples of AF demagnetization and decay curves of samples from Site 1140 are shown. Sediments of the lithological unit 1A (0 m - 10.1 m) are magnetically very hard (median destructive field MDF is approximately 60 mT) (Figure A.5A). The characteristic magnetization has a single component without overprint. Sediments of Unit 1B (10.1 m - 234.52 m) are magnetically soft with a MDF of approximately 30 mT (Figure A.5B) and have partly a secondary magnetic component which could easily be destroyed with demagnetization at 20 mT.

The AF demagnetization experiments of about 100 single samples from Site 1140 confirmed in all sections the results obtained during shipboard continuous measurements of the archive halves. No additional information could be obtained for the magnetostratigraphy from discrete sample measurements at this site. The sedimentation rate was obtained by correlation of biostratigraphic and magnetostratigraphic data plotted versus depth and is available on the CD of Appendix C.

A.4 Rock magnetism of sediments of Sites 1138 and 1140

A series of rock magnetic investigations on sediment samples has been carried out to characterize the carriers of magnetization. Thirteen samples were selected from Hole 1138A and seven samples from Hole 1140A. Differences in lithology and in AF demagnetization characteristics were used as a selection criterion.

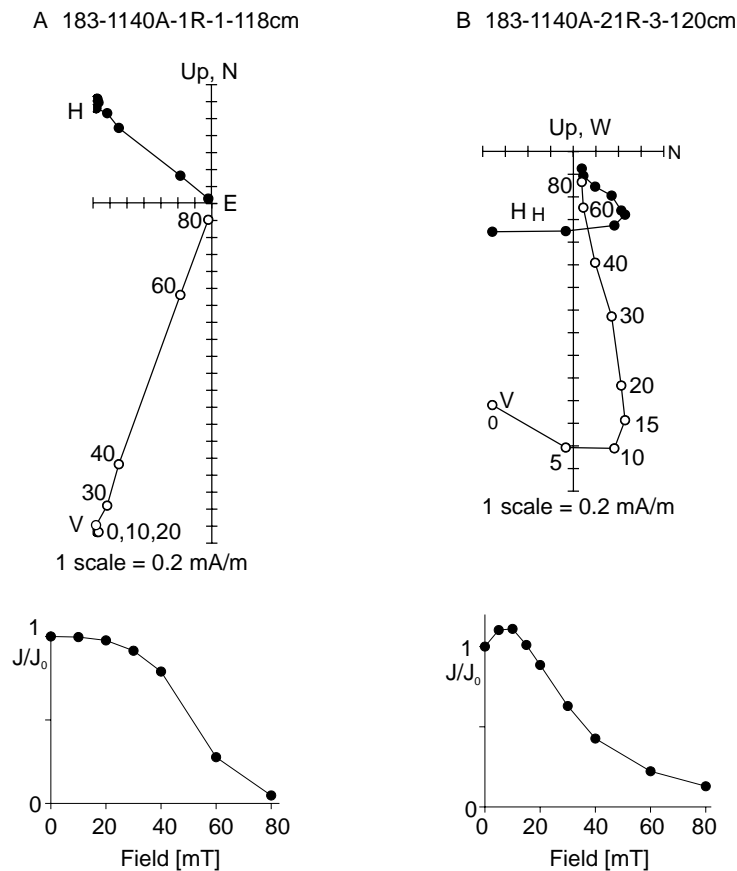


Figure A.5: Zijderveld-diagrams of sediments from Site 1140.

A.4.1 IRM Analysis

The selected samples were used in isothermal remanence acquisition (IRM) experiments in which the samples were placed in progressively stronger magnetic fields up to a maximum of 230 mT and their magnetization measured.

The results of these IRM experiments (Figure A.6) show that samples display two types of behavior. Samples of Site 1138 (Figure A.6A) and most of Site 1140 (Figure A.6B) show a sharp increase in magnetization in fields less than 150 mT followed by a slow increase through 230 mT. The rapid increase of the magnetization in low fields is typical for magnetite or Fe-Ti-Spinel, which because of its high spontaneous magnetization tends to dominate the IRM even when it is less abundant than other minerals. The second type (e.g., sample 183-1140A-21R-4-73cm) displays a more continuous increase up to 230 mT and might be due to a presence of a high-coercivity mineral. Five of the selected samples of Site 1138 are too weakly magnetic to measure IRM acquisition curves (samples of cores 43, 58, 59, 68, 73).

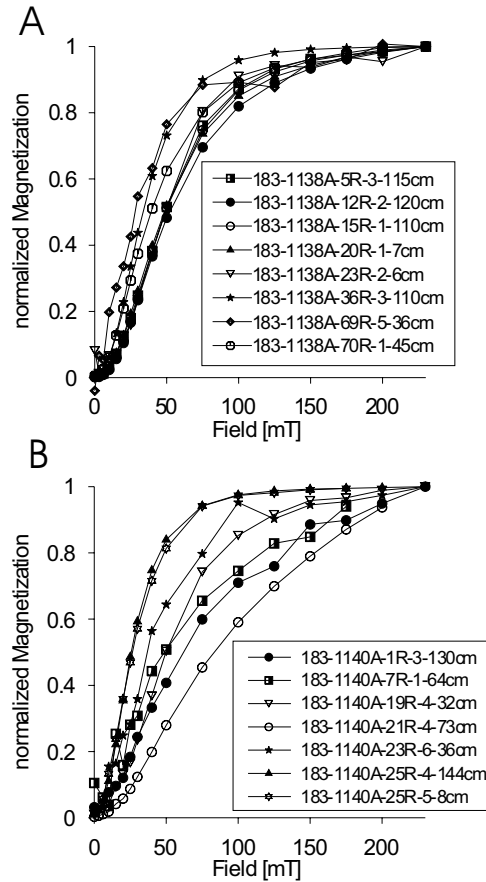


Figure A.6: IRM analysis of sediment samples of Site 1138 (A) and Site 1140 (B).

A.4.2 Hysteresis Analysis

Hysteresis parameters were obtained from hysteresis loops for a determination of the magnetic domain state. Of interest were the coercive force H_c and the ratio of saturation remanence I_{rs} over saturation magnetization I_s . The coercivity of remanence H_{cr} was determined measuring the backfield curves of the 16 samples which contained sufficient ferrimagnetic material for a determination of hysteresis parameters.

Hysteresis loops of samples of Site 1138 show four different characteristic behaviors. Very broad hysteresis loops with high H_c could be typical for single domain particles of magnetite (Figure A.7A). Some samples show clearly a diamagnetic behavior at high fields, superimposed by a ferrimagnetic component which dominates at smaller fields (Figure A.7B). Very weakly magnetic samples with a high content of calcite also show a strong diamagnetic component with a superimposed ferrimagnetic component (Figure A.7C). Hysteresis loops with a strong paramagnetic component have been corrected before interpretation (Figure A.7D). Hysteresis loops of samples of Site 1140 all show a typical behavior for titanomagnetite as magnetic carrier with a paramagnetic component which differs from sample to sample (Figure A.7E,F).

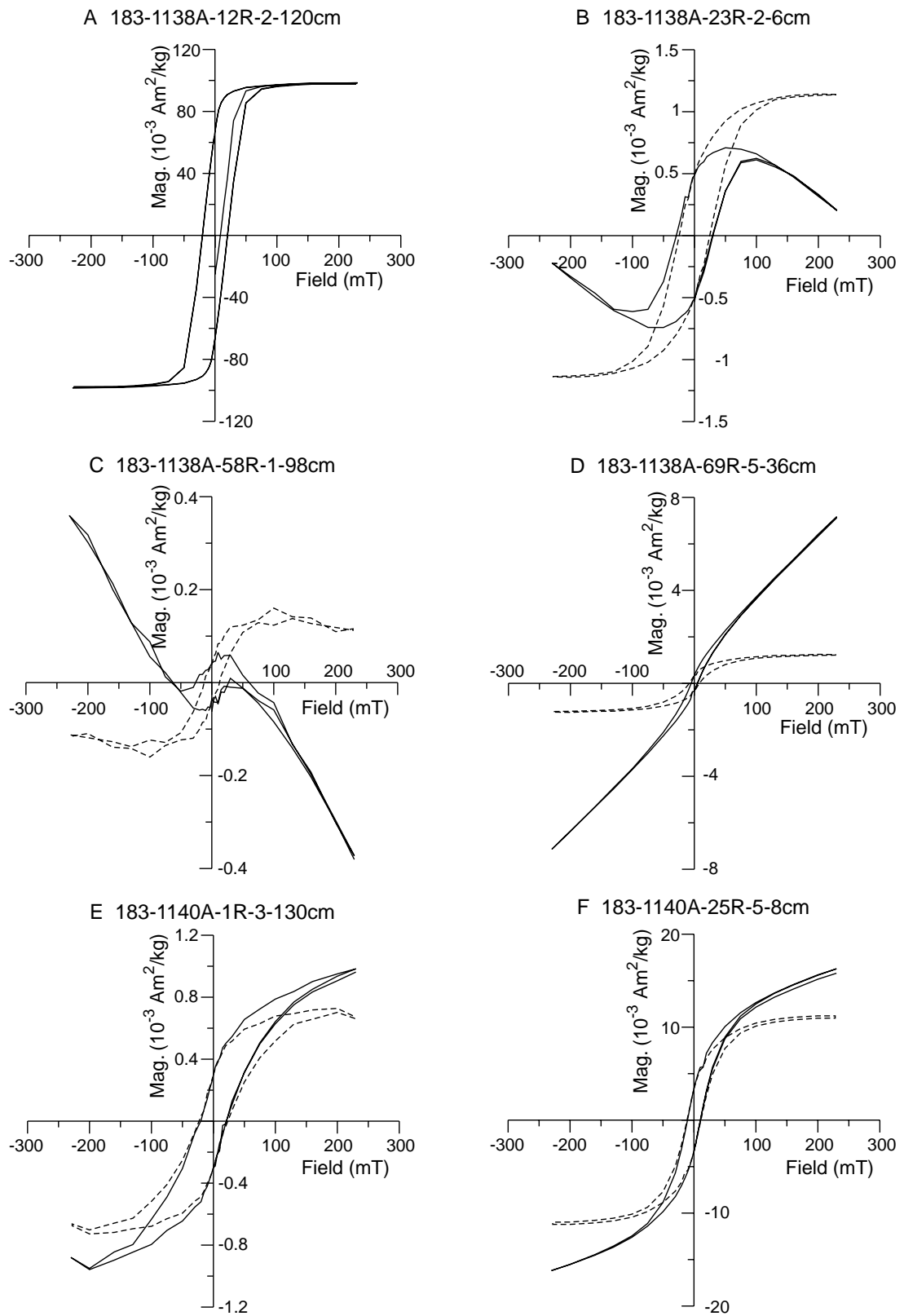


Figure A.7: Hysteresis curves of sediments of Sites 1138 (A-D) and 1140 (E,F).

Following the method of *Day et al.* [1977] the domain status was determined. The results from almost all samples are characteristic for PSD (pseudo single domain) particles. Two of the selected samples show characteristics of SD (single domain) particles.

A.4.3 Thermomagnetic Analysis

For thermomagnetic analyses some selected samples were heated between room temperature and 700°C and cooled down back to room temperature in the presence of a magnetic field (100 mT). For Site 1138, two representative examples are shown in Figure A.8A and B.

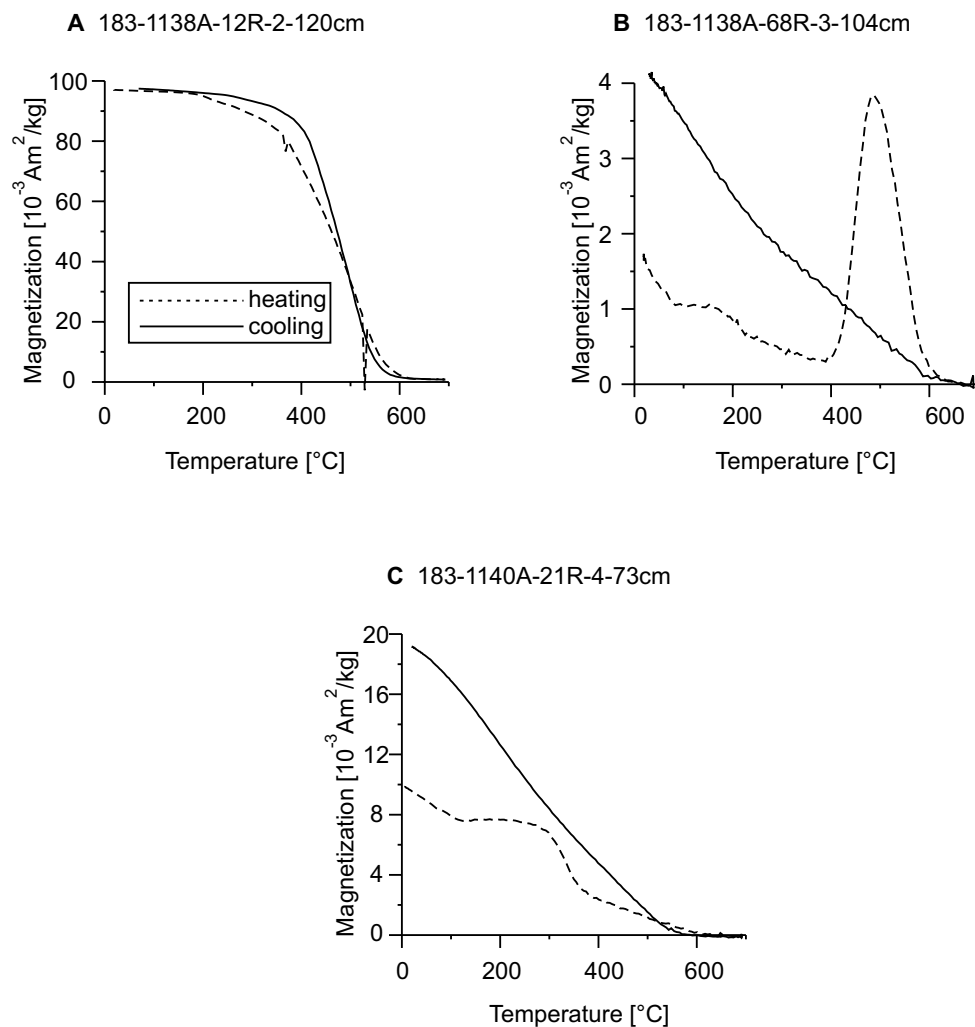


Figure A.8: Thermomagnetic measurements on sediments of Sites 1138 (A and B) and 1140 (C).

Sample 183-1138A-12R-2-120cm (Figure A.8A) shows reversible behavior during the heating-cooling cycle, indicating that no secondary mineral phase has been produced during heating. The constant intensity between 20°C and 400°C is followed by a major,

steep decline in intensity between 400°C and 600°C that is consistent with the removal of a mineral whose blocking temperature lies within this range. In the light of the results of the IRM study it is likely that this mineral is magnetite (or a low Ti-magnetite).

Irreversible behavior during the treatment cycle is shown by sample 183-1138A-68R-3-104cm (Figure A.8B). The heating curve of this sample shows a sudden decrease in intensity between 20°C and 80°C, which might be due to dehydration of the sample and simply represents a mass loss. This initial decrease is followed by a constant intensity up to 180°C and another decrease between 180°C and 400°C, which is ascribed to the removal of a low blocking temperature mineral. The sudden high peak after 400°C is due to the formation of secondary magnetite.

For Site 1140, sample 183-1140A-21R-4-73cm is shown in Figure A.8C. Its irreversible behavior, consistent with the conversion of a low-magnetization component to a higher magnetization component, is somehow similar to the one for Sample 183-1138A-68R-3-104cm. After a decrease between 20°C and 100°C, which might be due to mass-loss, and a following constant magnetization up to 300°C, a sudden decrease from 300°C to 350°C is observed, which is ascribed to the removal of a low blocking temperature mineral. From 350°C to 600°C a somewhat continuous decrease is displayed, typical for formation of secondary magnetite.

Appendix B

Magnetozones in sediments, Site 1138

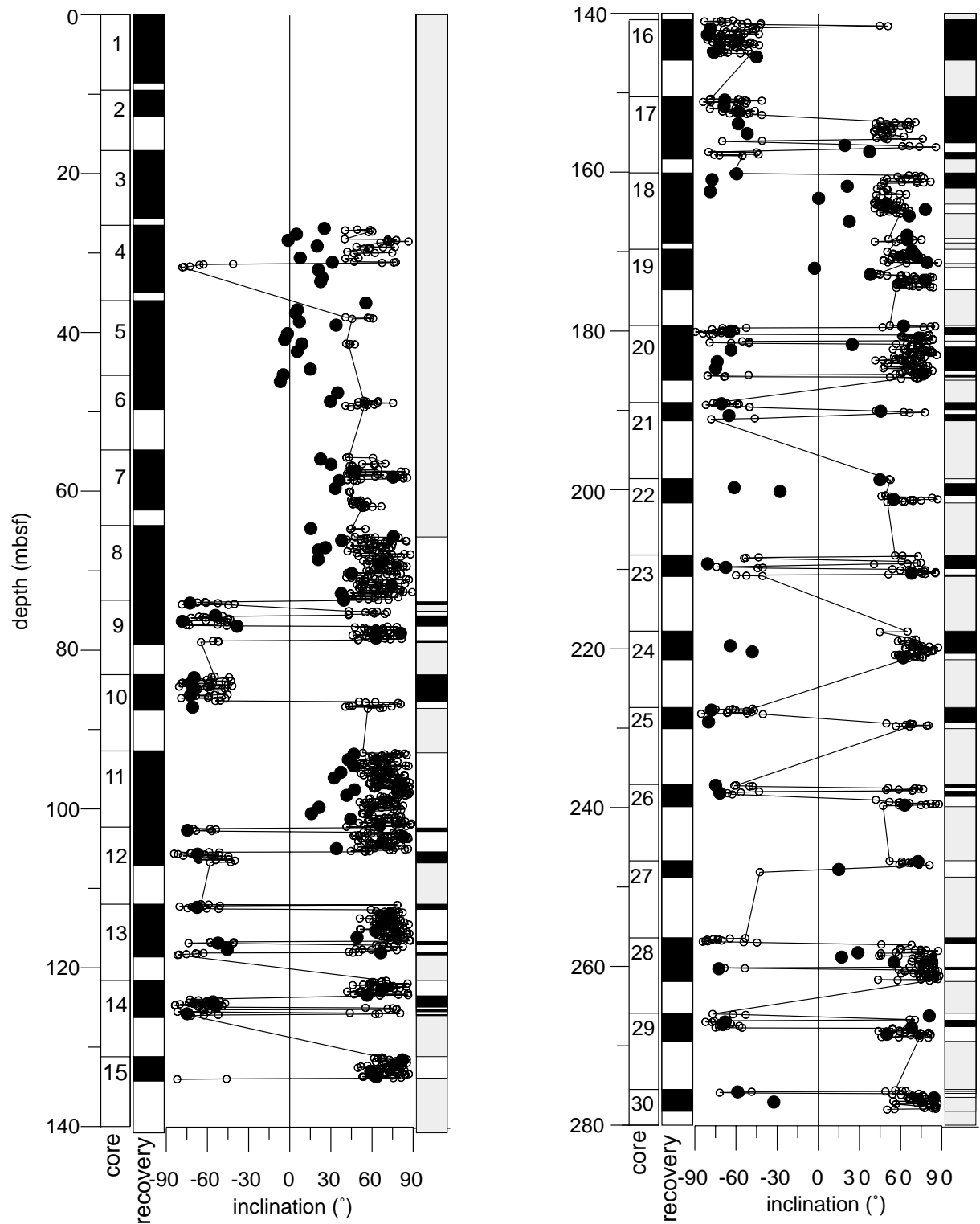


Figure B.1: Complete set of inclination data for sediments from Site 1138. Small circles represent ship-board continuous measurements, black dots represent results from demagnetization of discrete samples. The black and white bars in the right hand column indicate normal and reverse polarity, respectively. Shaded bars are zones without recovery or with unreliable inclination data.

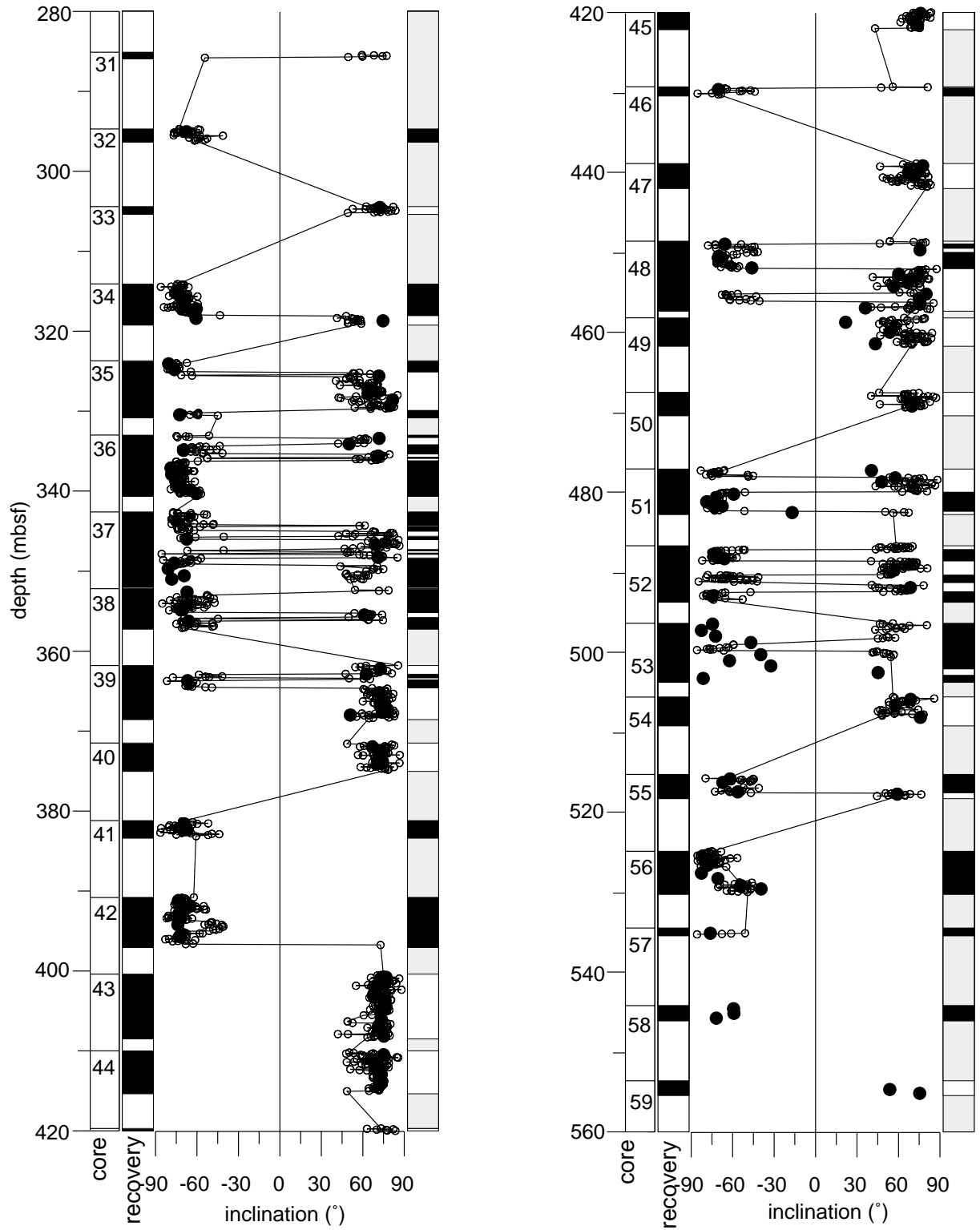


Figure B.1 (continuation).

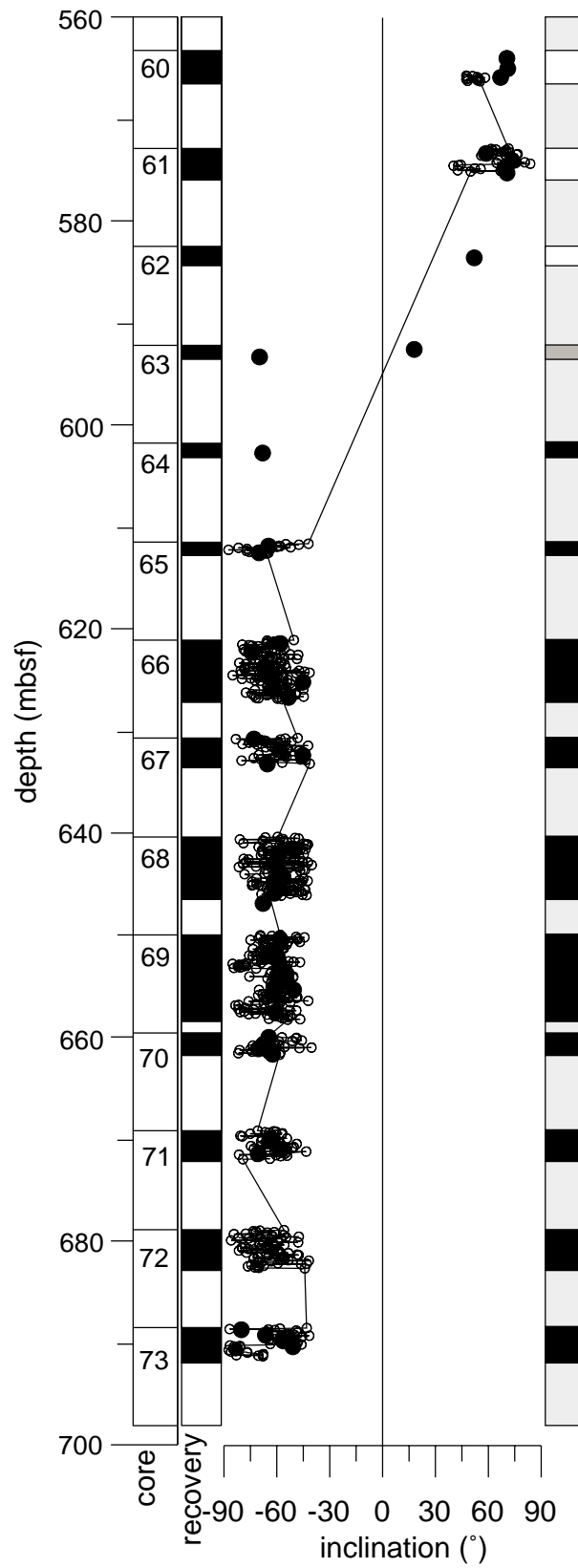


Figure B.1 (continuation).

Curriculum Vitae

14. Sept. 72 Geboren in Rosenheim als Kind von Anna und Franz Antretter

Sept. 78 bis Juli 82 Einschulung in die Grundschule in Stephanskirchen

Sept. 82 bis Juni 91 Übertritt in den musischen Zweig des Ignaz-Günther-Gymnasium in Rosenheim

Juni 91 Erwerb der allgemeinen Hochschulreife

Nov. 91 bis Okt. 97 Studium der Geophysik an der Ludwig-Maximilians-Universität München

März 94 Erwerb des Vordiploms in Geophysik

Nov. 95 bis Mai 96 Studium der Geologie und Physik in Pisa / Italien im Rahmen des Erasmus Programms

Nov. 97 Erwerb des Diploms in Geophysik an der LMU München. Diplomarbeit über den Einsatz von Bohrlochradar an hangrutschgefährdeten Gebieten

Jan. 98 bis Juli 98 Stipendiatin des Alpe-Adria Programms an der Università degli Studi di Trento und Mitarbeit am Servizio geologico di Trento, Italien

seit August 98 Anstellung als wissenschaftliche Mitarbeiterin am Institut für Geophysik bei einer Drittmittelstelle der Deutschen Forschungsgemeinschaft (DFG). Thema: Drift des Kerguelen Hotspot seit der Kreide anhand paläomagnetischer Breitenbestimmungen an Basalten von ODP Leg 183

Dez. 98 bis Feb. 99 Teilnahme an der Forschungsfahrt zum Kerguelen Plateau, ODP Leg 183

Jan. 00 bis März 00 Forschungsaufenthalt an der University of Hawai'i

Sept. 00 bis Nov. 00 Teilnahme an der Forschungsfahrt zum Ontong Java Plateau, ODP Leg 192